U.S. DEPARTMENT OF THE INTERIOR
U.S. GEOLOGICAL SURVEY

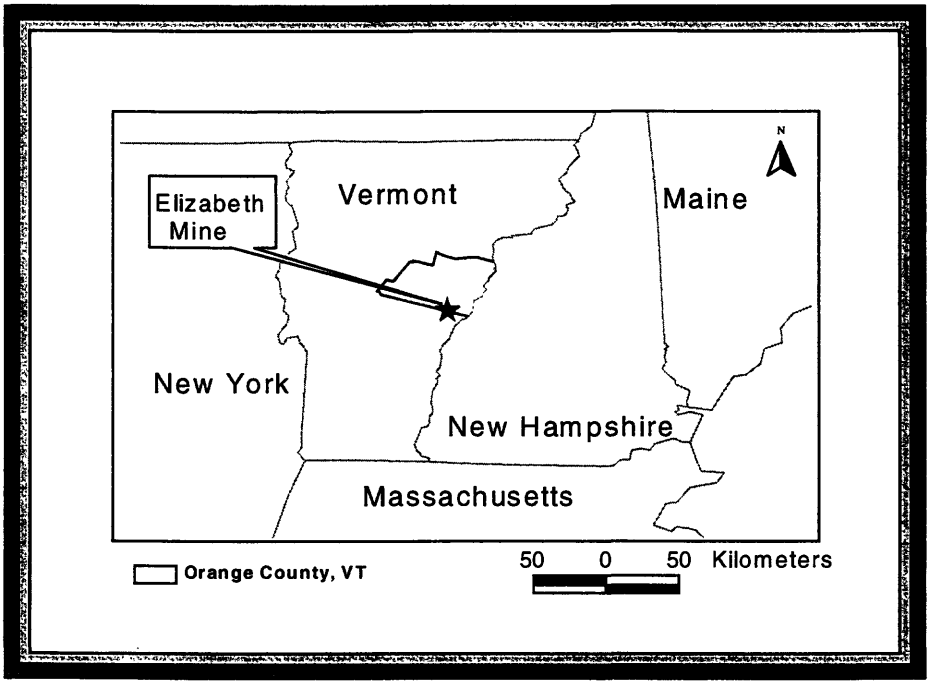

Characterization of Mine Waste at the Elizabeth Copper Mine, Orange County, Vermont

by

Jane M. Hammarstrom[1], Allen L. Meier[2], John C. Jackson[1], Ryan Barden[1], Peggie J. Wormington[1], John D. Wormington[1], and Robert R. Seal, II[1]

Open-File Report 99-564

[1] U.S. Geological Survey, 954 National Center, Reston, VA 20192
[2] U.S. Geological Survey, 973 Denver Federal Center, Denver, CO 80225

TABLE OF CONTENTS

FIGURES

TABLES

Figure 1. Copperas Brook confluence with the West Branch of the Ompompanoosuc River, about 0.5 km downstream from the base of the tailings at the Elizabeth mine site. The distinctive orange-red color of iron-rich coatings on the streambed and river rock is a hallmark of acid mine drainage.

INTRODUCTION

The Elizabeth mineral deposit, in the southern part of Orange County in east-central Vermont, was discovered in 1793. The deposit was developed in the early 1800s for copperas (iron sulfate) production from the iron-sulfide mineral pyrrhotite. Elizabeth is one of the oldest mines in the United States. From the 1830s to 1958, the deposit was mined for copper from chalcopyrite. Before the development of large copper deposits in Michigan, the Elizabeth mine was one of the largest domestic producers of copper. In the 1950s, it was the only operating metal mine in the northeastern United States. Sulfide ores of the Elizabeth mine constitute an excellent example of a Besshi-type massive sulfide deposit. These types of mineral deposits have the potential to generate considerable acid and contribute metals to the surrounding environment for two main reasons: (1) the ores are very rich in iron-sulfide minerals which are likely to produce acid and release metals upon weathering, and (2) the host rocks are carbonate-poor and have little or no capacity to neutralize any acid generated from weathering of sulfide minerals. Drainage from extensive mine waste piles and tailings (>30 acres) at Elizabeth enters Copperas Brook, which empties into the West Branch of the Ompompanoosuc River (figs. 1, 2). The West Branch joins the main Ompompanoosuc River about 5 kilometers east of the Elizabeth mine. In the 1980s, the Army Corps of Engineers and the U.S. Environmental Protection Agency (EPA) conducted limited site screening studies in response to concerns about the abandoned mine site as a source of heavy metals and silt affecting Copperas Brook and the Ompompanoosuc River; they concluded that the mine has had an adverse effect on local water quality.

The U.S. Geological Survey is currently (1999) cooperating with the Elizabeth Mine Study Group to characterize acid mine drainage from the site (Seal and others, 1999) as part of a broader study of the environmental behavior of massive sulfide deposits. Preliminary USGS water quality data are included in a report on hydrologic characterization and reclamation options prepared for the Elizabeth Mine Study Group (Barg and others, 1999). The water data show elevated concentrations of dissolved iron, aluminum, and acidity downstream from the tailings. Preliminary evaluation suggests that the heavy metals copper, zinc, and cadmium exceed U.S. EPA guidelines for acute toxicity for aquatic ecosystems (Seal and others, 1999). Increased metal loads from dissolution of sulfate salts during storm events degrade the water quality and aquatic biology of Copperas Brook. In conjunction with the USGS water quality study, the site was visited in August, 1998, and different geologic materials were sampled to characterize the mineralogy and chemistry of solid phases.

Mineralogy is an important control on water chemistry because the primary minerals in ore and host rock, and the secondary minerals that form during weathering of ore and tailings, provide the source for metals and acidity in associated waters. Soluble efflorescent sulfate salts forming on mine dump soils and tailings piles at Elizabeth are an important source of metals that affect surface runoff from the extensive mine waste on short time scales. Host rocks and mine waste composed mainly of common rock-forming minerals such as mica and feldspar release aluminum upon weathering and some of the minerals, although less effective than carbonate minerals, can consume some acidity.

Results of field observations and measurements, mineralogic data, and geochemical analyses for samples collected at Elizabeth in 1998 are summarized in this report, preceded by a general overview of environmental signatures associated with massive sulfide deposits elsewhere. X-ray powder diffraction (XRD), scanning electron microscopy (SEM), and electron microprobe analysis (EMPA) were used to identify the minerals; mineralogic and geochemical data are used to track the distribution of metals during weathering. These data provide preliminary information about the mineralogic residence, concentrations, and spatial distributions of metals and other elements in the solid materials on the site after 50 years (or more) of weathering and oxidation. Together with water analyses, these data can be used to help focus plans for site reclamation by providing information on the character of materials impacting Copperas Brook from the Elizabeth mine site.

ENVIRONMENTAL SIGNATURES OF MASSIVE SULFIDE DEPOSITS

Besshi-type massive sulfide deposits (named after a mine in Besshi, Japan) are a class of strata-bound mineral deposits that form in thick sequences of clastic sedimentary rocks interlayered with minor basalt (Slack, 1993). Besshi-type deposits range in size from less than one to over 180 million tonnes of ore. At a size of 2.9 million tonnes, the Elizabeth deposit is one of the smaller examples of this type. The deposits are typically copper-rich, but some also produce zinc, silver, and gold. The deposits are enriched in iron and sulfur, and many are initially mined for their near-surface iron sulfide minerals and subsequently exploited at deeper levels for copper and base metals. Other metals such as cobalt, molybdenum, tin, and lead may be present in minor amounts. The ore is concentrated in pods or lenses, and the deposits probably formed in ancient seafloor geothermal settings analogous to the modern black smoker deposits forming in deep ocean-floor settings in the Guaymas Basin of the Gulf of California (Slack, 1993).

Besshi-type mineral deposits tend to develop acid mine drainage and other environmental problems (Taylor and others, 1995) because (1) they contain massive concentrations of sulfide minerals that include abundant iron as well as base metals, (2) the iron sulfide minerals react with air and water during weathering to produce acid and release metals, and (3) host rocks typically lack effective acid-neutralizing minerals such as calcite. Some of the most acidic waters ever recorded are associated with drainage from massive sulfide deposits such as at the Iron Mountain Superfund site in California (Nordstrom and Alpers, 1999). Most metals are more mobile under acidic conditions and, therefore, waters associated with massive sulfide deposits tend to have low pH values and high dissolved metal concentrations (Plumlee, 1999). Water chemistry from these mine sites is a function of the geochemical and biogeochemical processes that operated at the site, the geology of the mineral

the geochemical and biogeochemical processes that operated at the site, the geology of the mineral deposit, climate, and mining and mineral processing methods used. Geologic controls on water quality and other environmental signatures of mineral deposits include ore and waste rock mineralogy and chemistry, mineral resistance to oxidation and weathering, mineral textures, and precipitation and dissolution of secondary minerals. In general, the pH of mine drainage varies depending on the balance between acid-producing and acid-consuming reactions that occur during weathering, the relative rates of these reactions, and the accessibility of minerals that contribute to these reactions (Smith and others, 1994). Reactions that produce acid include oxidation of iron sulfide minerals, hydrolysis of metal cations, and precipitation of hydrous metal-oxide minerals. Thus, mineralogy is important because (1) the primary ore and gangue minerals (the nonmetalliferous minerals associated with ore) provide a source of metals and other elements that can be released into solution upon weathering and produce or consume acid, and (2) any secondary minerals that form during the weathering process can temporarily sequester metals, recycling them and generating acidity in the environment as conditions, such as rainstorms or temperature, change.

The major ore minerals in Besshi-type deposits are pyrrhotite ($Fe_{1-x}S$), pyrite (FeS_2), and chalcopyrite ($CuFeS_2$). Minor ore minerals include magnetite and a number of other sulfides such as sphalerite ((Zn,Fe)S), arsenopyrite (FeAsS), galena (PbS), cobaltite (CoAsS), tetrahedrite ($(Cu,Fe,Ag,Zn)_{12}Sb_4S_{13}$), cubanite ($CuFe_2S_3$), and molybdenite ($MoS_2$). A number of potentially toxic metals such as cadmium, antimony, arsenic, and selenium may be present as major components or as trace elements that substitute for major components (e.g., Cd for the Zn in sphalerite) in these minerals. These elements can be released during mining, processing, natural weathering of the deposit, and weathering of the mine waste and tailings. Massive sulfide ores are typically finely ground during processing to reduce particle size for separating the different minerals and recovery of metals by a process known as flotation. In general, finer grained minerals weather faster than coarser grained minerals because of their greater surface area. Similarly, minerals that deviate from ideal composition weather faster than pure phases (Kwong, 1993; Kwong and Lawrence, 1994) and some sulfide minerals tend to decompose faster than others (Jambor, 1994). Weathering and oxidation of sulfide minerals in ore, waste rock, or tailings can release acid and metals directly to surface runoff or ground waters. More importantly, these processes recycle metals and acid. Secondary minerals form by evaporation of metal-rich solutions during dry periods and redissolve with rain or snow melt that releases pulses of acid and metals to aquatic systems. Secondary minerals can accumulate as efflorescent salt crusts and as cemented layers in tailings. Many of these secondary minerals are hydrates that are stable under very narrow ranges of temperature and relative humidity, and can appear and disappear within hours depending on weather conditions. Dissolved iron (from weathering and oxidation of the iron sulfide minerals) and aluminum (from weathering of the silicate minerals in the host rocks) precipitate as poorly crystalline oxyhydroxide mineral slimes under certain conditions of pH, and can affect aquatic habitats by increasing turbidity or interfering with gill function; these same minerals can remove metals from waters by adsorption.

THE ELIZABETH MINE

Location and geologic setting

The Elizabeth mine is located about 3 kilometers southeast of the village of South Strafford, on the east flank of Copperas Hill. The large open pits and tailings are shown on the USGS South Strafford 1:24,000-scale quadrangle map (fig. 2). Underground workings were accessed from the large open cuts (south pit and north pit) as well as from adits and vertical shafts. The mine area is within the headwaters for Copperas Brook, which flows northward through a wooded area for about a kilometer before it flows into the West Branch of the Ompompanoosuc River.

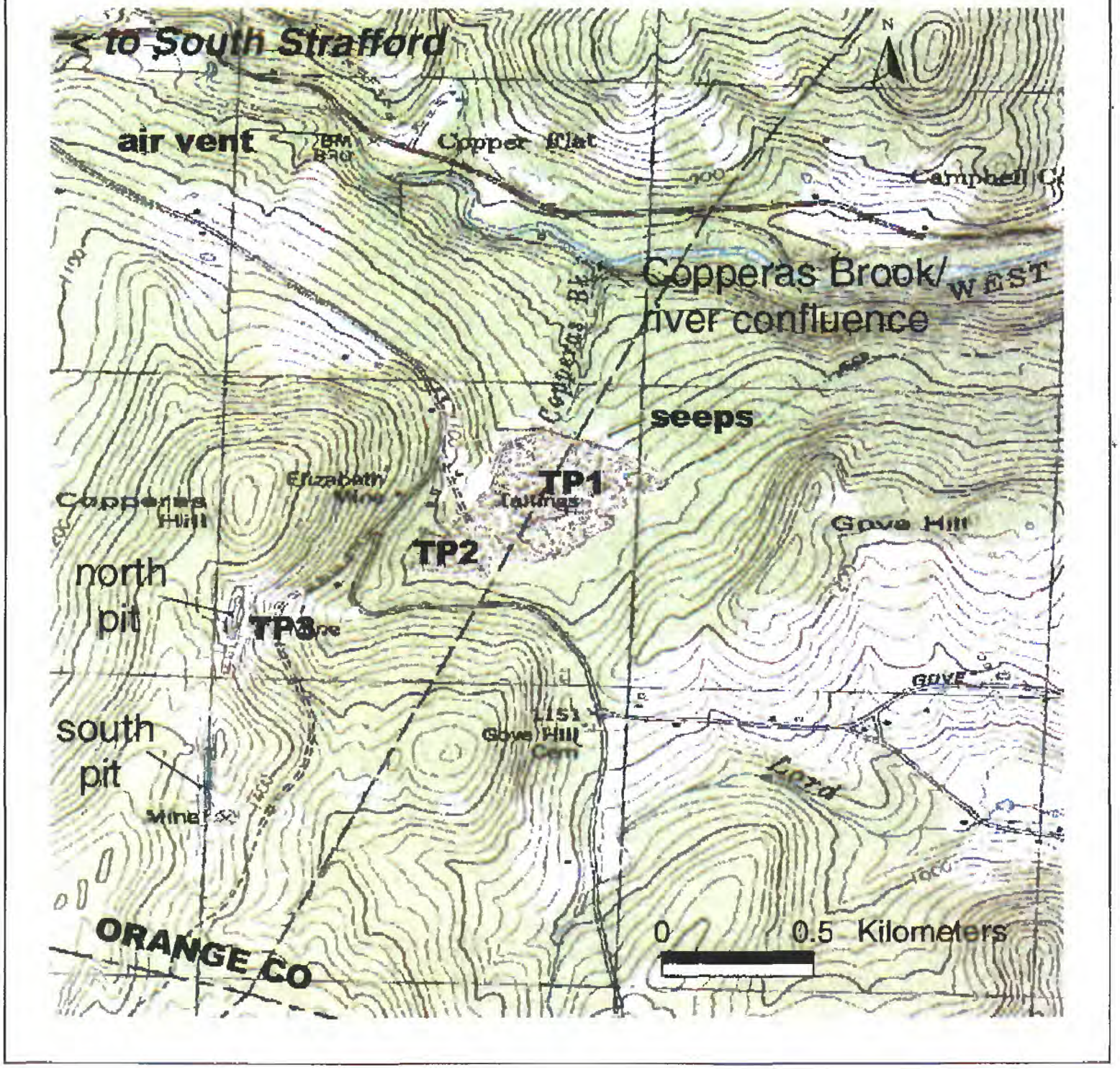

Figure 2. Elizabeth mine area as shown on part of the South Strafford 1:24,000-scale quadrangle. Labeled subareas sampled for this study are described in the text. The tic mark shown south of Copper Flat is at latitude 43° 50' north, longitude 72° 20' west.

Elizabeth was the southernmost and largest of the developed massive sulfide deposits of the Vermont Copper Belt. The Belt includes a number of mines and prospects that crop out west of the Connecticut Valley. The deposits are hosted by metamorphosed sedimentary rocks of Early Devonian age. The Gile Mountain Formation, the host rock for the Elizabeth and Ely deposits, is a sequence of silica-rich clastic rocks including pelite, quartzite, and metagraywacke, with minor amounts of mafic metaigneous rocks, such as hornblende schist and amphibolite. Deposits at Pike Hill occur in carbonate-rich rocks of the Waits River Formation. Both of these rock units were originally deposited by turbidity currents on an ancient ocean floor, covered with basaltic tuff (Standing Pond Volcanics), and following subsequent deposition of sediments and volcanics, were metamorphosed and deformed. Several smaller deposits (e.g., Cookville, Orange, Gove) are associated with the volcanic rocks. From

an environmental standpoint, one would predict that tailings and mine waste from any of these deposits likely impact the surrounding watershed because the deposits all share the characteristics of Besshi-type massive sulfide deposits.

A number of unusual rock types such as albite-, garnet-, and tourmaline-rich rocks are present in the local Elizabeth mine area. Ore bodies are sheetlike, but complexly folded. The nature of the original rock types and geometry of the mineral deposit have been obscured by the complicated geologic history of the area. For details of the stratigraphy, structure, and origins of the mineral deposits of the copper district, the interested reader is referred to Slack and others (1993) and references therein.

Mine history and previous studies

The Elizabeth mine was discovered in 1793 but at that time was unsuccessfully exploited for iron. In the 1800s, the iron sulfide mineral pyrrhotite was mined and processed on site to produce copperas at the Strafford Copperas Works, which is believed to have occupied the area adjacent to the north pit (fig. 2). Copperas, also known as green vitriol, is an informal name for the hydrated ferrous iron sulfate mineral melanterite ($FeSO_4 \cdot 7H_2O$). Melanterite was produced from pyrrhotite by igniting and then leaching the ore to decompose the sulfides, collecting the leachate liquor in evaporators, boiling the concentrate to an appropriate strength, and then evaporating the solution to form large green crystals of copperas in vats (Hitchcock and others, 1861). Sticks, branches, and timbers were used as substrates to seed crystallization. Copperas was marketed as a mordant in dyes and inks, and was also used as a disinfectant for purifying sewers. Ironically, the mineral melanterite, which was once the product of mining at Elizabeth, is now forming by the natural weathering of exposed sulfide-rich ore and mine waste rather than by a human-engineered process. Melanterite, and other efflorescent salts identified in this study, are readily soluble sources of metals and acidity that contribute to the degradation of water quality in Copperas Brook.

Open-pit copper mining at Elizabeth started in 1830 and underground mining began in 1886. The deposit was worked for copper until 1930, and was reopened by the Vermont Copper Company from 1943 until 1958 (Annis and others, 1983). The mine produced approximately 2.9 million tonnes (3.2 million short tons) of ore averaging 1.8 percent copper and 0.5 percent zinc, as well as minor silver and gold (Gair and Slack, 1980). The geology and history of the Elizabeth mine and the genesis of the mineral deposits of the Vermont copper belt have been addressed in many previous studies (Hitchcock and others, 1861; Wheeler, 1883; Howe, 1886; Smyth and Smith, 1904; Judson, 1909; Fay, 1909; Anderson, 1931; White, 1943; White and Eric, 1944; Benson and others, 1950; Lutjen and Kearney, 1953; Howard, 1959a, 1969; McKinstry and Mikkola, 1954; Jenks, 1968; Gair and Slack, 1980; Annis and others, 1983; Slack and others, 1993).

The Elizabeth mine was developed in open pits and in extensive underground workings. Water was a problem in the open pits, but relatively little water entered the underground workings during mining (125 gallons per minute reported in the 1950s; Lutjen and Kearney, 1953). Ore was processed on-site over a period of more than 100 years by a variety of methods. Copper smelters operated at the mine from 1830 to 1839, from 1861 to 1872, and from 1880 to 1888 (Benson and others, 1950). A flotation mill was erected during World War I and a second flotation plant operated from about 1927 to 1930. The mine was reorganized under the Vermont Copper Company in 1942 and reopened with a modern flotation mill.

Preexisting mine dumps were reprocessed in the modern mill and flotation plant during 1949 and 1950. These older dumps were reportedly acidic from ferrous sulfate formation generated by burning; oxidation of unstable pyrrhotite in the tailings apparently was susceptible to spontaneous combustion. Buildings constructed during this last phase of the mine operation remain on the site (fig. 3). In the 1940s, 180 to 680 tonnes (200 to 750 short tons) of ore were milled daily (Benson and others, 1950). The ore was reduced to a particle size of 2 cm (3/4 in) or less before entering the copper concentration circuit where a Marcy mill was used to grind 60 percent of the ore to -200 mesh for flotation. In order to float pyrrhotite from the rest of the ore, copper sulfate or sulphuric acid (or both) were added to the pulp, and a pH of 9.0 to 9.3 was maintained in the copper recovery circuit by adding lime to truckloads of ore as they were dumped into the coarse ore bin (Lutjen and Kearney, 1953;

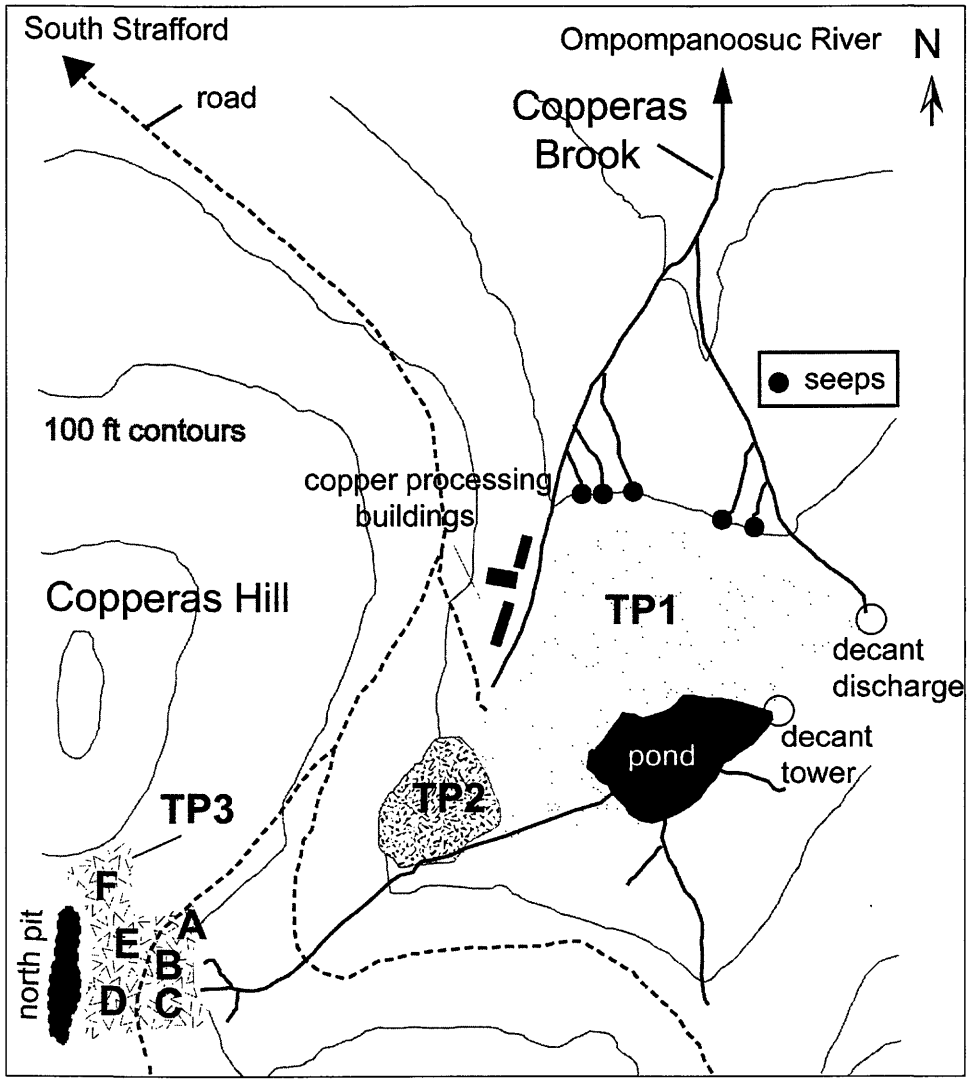

Figure 3. Detailed sketch map of the Elizabeth mine site (based on Young, 1991).

Benson and others, 1950). Other reagents used in the flotation circuit included cyanide, pentasol amyl xanthate, and a frother of pine oil and pentasol 124 alcohol. Sandy tailings were dammed to form an impoundment near the concentrator that was designed to hold several million tons of tailings (Benson and others, 1950). These fine-grained tailings are present in the 30 acres designated as tailings pile 1 (TP1 on figs. 2 and 3). Copper and pyrrhotite tails from the flotation circuit were separated because the pyrrhotite tailings contained fine mica and talc slimes that tended to slide when the tailings got wet. Concrete pipes were installed to dewater the tailings to address this problem. Decant towers (fig. 3) that drained the tailings pile surface are still present on the site although the underground pipes have collapsed.

In the early years of operation at Elizabeth, copper was smelted on-site. Copper concentrates produced in the modern flotation plant were shipped to a smelter in New York; about a third of the pyrrhotite produced (70 short tons per day) was shipped to a paper company for manufacture of sulfur. Some magnetic pyrrhotite was sold in a pilot project for manufacturing electrolytic iron. The mine operated under government subsidy for many years. At times, the mine employed as many as 200 people and played an important role in the local economy for over 150 years.

Mine dumps and tailings from the Elizabeth mine have been exposed to weathering processes since at least 1958. The south pit and north pit areas (figs. 3) represent the oldest workings. Most of the ore was produced from underground workings accessed through the adits in the walls of the north pit. Underground workings extend to the West Branch of the Ompompanoosuc River; where the underground air ventilation system now discharges ground water to the river about one kilometer upstream from the confluence of Copperas Brook (fig. 2). In a 1991 EPA study (Young, 1991), the mine site was surveyed and tailings piles were designated as tailings piles 1, 2, and 3 (fig. 3). We have retained those designations throughout this report. Tailings piles 1 (TP1, 30 acres) and 2 (TP2, 5 acres) comprise fine-grained tailings from the on-site flotation mill that operated during the most recent period of mining (1943 to 1958). The piles have steeply dipping, bare, eroded north slopes and partially vegetated flat tops. Tailings pile 3 (TP3) consists of a 6-acre mine waste pile adjacent to the open cut of the north pit; TP3 represents waste from mining operations in the 1800s. Copperas Brook flows from the base of TP3, through a divide in TP2 onto the top surface of TP1, where it enters a small pond. Decant towers divert water from the surface of TP1 through concrete pipes to a discharge point at the northeast corner of the pile (fig. 3). Waters from the discharge and from seeps along the base of tailings pile 1 coalesce to form Copperas Brook in the wooded areas and wetlands below the tailings.

In addition to the EPA study, Barg and others (1999) characterized hydrology and remediation options for the Elizabeth mine. Other studies on environmental aspects of Elizabeth include a study of water quality implications associated with the Union Village dam project downstream from the mine (Barth, 1984) and a hydraulic evaluation and revegetation study conducted by the U.S. Army Corps of Engineers (Department of the Army, 1989). Geobotanical studies of tree species showed that birch at the Elizabeth mine site accumulate copper, zinc, and cobalt and show effects of stunted growth (Power and Milton,1990). Slack and others (1990) documented geochemical dispersion of copper, zinc, cadmium, cobalt, silver, boron, and manganese downstream from mine dumps at Elizabeth, Ely, and Pike Hill in their study of the geochemistry of stream sediments and heavy mineral concentrates from the Orange County copper district. Some of these previous studies include chemical data on tailings and stream sediments, but no mineralogic data.

METHODS

A variety of solid geologic materials occurring at the Elizabeth mine can interact with surface and ground waters to contribute, or remove, metals and other elements to and from the aquatic habitat. These materials include bedrock outcrop exposed in pit walls, weathered chunks of ore sitting out on bare waste piles, slag, soils that develop on mine waste piles, tailings from on-site ore processing, stream sediments, efflorescent salt minerals, and ochre deposits. By compiling mineralogic and geochemical data on these different sample types, the fate of different elements in the environment can be tracked and contributions of different materials to the waters associated with the mine can be evaluated. During August, 1998, detailed surface sampling of solid materials was conducted in the mine area. Stream sediments were collected at water sampling sites (Seal and others, 1999) upstream and downstream from the confluence of Copperas Brook, and from the main Ompompanoosuc River above and below its junction with the West Branch. Sample localities discussed in the text are shown on part of the South Strafford 1: 24, 000 quadrangle map (fig. 2) and on a sketch map of the site (fig. 3). Representative samples of different types of materials were collected and several techniques were used to determine mineralogy and chemistry. Primary and secondary minerals identified at the Elizabeth mine are listed in table 1 together with their ideal chemical formulas and, for secondary minerals, a ranking of weathering behavior. Iron, for example, is present in several different primary sulfide ore minerals as well as in relatively fast-weathering common minerals that comprise the wallrock around the ore. The fact that a number of different secondary minerals contain iron (both oxides and efflorescent sulfate salts) indicates that iron is mobile in the environment at the Elizabeth mine. Additional secondary minerals probably occur at Elizabeth, but have not yet been identified because they are, by nature, ephemeral and may form and dissolve in periods as short as a few hours.

Table 1. Mineralogy of the Elizabeth mine.
[Chemical formulas from Mandarino, 1999; relative weathering rates from Kwong, 1993]

Ore minerals	
Mineral name	Chemical formula
chalcopyrite	$CuFeS_2$
cubanite	$CuFe_2S_3$
galena	PbS
marcasite	FeS_2
molybdenite	MoS_2
pyrite	FeS_2
pyrrhotite	$Fe_{1-x}S$ (x = 0 to 0.17)
sphalerite	ZnS
tetrahedrite-tennantite	$(Cu,Fe,Ag,Zn)_{12}Sb_4S_{13}$
valleriite	$4(Fe,Cu)S \cdot 3\ Mg,Al)(OH)_2$

Gangue and wallrock minerals	
Mineral name	Chemical formula
Dissolving	
calcite	$CaCO_3$
Fast to intermediate weathering	
amphibole (tremolite variety)	$Ca_2Mg_5Si_8O_{22}(OH)_2$
biotite mica	$K(Fe,Mg)_2Al_3Si_2O_{10}(OH)_2$
chlorite	$(Mg,Fe)_5Al(Si_3Al)O_{10}(OH)_8$
epidote	$Ca_2(Fe^{3+},Al)_3(SiO_4)_3(OH)$
garnet (spessartine variety)	$Mn_3Al_2(SiO_4)_3$
talc	$Mg_3Si_4O_{10}(OH)_2$
Slow weathering to inert	
apatite	$Ca_5(PO_4)_3F$
graphite	C
muscovite mica/sericite	$KAl_3Si_3O_{10}(OH)_2$
plagioclase feldpsar	$NaAlSi_3O_8$
phlogopite mica	$KMg_3AlSi_3O_{10}(OH)_2$
quartz	SiO_2
rutile	TiO_2
tourmaline	$Na(Fe,Mg)_3Al_6(BO_3)_3Si_6O_{18}(OH)_4$
vesuvianite(idocrase)	$Ca_{10}Mg_2Al_4(SiO_4)_5(Si_2O_7)_2(OH)$
wollastonite	$CaSiO_3$

Table 1. Continued

Secondary minerals		
Mineral name	Chemical formula	Color
	very soluble	
aluminite(?)	$Al_2(SO_4)(OH)_4 \cdot 7H_2O$	white
alunogen	$Al_2(SO_4)_3 \cdot 17H_2O$	white
melanterite	$FeSO_4 \cdot 7H_2O$	green
rozenite	$FeSO_4 \cdot 4H_2O$	white
	soluble	
halothrichite-pickeringite	$(Fe,Mg)Al_2(SO_4)_4 \cdot 22H_2O$	white, fibrous
siderotil	$Fe^{2+}SO_4 \cdot 5H_2O$	light blue to white
	slightly soluble	
gypsum	$CaSO_4 \cdot 2H_2O$	white
	relatively insoluble	
ferrihydrite	$5Fe^{3+}{}_2O_3 \cdot 9H_2O$	reddish brown
goethite	$Fe^{3+}O(OH)$	yellowish brown
hematite	α - Fe_2O_3	black, brown, blood red
jarosite	$K_2Fe^{3+}{}_6(SO_4)_4(OH)_{12}$	straw yellow
schwertmannite	$Fe^{3+}{}_{16}O_{16}(OH)_{12}(SO_4)_2$	yellow

Descriptions and locations of rock, slag, mineral, mine dump soils, tailings soils, and ochre samples are tabulated by subarea in Appendix A . Locations were determined in the field by global positioning system (GPS) or were taken from the topographic map if no GPS satellite readings could be obtained. Details of analytical methods used for determinative mineralogy and chemistry are given in Appendix B.

Rock and slag samples were collected from surface outcrops and mine dumps. In the laboratory, samples were reduced with a jaw crusher and ground to <100 mesh in a ceramic-lined percussion mill to obtain a minimum of 70 g of powder for chemical analysis. For some samples, polished thin sections were prepared for quantitative electron microprobe analysis of minerals. Mineral grains and fragments of rocks also were hand-picked under a binocular microscope and mounted on carbon planchets for scanning electron microscope studies.

Soil fractions (<2 mm) of mine dumps and tailings surfaces were sampled with a stainless steel trowel, sieved into a plastic pan using a solder-free 8-mesh screen, and stored in plastic bags. A minimum of 1 kg of sample was composited from 30 increments collected on a random grid over defined sampling areas. Composite sample areas were chosen on the basis of distinctive features such as natural physical breaks and age of waste piles, surface color or texture, and tops of piles versus steep eroded slopes. Shovel- and core-type soil augers up to 150 cm long were used to sample the stratigraphy of the waste piles. In the laboratory, samples were mixed, split, and ground to <100 mesh in a ceramic-lined percussion mill to obtain a minimum of 70 g for chemical analysis. Paste pH was measured in the field (Appendix B). Paste pH is a static technique used in soil science. By exposing soil-sized material to near-neutral to slightly acidic deionized water and measuring the pH of the resulting paste, one can get a quick measure of the relative acid-generating (pH<4) or acid-neutralizing (pH>7) potential of the material. The paste pH technique does not replace acid-base accounting procedures used to classify acid-generating material and prescribe remediation treatments such as addition of lime;

however, it does provide an indication of what will happen when the material is exposed to surface runoff from rain or snowmelt.

Rocks, slag, tailings, and ochre deposits were analyzed by inductively coupled plasma mass spectrometry (ICP-MS) in USGS laboratories in Denver, CO and by inductively coupled plasma-atomic emission spectroscopy (ICP-AES) by XRAL Laboratories of Don Mills, Ontario using USGS analysis protocols (Arbogast, 1996). Some samples were analyzed for major rock-forming elements (reported as oxide weight per cent) by wavelength dispersive x-ray fluorescence spectroscopy (WD-XRF) in USGS laboratories in Denver, CO. Splits of the samples were sent to XRAL Laboratories for analysis of total carbon, carbonate carbon, and total sulfur by LECO methods; mercury by cold vapor aromic absorption spectrometry (CVAC); gold by graphite furnace atomic absorption spectrophotometry (GFAA); and selected trace metals (As,Se, and Sb) by a hydride generation technique (HYD). Total sulfur contents provide a measure of the maximum potential acidity that a material may produce. Unpublished geochemical data for ore samples (Harvard University collection) from the historic underground workings provided by John Slack (USGS) are included in this report (table 3). Tailings soil color was determined by comparison of dry, <2 mm material, in sunlight with Munsell soil color charts. Soil mineralogy was determined by x-ray diffraction on powder mounts.

Stream sediments were collected at water sampling sites in and adjacent to the mine area. Samples of one kilogram or more were collected with a stainless steel scoop, washed through an 8-mesh solder-free screen into a plastic pan, and stored in plastic bags. Each sample represents a 30-increment composite across the stream. Where streams are narrow (<3 m wide), the increments represent 10 traverses of three samples across the stream. For wider streams, the sampling interval was adjusted. In the laboratory, the sediments were air dried in plastic pans, weighed, sieved to remove material coarser than 80 mesh, reweighed, and ground in a ceramic-lined percussion mill to obtain a minimum of 70 g of powder for chemical analysis. The <80 mesh fraction of the stream sediment represents the finer-grained portion of the sediment that is most likely to be transported downstream, to contribute to stream turbidity, and to affect aquatic and benthic species. Stream sediments were analyzed for 40 elements by ICP-AES by XRAL Laboratories using USGS protocols for analysis. (Arbogast, 1996).

Mineral samples of efflorescent salts were collected using tweezers or a knife blade and stored in plastic vials or in mineral oil to preserve hydration state. Samples were examined under a binocular microscope and hand-picked for mineral identification by x-ray diffraction and scanning electron microscopy. Heavy liquids were used on tailings and ochre deposits to separate minerals with high specific gravity for identification by SEM or EMPA.

OVERVIEW OF SAMPLE SITES

Field observations and localities sampled are discussed in terms of discrete subareas (figs. 2 and 3), starting with the southernmost areas that are proximal to the underground workings and ending with the northernmost samples collected along Copperas Brook and the West Branch of the Ompompanoosuc River. Aspects of mineralogy relevant to each site are noted (see table 1 for key to minerals) in the overview discussion. Tailings characteristics are summarized in table 2. Mineralogic and geochemical data are discussed by sample type (ore, tailings, salts, etc.) in the Results section of this report below. Data are given in tables 3-10; within each table, data are organized by subarea.

South pit area

The south (No. 2) pit area represents some of the oldest workings at the Elizabeth mine. The pit is flooded at its north end (fig. 4A). The south end is a deep trench that exposes bedrock along the pit walls. Slack and others (1993) provided a detailed description of the lithologies and structures exposed in the pit walls. The pit exposes bedrock composed of quartzite, biotite schist, coarse garnet-mica schist, amphibolite, and massive sulfide ore (Slack and others, 1993, fig. 13). Under protected overhangs, some of the exposed pit walls are covered with thin (<1 mm thick) coatings of white, orange,

A

B

Figure 4. Photos of the South Pit area. A, Flooded north end of the south pit and haulageway, looking north. B, Gypsum encrustation on sheltered parts of pit walls. Note pen for scale.

blue, and green minerals that form vertical color bands. X-ray powder diffraction identified these color bands as mixtures of jarosite, feldspar, chlorite, mica, and quartz. Locally, thick (up to 1 cm) encrustations of coarse, yellowish crystals of gypsum coat pit walls over vertical distances of 1 to 2 m (fig. 4B). Occurrence of the sulfate minerals jarosite and gypsum indicates that sulfide minerals in the bedrock are actively oxidizing on pit wall surfaces. Loose pieces of weathered ore on the pit floor are coated with rusty- colored iron oxyhydroxide minerals on exposed surfaces ; "bathtub rings" of white salts form a border on the rocks at the soil/rock interface, marking the area where sulfate salts precipitate during wet/dry cycles. A paste pH value of 2.9 obtained on a composite soil sample from the dry floor of the south end of the pit indicates that the soils contain readily available acidity from prior acid generation. A composite wall rock sample of relatively fresh garnet amphibolite schist (98JH-SP-R1) from the north side of the haulageway and weathered mica schist (98JH-SP-R4) were collected to determine the trace metal, sulfur, and carbonate content of pit bedrock (table 4). No extensive piles of mine waste are associated with this pit. Intermittent drainage flows along the old haulageway. Twenty two percent of the sediment that collects in the intermittent stream channels in the ore haulageway is fine-grained (<80 mesh). A drainage divide separates the south and north pit areas; therefore, surface flow from the south pit area does not enter Copperas Brook.

North pit area (Tailings pile 3)

Tailings pile 3 (TP3) is a 6-acre pile of mine waste from the pre-1942 phase of mining operations (fig. 3). The pile extends from the open cut of the north pit, across a dirt road, to an area just above the top of tailings pile 2. Although we use the term "tailings pile", the nature of the surface material in this area is quite different from the fine-grained processed tailings of piles 1 and 2. The term "mine dump" or mine spoil is more appropriate than "tailings" because we are unsure of the degree to which metals were removed from the waste material during processing. This pile is composed of waste from the earliest mining, when ore recovery was not as refined. Thus, one would expect more metals to be present in the soil cover here than in the tailings from the 1950s-era flotation plant (TP1, TP2). TP3 is essentially devoid of vegetation and the north-facing slopes of the waste piles have deep erosion gullies (fig. 5). The pile is extremely heterogeneous in color and texture, and surface runoff from this pile contributes to the headwaters of Copperas Brook that emanate from the base of the pile. We arbitrarily divided tailings pile 3 into 6 subareas (A-F) on the basis of surface color and collected composite samples of each subarea for mineralogy, paste pH measurements (table 2), and chemistry (table 6). Slag and timber are present in the central part of the area (piles B and E). Color variations from pile to pile reflect the dominant soil minerals. Hematite is especially abundant in the central part of TP3 (subarea TP3-B and TP3-D) on both sides of the road, where slag is noted and pieces of lumber are strewn about. This pattern suggests that the central part of TP3 was the site of historic ore processing, possibly one of the early smelter operations. Hematite most likely formed from oxidation and burning, rather than through any natural weathering process that affected the mine waste. Paste pH values for the surface composites over each subarea are all extremely acidic (2.1 to 3.2). Piles that are yellowish in color are jarosite-rich and tend to have slightly lower paste pH values than the redder, hematite-rich piles (table 2). Jarosite is an iron hydroxy sulfate mineral that is typically straw yellow, forming from oxidized acid mine waters that contain dissolved ferrous iron, sulfate, and potassium. A shovel auger was used to examine the upper 150 cm of material at the center of each pile (GPS locations noted in Appendix A). Changes in color or texture were logged and selected intervals were sampled for paste pH measurement and mineralogy (table 4). The only hole that penetrated unoxidized black tailings was TP3-F, where tailings composed of chalcopyrite, sphalerite, covellite, quartz, mica, and siderotil (but no pyrrhotite) were encountered at a depth of 105 cm below the surface. In general, the paste pH values for the composite surface soils are lower than, or the same as, the material encountered at depth. None of the material in the top 150 cm of any part of TP3 approached a near-neutral pH. Quartz (inert) and white mica (very slow weathering) are ubiquitous and provide no practical neutralization potential.

The most striking feature of the pile is the presence of thick coatings of white efflorescent salts on loose pieces of oxidized ore on dry days that give pile surface the appearance of being covered with "snowballs" (fig. 5C); these salts essentially disappear during storm events. XRD data show that these

A

B

C

D

Figure 5. Photos of the north pit area (tailings pile 3). A, Center of subarea TP3-A. The yellow color is due to jarosite. B. Center of subarea TP3-B. Red color due to hematite; red and black slag occur in this pile. C, "Snowballs" of weathered sulfide ore coated with white efflorescent salt minerals littering the surface of subarea TP3-F on a dry day. D , Close-up view of blue efflorescent salt crust on TP3 mine dump soil.

Table 2. Tailings characteristics.

[Measurements are for 30-increment surface soil samples (<2 mm fraction) composited over the pile described; see fig. 3 for locations of piles]

Sample	Description	Munsell color	Mineralogy	Paste pH
	North pit area (tailings pile 3)			
TP3-A	Northernmost pile east of the road characterized by a yellow-brown soil color.	yellow 2.5Y 7/6	jarosite + quartz	2.4
TP3-B	Central pile east of road; appears to be site of historic processing. Surface soil is very heterogeneous, local blue-green iridescent copper coatings on slag. Red to black soil on pile surface.	dark reddish brown 5 YR 3/2	hematite + quartz	2.6
TP3-C	Southernmost pile east of the road. Surface runoff from this pile directly affects water sample site LIZM13. Red to orange soil with white salts.	reddish brown 2.5Y 4/4	hematite + quartz + mica + feldspar	2.6
TP3-D	Southernmost pile west of the road. Yellow-brown soil similar to TP3-A.	brownish yellow 10YR 6/8	jarosite + quartz	2.1
TP3-E	Central pile west of road. Red soil with some black material, but lacks the slag noted on TP3-B.	red 2.5YR 4/6	hematite + quartz + mica	3.2
TP3-F	Northernmost pile west of the road and adjacent to the north end of the north pit. Orange soil littered with salt-coated ("snowballs") loose pieces of weathered ore.	yellowish brown 10YR 5/6	mica + quartz + jarosite + goethite	2.2
	Tailings pile 2			
TP2-1	Partially vegetated, flat top of tailings pile 2.	strong brown 7.5YR 5/8	jarosite + quartz + mica + plagioclase feldspar	5.5
TP2-2	Bare, eroded north slope of tailings pile 2.	strong brown 7.5YR 5/8	jarosite + goethite + quartz + plagioclase feldspar + mica	3.2
	Tailings pile 1			
TP1-1	Bare area of flat top of tailings pile 1 adjacent to the pond.	strong brown 7.5YR 5/8	quartz + mica + goethite + jarosite	3
TP1-2	Vegetated area on flat top of tailings pile 1.	strong brown 7.5YR 5/8	quartz + mica + goethite + jarosite	5.9
TP1-3	Steep, bare eroded north slope of tailings pile 1 with seeps along the base.	strong brown 7.5YR 5/8	quartz + mica + goethite + jarosite	2.8

very soluble salts are a mixture of melanterite and rozenite (table 1). SEM studies confirm that these salts contain iron and sulfur. Melanterite is typically blue-green and rozenite is white. Melanterite dehydrates to rozenite and fine-grained melanterite can appear white. No blue-green salts were noted in these snowball coatings. Locally, blue copper bearing efflorescent salts (fig. 5D) of the siderotil group coat surface soils. The relatively insoluble mineral gypsum is ubiquitous on surface soils as thin crusts and clusters of crystals that protrude from the soil surface like small organ pipes. Unlike melanterite and rozenite, the sulfate minerals gypsum and jarosite persist in wet weather.

Tailings pile 2

Tailings pile 2 (TP2) is a relatively small pile (5 acres) of waste from the 20th century mine operations. TP2 rises above the flat top of tailings pile 1 (TP1) and is bisected on its east side by the headwaters of Copperas Brook (fig. 3). The steep north face of the pile is bare and deeply eroded (fig. 6A). Soils developed on the tailings are oxidized; none of the weathered ores described above for TP3 are noted on TP2. Some vegetation is present on the flat top of the pile. Holes were dug with a shovel at two locations on top of the pile where black, unoxidized sulfide mineral tailings were encountered at depths of 15 to 60 cm below the surface. Tailings are overlain by yellow-green, clayey layers and local 2.5 cm thick hardpan layers. The surface layer (upper 13 to 30 cm) of the pile is reddish-brown topsoil with abundant plant roots. Near the base of the pile (fig. 6B), black tailings are overlain by nearly monomineralic layers of gray to white mica, yellow jarosite, and hardpan crusts that range from 0.5 cm to several cm thick. The hardpans may have formed in situ within the pile, or they may represent paleosurfaces that formed as surface layers exposed to oxidation and weathering as tailings were deposited over time. Hardpan ledges and crusts are actively forming on the present tailings surfaces wherever water is flowing. White crystals of gypsum coat the surface of TP2. White slime precipitates very locally along the Copperas Brook headwaters (fig. 6A) that bisect TP2, where ground water seeps in from the undisturbed area to the east of the pile. In acid mine drainage settings, white precipitates of amorphous or very poorly crystalline aluminum minerals commonly form where near-neutral waters mix with acidic waters (Alpers and others, 1994). White slime precipitates collected at the topographic break in TP2 is amorphous; SEM spectra show that it contains aluminum>sulfur>minor silicon. Some lime (or limestone) and topsoil were apparently added to the top of the pile after the mine closed. The effect of the treatment and(or) vegetation is apparent from the higher paste pH values obtained for the vegetated top of the pile (5.5), compared to the bare eroded slope (3.1).

Tailings pile 1

Tailings pile 1 (TP1) is a 30-acre accumulation of very fine-grained tailings (various amounts of pyrrhotite, jarosite, melanterite, goethite, gypsum, mica, feldspar, quartz, hornblende, talc, chlorite) from the most recent (1958) phase of the mining operations. The pile rises 30 m above the natural streambed of Copperas Brook (fig. 7A). The top of the pile is relatively flat and partly vegetated. A decant tower at the edge of a tailings pond on the eastern side of the pile diverts some water to a discharge point at the northeast corner of the pile (fig. 3). The top and north slope surfaces are oxidized. Adjacent to the south end of the pond, water-saturated, unoxidized black tailings are present about 25 cm below the surface and unoxidized tailings are exposed, or under a shallow cover, along the sides of the pile. Adjacent to piezometer MP3 at the north edge of the pond, an auger sample (fig. 7B) to a depth of 91 cm (36") shows relatively dry oxidized tailings (orange) overlying 2.5 cm (1") thick layers of black tailings, green clays, wet fine-grained black tailings, and drier coarse black tailings. Vertical variations in texture and wetness indicate that different layers within the tailings have different porosities. The entire tailings pile behaves as an artificial aquifer with a complex internal hydrology and chemistry. Hardpans are actively forming along the stream across the tailings surface that drains into the pond. Blue salt crusts were observed in a small area near the pond (fig. 7A). Sediment at the bottom of the pond is a very fine-grained orange ooze that contains pyrrhotite, gypsum, and jarosite. Unoxidized tailings were encountered at about 15 cm (6") below the top of the sediment column at the southern end of the pond in August, 1998. The level of the pond varies seasonally. Repeated cycles of evaporation, salt

A

B

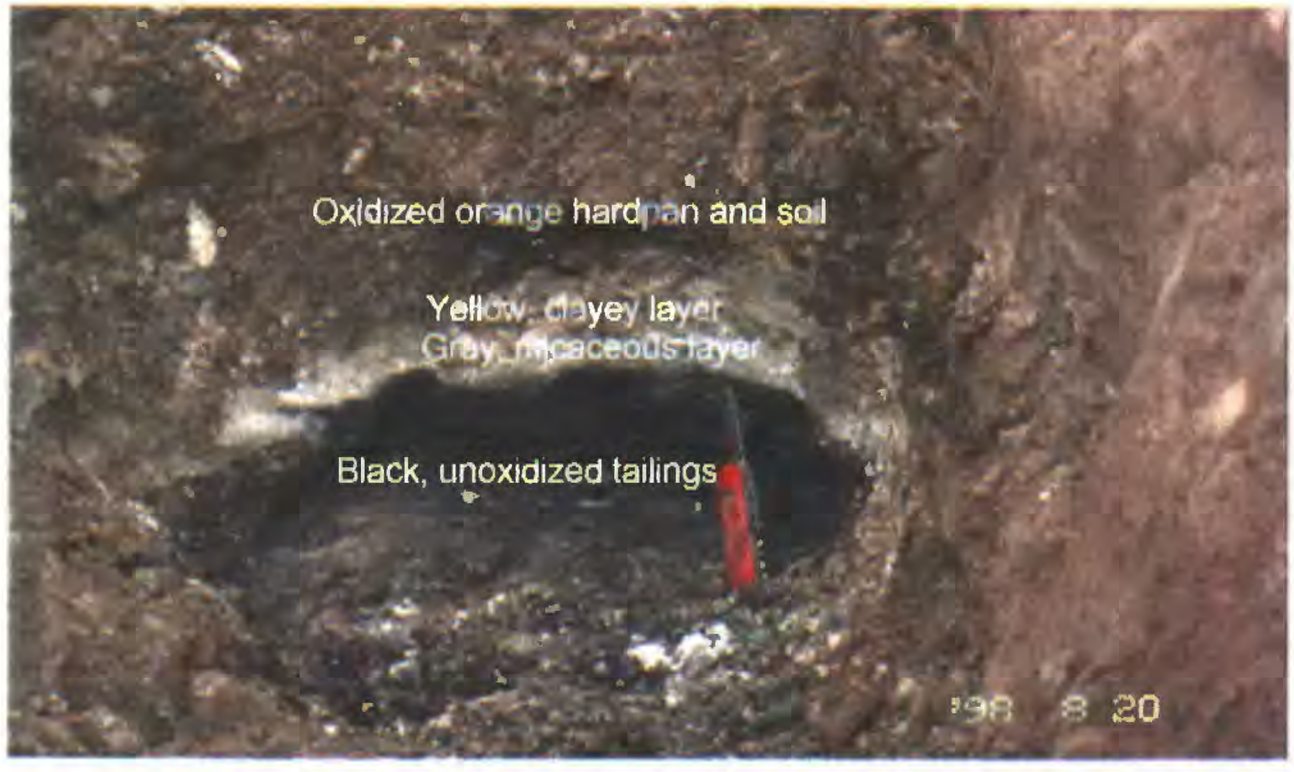

Figure 6. Photos of tailings pile 2. A, Bare, eroded north slope of TP2. Surface runoff from TP3 forms the headwaters of Copperas Brook that bisect TP2 and flow out onto the flat top of TP1 and into the pond. B, Layering in tailings at base of TP2 exposed by scraping off surface material.

formation, and subsequent salt dissolution on the tailings surface, near the margins of the pond, contribute to the acidity of the pond water (pH 2.6).

Seeps at the base of tailings pile 1

Near-neutral (pH 6.1 to 6.9) ground-water seeps occur along the base of the northern slope of TP1 (Seal and others, 1999). Waters from these seeps and water from the decant discharge pipe at the northeastern corner of the pile coalesce to form Copperas Brook (fig. 2). Bright red and orange mucks mark the seeps (fig. 8A). Dissolved iron in the seep waters oxidizes from ferrous iron (Fe^{2+}) to ferric iron (Fe^{3+}) as it contacts air, precipitating out of solution and forming ochre deposits of iron hydroxysulfate and iron oxyhydroxide minerals. Abundant organic material (leaves, small twigs) is incorporated in these mucks and becomes preserved in hardpan crusts as they build up (fig. 8B). Other studies (Ferris and others, 1989; Yapp and Poths, 1986) have noted that it is common to find concentrations of organic matter in natural goethite and ferrihydrite precipitates suggesting that bacterial cells may serve as nucleation sites for mineral growth. XRD and SEM confirm that the clayey yellow mud found near the seeps is essentially pure jarosite (sample LIZM6). In the wettest parts of the seeps, a yellow slime of poorly crystalline schwertmannite (table 1) is associated with goethite. A small area of wetlands with cattails and phragmites occurs at the lower end of the seeps.

Copperas Brook

A number of stream branches coalesce at water sample site LIZM18, below TP1 and the seeps, to form the main channel of Copperas Brook that flows into the West Branch of the Ompompanoosuc River (fig. 3). Ochre hardpans are associated with all of these side streams as well as with the main stream at its confluence with the river. As ochre minerals precipitate, acidity is produced and the associated surface waters become acidic as a result of oxidation and hydrolysis of dissolved iron. Just above the confluence with the river, the surface waters of Copperas Brook have a pH of about 2.7 (Seal and others, 1999). Rocks along the river are coated with red to orange precipitates for over a kilometer downstream.

Air shaft along the West Branch of the Ompompanoosuc River

About 1 kilometer upstream from Copperas Brook, an air shaft that provided ventilation for the underground workings of the mine discharges ground water onto the south bank of the West Branch of the Ompompanoosuc River and into a side stream. The discharge pipe is covered with an iron grate that is coated with white aluminum minerals (fig. 8C) that have precipitated out of the water. These white minerals coat the bottom of the stream and rocks that form a small waterfall. The whole area for about 7 meters around the pipe is an ochre muck that incorporates a lot of organic material. The pH of the water coming out of the pipe is 5.0. Aluminous precipitates ("white slimes") are typically found where acidic (pH<5) waters mix with near-neutral waters that elevate the pH values to around 5, the pH value where aqueous aluminum hydrolyzes to form $Al(OH)^{2+}$. The white material coating the rocks below the grate was scraped off with a knife, dried in air in the lab, and examined by XRD and SEM. Due to its amorphous nature, the material gave a very poor XRD pattern with broad, indistinct peaks. The peaks are consistent with, but are not unique to, any of a number of aluminum hydroxide and aluminum hydroxysulfate minerals. SEM spectra show that aluminum is the dominant component, with minor, subequal amounts of sulfur, iron, and silicon.

A

B

C

Figure 7. TP1. A, Deeply eroded, bare north slope of TP1. Surface runoff from this slope contributes to degradation of water quality of Copperas Brook. B, Soil auger profile of tailings from the top of TP1 adjacent to piezometer site MP3; auger is 91 cm (36") long. C, Close-up of bluish-white salts that form on damp tailings adjacent to the pond.

A

B

C

Figure 8. Photos of actively precipitating secondary minerals. A, Iron-rich ochre protohardpan forming at near-neutral seeps. B, Close-up of "fossilized" leaves incorporated in hardpan. C, White, amorphous aluminum precipitates at the air vent.

RESULTS

Geochemical data are presented in a series of tables, grouped by sample type (tables 3-8, 10). Major rock-forming elements or oxides are reported in weight percent (%) at the beginning of each table, followed by (1) minor and trace element data reported in parts per million (ppm); (2) water, carbon species, and total sulfur; and (3) selected metal ratios. A number of elements were determined by more than one method, such as iron which is reported by both ICP-MS and by ICP-AES. See Appendix B for detection limits and references for each method. Some concentrations are reported as qualified values, indicating that the concentration measured was greater than (>) or less than (<) the detection limit of the analytical technique. Within tables, samples are arranged from south (proximal to the mine workings) to north (distal to the mine workings). Concentrations of total base metals (Cu+Co+Cd+Ni+Pb+Zn) are computed as well as selected metal ratios for comparison of variations among sample types. The variation of metal abundances within sample types and among different sample media is illustrated in a series of bar graphs (figs. 9 and 10). Note that most metal concentrations are plotted on a logarthimic scale.

Minerals identified at the Elizabeth mine are listed, together with their ideal chemical formulas, by subgroup (ore, gangue, secondary minerals) in table 1. Minerals are listed in alphabetical order within each subgroup. Gangue minerals are listed in terms of their ease of weathering; for secondary minerals, typical color and relative solubility are noted. Examples of XRD and SEM data are included below. EMPA data for sulfide minerals in ore and tailings are given in table 9.

Ore

Geochemical data for representative massive sulfide ore samples from the historic underground workings were provided by J. F. Slack (table 3). Ore samples are highly variable in their sulfide mineral content (table 3A); however, pyrrhotite is the dominant ore mineral. Unpublished quantitative geochemical data are listed for three samples (table 3B). Semiquantitative (SQS) and atomic absorption data presented by Slack and others (1986) for selected elements for six samples (table 3C) are less precise, but are still useful for demonstrating the chemical signature of the material that was mined at Elizabeth. These data show that (1) the ores were variable in composition but extremely enriched in base metals (4 to 25 wt. %); (2) copper is the dominant base metal followed by zinc; lead comprises less than 1 % of total base metals; (3) the ores are uniformly iron-rich; (4) the ore itself contains very little aluminum, so any aluminum that enters the aquatic ecosystem results from weathering of gangue and host rock minerals; (5) contents of copper and zinc, and to a lesser extent arsenic and cadmium, are one to two orders of magnitude higher in ore than in any of the other types of samples collected on the site (fig. 9); (6) mercury concentrations are about 2 ppm or less in all solid sample media; and (7) selenium is present in concentrations of up to 100 ppm in pyrrhotite-rich ore.

Host rock

Silicate-rich rock exposed in the walls of the south pit (table 4) contains >0.7 wt. % base metals, significant concentrations of sulfur (>0.5 wt. %), and in places, a minor amount of carbonate carbon (<2 wt. %). Sulfide minerals in the wallrock weather to produce the sulfate that forms gypsum crusts and other salt coatings on pit walls. Wallrock is a major source of aluminum (~15 weight per cent Al_2O_3) and manganese. Most metal concentrations in wallrock are one or two orders of magnitude less than in ore (fig. 9). Relative to ore, cobalt is depleted and nickel and chromium are enriched in wallrock.

Slag

Slag (table 5) is a product of on-site smelting during the early years of the mine operation. Both red and black slag are locally abundant in tailings pile 3B. Some slag surfaces are iridescent due to the oxidation of copper to produce "peacock ore". Although slag is not volumetrically significant at the mine, it does represent a significant source of copper and zinc. The slag contains about 1 wt.% sulfur.

Table 3. Ore samples.

A. Sample descriptions.
[Data from Slack and others, 1986; Unpublished data, 1999, provided by J.F. Slack, USGS]

Sample Number	Sample Description
EZ-39	Harvard University collection sample from underground. Massive, coarse grained pyrrhotite (50%) and chalcopyrite (40%) plus minor quartz inclusions and sphalerite (5%).
EZ-45	Very fine-grained massive pyrrhotite ore with chalcopyrite.
EZ-56	Harvard University collection sample from underground consisting of massive coarse, granular pyrite (60%), quartz (30%), and chalcopyrite (10%).
EZ-102	Harvard University collection sample from underground consisting of massive pyrrhotite and chalcopyrite with quartz inclusions.
EZ-1023	Harvard University collection sample of sphalerite-rich calcite marble with very minor pyrite.
EZ-42A	Harvard University collection sample of pyrrhotite and chalcopyrite ore with minor sphalerite and quartz.
EZ-1031	Harvard University collection sample of massive chalcopyrite ore with very minor pyrrhotite and sphalerite.

B. Major and minor element data.
[See Appendix B for explanation of methods; n.r., not reported]

Element	Sample number / Method	Units	EZ-39	EZ-45	EZ-56
		Major elements			
Al	ICP-AES	%	0.03	0.31	0.225
Ca	ICP-AES	%	0.719	1.271	0.725
Fe	ICP-AES	%	30.6	28.2	30.3
K	ICP-AES	%	<0.01	0.06	0.07
Mg	ICP-AES	%	0.01	0.05	0.06
Na	ICP-AES	%	<0.005	0.014	<0.005
P	ICP-AES	%	0.12	0.165	0.04
Ti	ICP-AES	%	<0.005	0.018	0.006
		Minor elements			
Ag	ICP-AES	ppm	63	78	14
As	HYD	ppm	53.1	81.1	106
As	ICP-AES	ppm	19	62	89
Au	GFAA	ppm	0.292	ins	0.76
Au	ICP-AES	ppm	<8	<8	<8
Ba	ICP-AES	ppm	<1	8	6
Be	ICP-AES	ppm	<1	<1	<1
Bi	ICP-AES	ppm	84	<50	51
Cd	ICP-AES	ppm	122	98	100
Ce	ICP-AES	ppm	<5	<5	<5
Co	ICP-AES	ppm	403	376	770
Cr	ICP-AES	ppm	40	30	44
Cu	ICP-AES	ppm	136,840	168,790	29,880
Eu	ICP-AES	ppm	<2	<2	<2
Ga	ICP-AES	ppm	<4	<4	<4
Ho	ICP-AES	ppm	<4	<4	<4
Hg	CVAC	ppm	2.29	0.77	1.44
La	ICP-AES	ppm	<2	<2	<2
Li	ICP-AES	ppm	<2	3	<2
Mn	ICP-AES	ppm	804	390	357
Mo	ICP-AES	ppm	41	32	52
Nb	ICP-AES	ppm	25	23	25
Nd	ICP-AES	ppm	<9	<9	<9
Ni	ICP-AES	ppm	43	30	<3
Pb	ICP-AES	ppm	205	232	201
Sb	HYD	ppm	1.1	1	<0.6
Sc	ICP-AES	ppm	3	4	<2
Se	HYD	ppm	30.5	31.2	52.3
Sn	ICP-AES	ppm	<50	<50	<50
Sr	ICP-AES	ppm	7	7	6
Ta	ICP-AES	ppm	<40	<40	<40
Te	GFAA	ppm	0.8	0.7	0.1
Th	ICP-AES	ppm	<6	<6	<6
Tl	GFAA	ppm	<0.1	0.3	0.4
U	ICP-AES	ppm	<100	<100	<100
V	ICP-AES	ppm	10	19	19
Y	ICP-AES	ppm	<2	<2	<2
Yb	ICP-AES	ppm	<1	<1	<1
Zn	ICP-AES	ppm	11,170	9,720	11,350
		Selected metal ratios			
Total base metals (BM)		ppm	148,783	179,246	42,301
Cu/BM			0.92	0.94	0.71
Zn/BM			0.08	0.05	0.27
Pb/BM			0.001	0.001	0.005
Cu/Zn			12.25	17.37	2.63

C. Minor element data.

[AA, atomic absorption spectrophotometry; SQS, semi-quantitative spectroscopy]

Sample Number			EZ-39	EZ-56	EZ-102	EZ-1023	EZ-42A	EZ-1031
Element	Method	Units						
Ag	SQS	ppm	150	46	150	0.38	81	64
As	SQS	ppm	<150	<150	<150	<150	200	<100
Au	AA	ppm	0.24	0.85	0.11	0.59	0.25	0.51
B	SQS	ppm	<6.8	<6.8	<6.8	<6.8	<6.8	<6.8
Ba	SQS	ppm	9.5	12	16	15	<1.5	6
Bi	SQS	ppm	28	<10	24	<10	<10	33
Cd	SQS	ppm	190	150	110	1300	170	260
Co	SQS	ppm	190	550	180	120	190	150
Cu	SQS	%	3.00	1.3	2.5	0.09	24	23
Hg	AA	ppm	1.7	1.4	1.4	0.36	0.4	0.12
Mn	SQS	ppm	1,300	520	440	8,600	710	770
Mo	SQS	ppm	15	71	45	170	n.r.	n.r.
Ni	SQS	ppm	37	11	43	4.4	58	44
Pb	SQS	ppm	390	290	240	67	33	49
Sb	SQS	ppm	<2	<32	<32	<32	<68	<68
Se	AA	ppm	22	15	34	10	15	50
Sn	SQS	ppm	n.r.	n.r.	<1.5	<1.5	n.r.	n.r.
Te	AA	ppm	2.2	1.4	0.8	0.09	1.2	2.8
Th	SQS	ppm	<0.8	<1.2	<1.6	<33.5	<3.5	<2.0
U	SQS	ppm	0.47	1.22	2.05	<0.46	0.91	1.13
V	SQS	ppm	5.7	9	33	5	6.1	11
W	SQS	ppm	<10	<10	<10	<10	<15	<15
Zn	SQS	%	2.6	2.6	1.1	12	2	2
Zr	SQS	ppm	10	<3.2	<10	39	<4.6	11
				Selected metal ratios				
Total base metals (BM)		ppm	56,807	40,001	36,573	122,391	260,451	250,503
Cu/BM			0.53	0.33	0.68	0.01	0.92	0.92
Zn/BM			0.46	0.65	0.30	0.98	0.08	0.08
Pb/BM			0.01	0.01	0.01	0.00	0.00	0.00
Cu/Zn			1.15	0.50	2.27	0.01	12.00	11.50

Table 4. Geochemical data for host rocks exposed in the south pit.
[See Appendix B for explanation of methods; LOI, loss on ignition; $FeTO_3$, total iron reported as Fe_2O_3; $C=CO_2$, carbonate carbon; CHM, FeO determined by titration; BM, total base metal concentration in ppm]

Sample No.			98JH-SP-R1	98JH-SP-R4				98JH-SP-R1	98JH-SP-R4
Major element oxides					Minor elements				
Element	Method	Units			Element	Method	Units		
SiO_2	WD-XRF	%	42.9	48.4	Nb	ICP-MS	ppm	2.1	0.89
Al_2O_3	WD-XRF	%	15.6	15.2	Ni	ICP-MS	ppm	120	53
$FeTO_3$	WD-XRF	%	8.01	8.03	Pb	ICP-MS	ppm	18	17
MgO	WD-XRF	%	5.54	10.1	Rb	ICP-MS	ppm	5.5	72
CaO	WD-XRF	%	15.8	2.36	Sb	ICP-MS	ppm	0.1	<0.1
Na_2O	WD-XRF	%	2.23	4.5	Sc	ICP-MS	ppm	26	21
K_2O	WD-XRF	%	0.18	2.1	Se	ICP-MS	ppm	2	2
TiO_2	WD-XRF	%	0.81	0.77	Sr	ICP-MS	ppm	220	33
P_2O_5	WD-XRF	%	0.09	0.08	Te	ICP-MS	ppm	< 0.1	< 0.1
MnO	WD-XRF	%	0.15	0.14	Th	ICP-MS	ppm	0.07	< 0.06
LOI	WD-XRF	%	6.77	4.92	Tl	ICP-MS	ppm	<0.1	<0.1
Total			98	97	U	ICP-MS	ppm	0.1	0.08
Major elements					V	ICP-MS	ppm	150	120
Element	Method	Units			Y	ICP-MS	ppm	21	4.1
Al	ICP-MS	%	8.7	8.1	Zn	ICP-MS	ppm	240	1,100
Ca	ICP-MS	%	11	1.6	Water, carbon, ferrous iron, and total sulfur				
Fe	ICP-MS	%	5.6	5.8					
K	ICP-MS	%	0.13	1.6	Total H2O	LECO	%	1.2	2.6
Mg	ICP-MS	%	3.9	7.1	H2O-	LECO	%	0.2	0.5
Na	ICP-MS	%	1.6	3.1	H2O+	LECO	%	1	2.1
Minor elements									
Ag	ICP-MS	ppm	0.16	0.32	FeO	CHM	%	6	5.5
As	ICP-MS	ppm	2	3					
Ba	ICP-MS	ppm	24	52	Total C	LECO	%	1.93	0.34
Be	ICP-MS	ppm	0.1	0.2	$C = CO_2$	LECO	%	1.89	0.27
Bi	ICP-MS	ppm	0.2	0.57	CO_2	LECO	%	6.92	0.99
Cd	ICP-MS	ppm	1.2	2.7	$C_{organic}$	LECO	%	0.04	0.07
Ce	ICP-MS	ppm	3.7	3					
Co	ICP-MS	ppm	47	34	Total S	LECO	%	0.51	2.26
Cr	ICP-MS	ppm	270	240					
Cs	ICP-MS	ppm	1.7	25	Selected metal ratios and calculated parameters				
Cu	ICP-MS	ppm	360	2,900	BM		ppm	786	4,107
Ga	ICP-MS	ppm	13	10					
Ge	ICP-MS	ppm	1.9	0.5	Cu/BM			0.46	0.71
Hg	CVAC	ppm	<0.02	<0.02	Zn/BM			0.30	0.27
In	ICP-MS	ppm	< 0.1	< 0.1	Pb/BM			0.02	0.00
La	ICP-MS	ppm	1.2	0.9					
Li	ICP-MS	ppm	38	80	Cu/Zn			1.5	2.6
Mn	ICP-MS	ppm	1,100	990					
Mo	ICP-MS	ppm	0.4	4.2	Fe/Al			0.64	0.72

Table 5. Geochemical data for slag in tailings pile 3 (north pit area).
[See Appendix B for explanation of methods; BM, total base metal concentration in ppm; sample 98JHNP-slag is a black slag, sample 98JHNP-B-RS is a red slag or clinker]

Sample No.			98JHNPB-slag	98JHNP-B-RS				98JHNPB-slag	98JHNP-B-RS
Major elements					Minor elements				
Element	Method	Units			Element	Method	Units		
Al	ICP-AES	%	2.21	3.59	Mn	ICP-AES	ppm	206	264
Al	ICP-MS	%	2.2	3.6	Mn	ICP-MS	ppm	140	210
Ca	ICP-AES	%	0.09	0.3	Nb	ICP-AES	ppm	<10	<10
Ca	ICP-MS	%	0.1	0.3	Ni	ICP-MS	ppm	46	22
Fe	ICP-AES	%	>30	>30	Pb	ICP-MS	ppm	13	77
Fe	ICP-MS	%	46	35	Sb	ICP-MS	ppm	<0.1	<0.1
K	ICP-AES	%	0.73	0.91	Sr	ICP-AES	ppm	<10	17
K	ICP-MS	%	0.72	0.95	Te	HYD	ppm	0.7	1
Mg	ICP-AES	%	0.37	0.64	Tl	HYD	ppm	0.2	0.9
Mg	ICP-MS	%	0.39	0.68	Tl	ICP-MS	ppm	0.3	0.9
Na	ICP-AES	%	0.2	0.69	V	ICP-MS	ppm	47	91
Na	ICP-MS	%	0.21	0.74	Y	ICP-AES	ppm	<10	<20
P	ICP-AES	%	<0.01	<0.01	Zn	ICP-MS	ppm	1,200	1,800
Si	ICP-AES	%	5.32	12.9	Zr	ICP-AES	ppm	22	47
Ti	ICP-AES	%	0.13	0.25					
Minor elements					Total S	LECO	%	1.11	1.15
Ag	ICP-MS	ppm	1	4					
As	HYD	ppm	4.5	7	Selected metal ratios and calculated parameters				
As	ICP-MS	ppm	5	5.9	BM		ppm	4,110	6,063
Au	GFAA	ppm	0.01	0.009					
Ba	ICP-AES	ppm	26	25	Cu/BM			0.63	0.66
Ba	ICP-MS	ppm	26	26	Zn/BM			0.29	0.30
Be	ICP-MS	ppm	<0.1	0.2	Pb/BM			0.00	0.01
Cd	ICP-MS	ppm	1.2	3.9					
Co	ICP-MS	ppm	250	160	Cu/Zn			2.17	2.22
Cr	ICP-AES	ppm	91	129					
Cu	ICP-MS	ppm	2,600	4,000	Fe/Al			21	10
Hg	CVAC	ppm	<0.02	0.06					

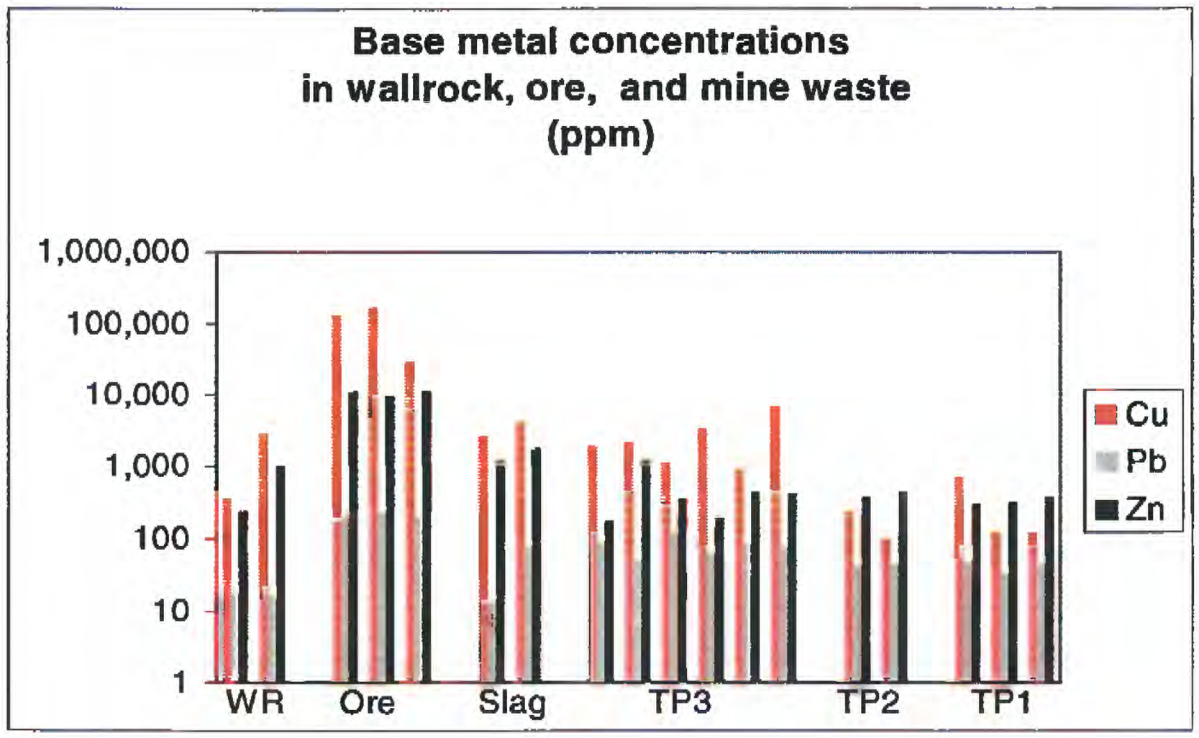

A

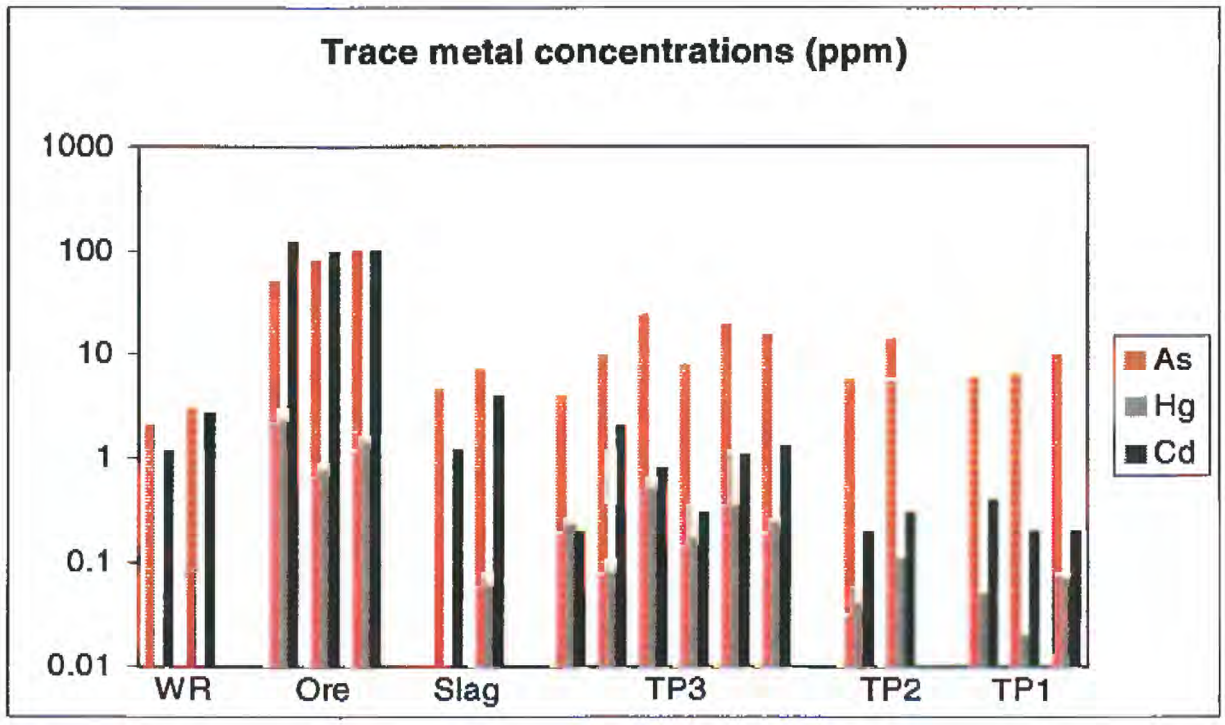

B

Figure 9. Bar graphs showing the variation in selected metal concentrations within, and among, different types of solid materials sampled at the Elizabeth mine. Note that the y-axis is a logarithmic scale for charts A, B, and C, and that Hg was not determined for all samples. WR, wallrock in the south pit; TP, composite tailings surface soils from TP1, TP2, and TP3.

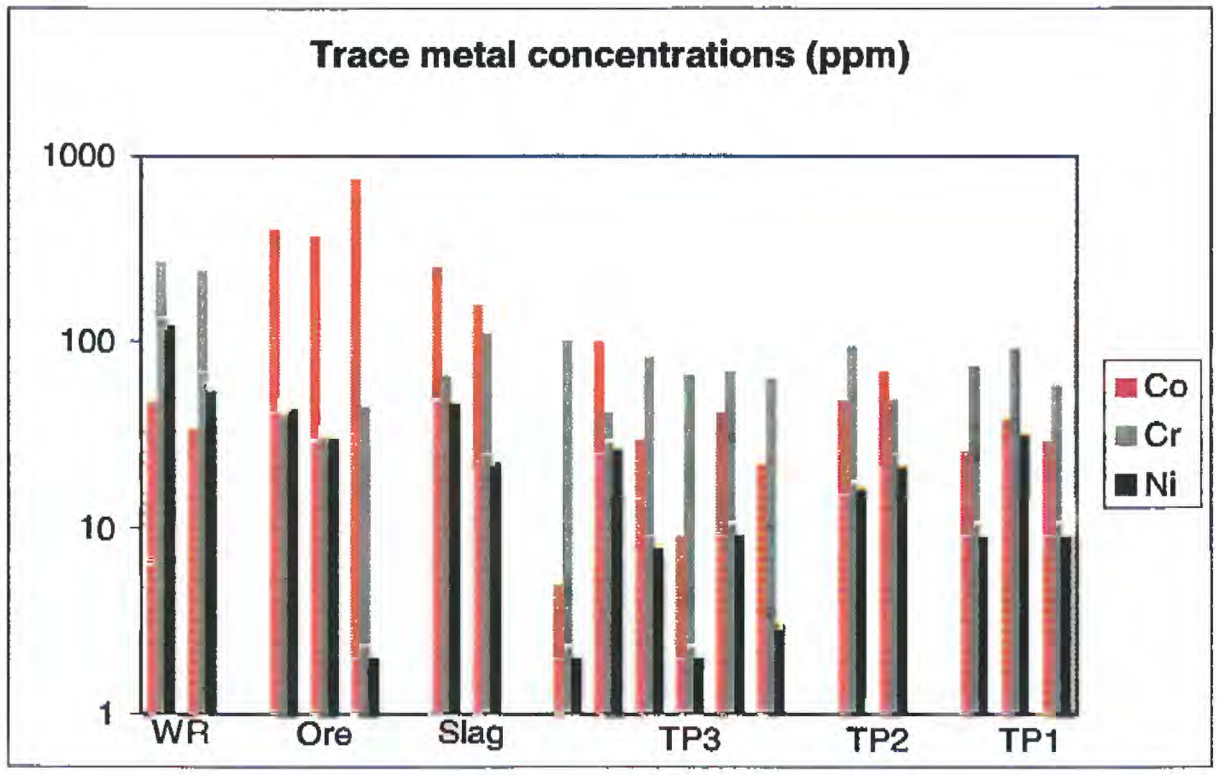

C

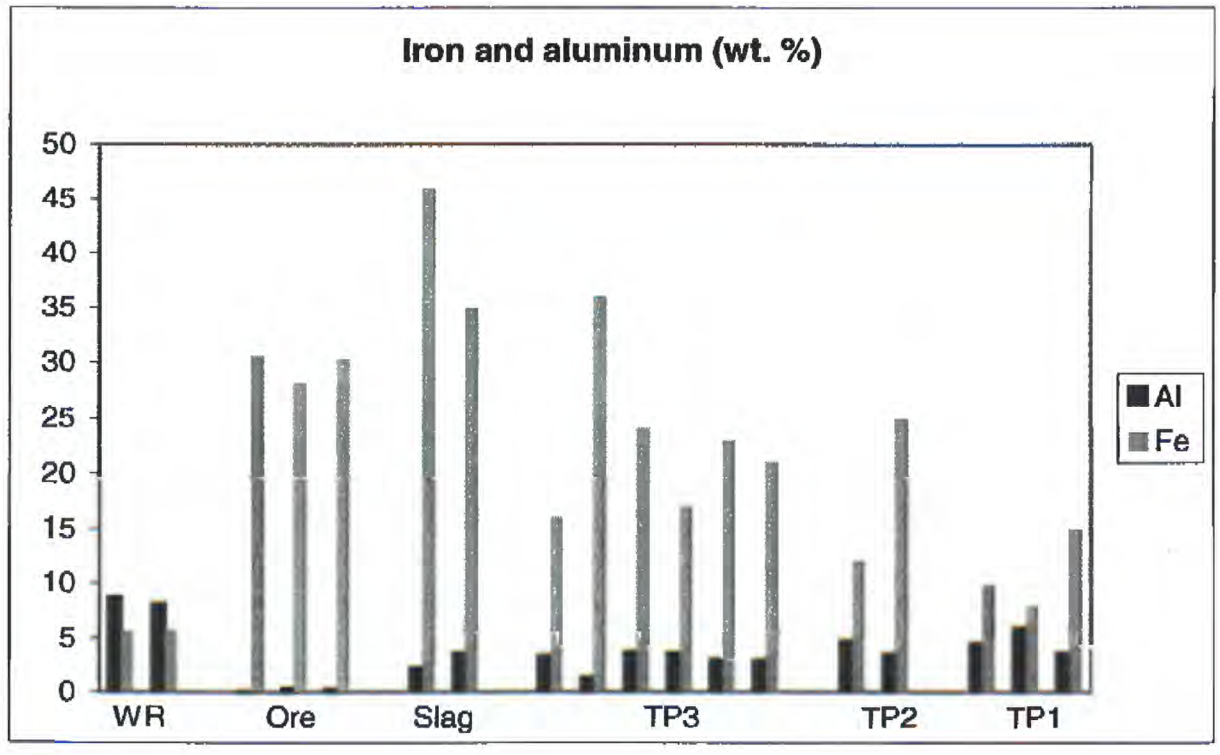

D

Figure 9. Continued.

Tailings

Composite surface samples

Multi-element geochemical data for composite surface-soil tailings (table 6) show systematic chemical differences between the older (TP3) and younger piles (TP1, TP2). Composite sample characteristics are described in table 2, and GPS locations for the approximate center of each subarea sampled are listed in Appendix A. All of the surface soils developed on the older tailings (TP3) are iron-rich relative to TP2 and TP1, which tend to have more aluminum. Contents of total base metals are high (>1,000 ppm) in all parts of TP3, compared with the variable, but lower base metal concentrations at the surfaces of TP1 and TP2 (<1,000 ppm). Copper is the dominant base metal in TP3, but zinc dominates the base metal suite (on a weight basis) for most of the areas of TP1 and TP2. Within TP3, the subareas characterized by hematite (TP3-B, C, and E) tend to have more iron and less sulfur than the subareas where jarosite is more abundant. TP3-F, the area littered with salt-encrusted weathered ore near the north pit, has the highest concentrations of base metals in the soil fraction of surface material of all areas sampled (>7,000 ppm or >0.7 wt. %). Total carbon concentrations are uniformly low (<0.5 wt. %) and most of the carbon is organic. The highest concentration of carbonate carbon and of calcium was obtained for sample TP1-2 from the vegetated, western part of the top of TP1. This may reflect remnants of limestone or lime added in the past to promote growth of a vegetative cover on the tailings.

Profiles through upper tailings surfaces

Vertical profiles through the near-surface part of the piles were obtained by digging down to black, unoxidized tailings. These profiles are by no means representative of the total variation within the piles. A detailed grid drilling program though the entire thickness of the piles would be necessary to determine the lateral and vertical extent of different layers. These data (table 7), along with the surface composite data described above, provide an indication of the geochemical signature of the materials on the site. One profile was collected about a third of the way (about 10 m) up from the base of TP1, above the seeps. The profile revealed a complex and colorful stratigraphy (fig. 10A) showing a grayish-white gypsum layer, yellow jarosite-rich layers, and two orange hardpan layers. Iron and total sulfur contents vary dramatically through the profile. Copper increases downward by over two orders of magnitude. Zinc is greater than, or equal to, copper in the upper parts of the profile; Cr>Co also but this trend reverses with depth. The other profile (fig. 10B) is from a hole dug on the flat top surface of TP2. Black, unoxidized tailings were encountered at a depth of 60 cm, overlain by a thin layer of yellow-green clayey material, hardpan, and orange soil. The upper most 30 cm soil zone was full of roots and organic debris and was not sampled. Unlike the TP1 profile, here Cu>Zn>Pb at all levels. Maximum cobalt concentrations observed are about 100 ppm whereas >1,000 ppm cobalt was measured in a pyrrhotite-rich layer in unoxidized from TP1 (table 7, key 6). Maximum cobalt concentrations observed in massive sulfide ores at the Elizabeth mine is <1,000 ppm (table 3); therefore, cobalt is enriched in the some waste materials relative to the ores.

Table 6. Geochemical data for composite waste dump and tailings soils.

[See Appendix B for explanation of methods. Each sample represents a 30-increment composite of <2 mm (soil fraction) surface material; n.d., not determined; LOI, loss on ignition; C=CO_2, carbonate carbon; BM, total base metal concentration in ppm. TP1-3R is a replicate for sample TP1-3.]

			Tailings pile 3					
	Field No.		TP3-A	TP3-B	TP3-C	TP3-D	TP3-E	TP3-F
Element	Method	Units						
			Major element oxides					
SiO_2	WD-XRF	%	41.6	16.5*	35.6*	41.3	39.6*	35.0*
Al_2O_3	WD-XRF	%	7.28	2.77*	7.70*	7.53	6.72*	6.67*
$FeTO_3$	WD-XRF	%	26.3	72.3*	40.8*	27.2	41.3*	34.8*
MgO	WD-XRF	%	1.23	<0.40*	0.58*	0.99	.56*	0.56*
CaO	WD-XRF	%	0.73	0.14*	0.54*	0.8	.53*	0.65*
Na_2O	WD-XRF	%	2.66	<0.40*	1.77*	2.06	1.58*	1.28*
K_2O	WD-XRF	%	1.72	0.70*	1.54*	1.68	1.16*	1.57*
TiO_2	WD-XRF	%	0.58	0.12*	0.79*	0.55	0.52*	0.46*
P_2O_5	WD-XRF	%	0.05	<0.20*	<0.14*	0.05	<0.14*	<0.14*
MnO	WD-XRF	%	0.03	<0.04*	0.03*	0.04	0.03*	<0.03*
LOI	WD-XRF	%	16.9	7.03*	10.1*	16.9	7.84*	17.0*
Total			99.1	99.6	99.5	99.1	99.8	98
			Major elements					
Al	ICP-MS	%	3.3	1.3	3.7	3.6	3	2.9
Ca	ICP-MS	%	0.4	0.09	0.3	0.51	0.3	0.4
Fe	ICP-MS	%	16	36	24	17	23	21
K	ICP-MS	%	1.2	0.48	1	1.2	0.76	1
Mg	ICP-MS	%	0.55	0.06	0.26	0.41	0.24	0.23
Na	ICP-MS	%	1.7	0.28	1.2	1.4	1	0.85
			Minor elements					
Ag	ICP-MS	ppm	3.3	8.9	24.2	7	11.8	10.7
As	ICP-MS	ppm	4	10	25	8	20	16
Ba	ICP-MS	ppm	32	14	44	65	30	55
Be	ICP-MS	ppm	0.2	0.1	0.2	0.2	0.2	0.2
Bi	ICP-MS	ppm	3.8	3.7	10	4.1	7.7	6.5
Cd	ICP-MS	ppm	0.2	2	0.8	0.3	1.1	1.3
Ce	ICP-MS	ppm	1.5	0.4	2.4	2.9	1.5	2.3
Co	ICP-MS	ppm	5	100	30	9.2	41	22
Cr	ICP-MS	ppm	100	41	81	65	68	62
Cs	ICP-MS	ppm	3.4	0.7	1.5	2.1	1.3	1.5
Cu	ICP-MS	ppm	1,800	2,100	1,100	3,200	850	6,600
Ga	ICP-MS	ppm	11	4.4	10	8.7	8.4	9.1
Ge	ICP-MS	ppm	0.8	0.4	1.2	0.8	0.8	0.8
Hg	CVAC	ppm	0.23	0.08	0.51	0.17	0.35	0.24
In	ICP-MS	ppm	0.2	0.3	0.4	0.3	0.3	0.3
La	ICP-MS	ppm	0.9	0.3	1.5	2	0.8	1.4
Li	ICP-MS	ppm	9.7	4.9	12	8.7	12	9.6
Mn	ICP-MS	ppm	170	65	220	230	170	83
Mo	ICP-MS	ppm	27	34	100	47	67	56
Nb	ICP-MS	ppm	< 0.2	< 0.2	0.5	0.5	0.3	0.6

Element	Field No. / Method	Units	Tailings pile 3 TP3-A	TP3-B	TP3-C	TP3-D	TP3-E	TP3-F
			Minor elements					
Ni	ICP-MS	ppm	<2	26	8	<2	9.2	3
Pb	ICP-MS	ppm	87	51	120	61	84	76
Rb	ICP-MS	ppm	55	17	36	56	27	40
Sb	ICP-MS	ppm	<0.1	0.1	0.2	<0.1	0.1	0.2
Sc	ICP-MS	ppm	7.8	2	10	6.9	7.3	6.5
Se	ICP-MS	ppm	39	45	170	55	100	75
Sr	ICP-MS	ppm	29	7.7	26	28	18	24
Te	ICP-MS	ppm	0.3	< 0.1	1.2	0.3	0.6	0.3
Th	ICP-MS	ppm	< 0.06	< 0.06	0.1	0.38	0.09	0.23
Tl	ICP-MS	ppm	<0.1	<0.1	<0.1	<0.1	<0.1	<0.1
U	ICP-MS	ppm	0.2	0.3	0.4	0.2	0.4	0.4
V	ICP-MS	ppm	90	32	84	78	70	83
Y	ICP-MS	ppm	1.8	0.7	1.5	2.3	1.3	1.9
Zn	ICP-MS	ppm	170	1,200	350	200	440	420
			Carbon, water, and sulfur					
Total C	LECO	%	0.06	0.04	0.12	0.1	0.19	0.26
CO_2	LECO	%	0.01	<0.01	<0.01	<0.01	<0.01	<0.01
$C{=}CO_2$	LECO	%	<0.003	<0.003	<0.003	<0.003	<0.003	<0.003
$C_{organic}$	LECO	%	0.06	0.04	0.12	0.1	0.19	0.26
Total H_2O	LECO	%	7.4	2.8	4.6	7.4	3.8	8.1
H_2O^+	LECO	%	6.5	2.5	4.1	6.3	3.4	6.6
H_2O^-	LECO	%	0.9	0.3	0.5	1.1	0.4	1.5
Total S	LECO	%	4.02	1.69	1.8	3.77	1.2	4.96
			Selected metal ratios and calculated parameters					
BM		ppm	2,062	3,479	1,609	3,471	1,425	7,122
Cu/BM			0.87	0.60	0.68	0.92	0.60	0.93
Zn/BM			0.08	0.34	0.22	0.06	0.31	0.06
Pb/BM			0.04	0.01	0.07	0.02	0.06	0.01
Cu/Zn			10.6	1.8	3.1	16.0	1.9	15.7
Fe/Al			5	28	6	5	8	7

* Samples with extreme iron concentrations (>30 % total iron as Fe_2O_3) were analyzed as partial weight samples and therefore have lower precision and lower detection than specified for the method in Appendix B.

Table 6.–Continued.

			Tailings pile 2		Tailings pile 1			
	Field No.		TP2-1	TP2-2	TP1-1	TP1-2	TP1-3	TP1-3R
Element	Method	Units						
			Major element oxides					
SiO_2	WD-XRF	%	n.d.	n.d.	61.8	63.3	50	n.d.
Al_2O_3	WD-XRF	%	n.d.	n.d.	8.93	10.6	7.88	n.d.
$FeTO_3$	WD-XRF	%	n.d.	n.d.	15.3	11.2	22.6	n.d.
MgO	WD-XRF	%	n.d.	n.d.	1.09	1.67	0.99	n.d.
CaO	WD-XRF	%	n.d.	n.d.	1.19	2.05	1.72	n.d.
Na_2O	WD-XRF	%	n.d.	n.d.	1.81	1.57	1.73	n.d.
K_2O	WD-XRF	%	n.d.	n.d.	1.51	1.7	1.65	n.d.
TiO_2	WD-XRF	%	n.d.	n.d.	0.63	0.76	0.73	n.d.
P_2O_5	WD-XRF	%	n.d.	n.d.	0.07	0.13	0.06	n.d.
MnO	WD-XRF	%	n.d.	n.d.	0.04	0.08	0.06	n.d.
LOI	WD-XRF	%	n.d.	n.d.	6.71	5.58	11.6	n.d.
Total			n.d.	n.d.	99.1	98.6	99	n.d.
			Major elements					
Al	ICP-MS	%	4.7	3.5	4.5	5.9	3.9	3.6
Al	ICP-AES	%	4.7	3.6	n.d.	n.d.	n.d.	3.65
Ca	ICP-MS	%	0.91	0.79	0.78	1.5	1.1	1.3
Ca	ICP-AES	%	0.84	0.72	n.d.	n.d.	n.d.	1.19
Fe	ICP-MS	%	12	25	9.8	7.9	15	15
Fe	ICP-AES	%	10.4	19.3	n.d.	n.d.	n.d.	12.5
K	ICP-MS	%	1.5	1.1	1.1	1.3	1.2	1.3
K	ICP-AES	%	1.35	0.92	n.d.	n.d.	n.d.	1.18
Mg	ICP-MS	%	0.9	0.52	0.51	1.2	0.47	0.43
Mg	ICP-AES	%	0.79	0.56	n.d.	n.d.	n.d.	0.45
Na	ICP-MS	%	1.4	1.4	1.2	1.2	1.2	1.3
Na	ICP-AES	%	1.28	1.24	n.d.	n.d.	n.d.	1.12
P	ICP-AES	%	0.02	0.01	n.d.	n.d.	n.d.	<0.01
Si	ICP-AES	%	23.6	16.9	n.d.	n.d.	n.d.	20.8
Ti	ICP-AES	%	0.43	0.52	n.d.	n.d.	n.d.	0.36
			Minor elements					
Ag	ICP-MS	ppm	0.81	0.58	1.8	0.87	1.3	1.8
As	ICP-MS	ppm	5.6	14	5.9	6.2	9.6	9.7
As	HYD	ppm	6.6	15.9	n.d.	n.d.	n.d.	11.6
Au	GFAA	ppm	0.16	0.029	n.d.	n.d.	n.d.	0.014
Ba	ICP-MS	ppm	140	73	120	280	100	100
Ba	ICP-AES	ppm	107	51	n.d.	n.d.	n.d.	78
Be	ICP-MS	ppm	1	0.5	0.8	1.7	0.6	0.6
Bi	ICP-MS	ppm	n.d.	n.d.	1.4	0.75	2.2	n.d.
Cd	ICP-MS	ppm	0.2	0.3	0.4	0.2	0.2	0.2
Ce	ICP-MS	ppm	n.d.	n.d.	7.9	36	7.4	n.d.
Co	ICP-MS	ppm	48	68	26	38	37	29
Cr	ICP-MS	ppm	93	48	72	91	63	57
Cr	ICP-AES	ppm	111	106	n.d.	n.d.	n.d.	67
Cs	ICP-MS	ppm	n.d.	n.d.	1.7	3.3	2.6	n.d.

Element	Method	Units	Tailings pile 2		Tailings pile 1			
			Minor elements					
Ga	ICP-MS	ppm	n.d.	n.d.	10	13	8.3	n.d.
Ge	ICP-MS	ppm	n.d.	n.d.	0.9	1.2	0.9	n.d.
Hg	CVAC	ppm	0.04	0.11	0.05	0.02	0.05	0.07
In	ICP-MS	ppm	n.d.	n.d.	0.1	0.1	0.1	n.d.
La	ICP-MS	ppm	n.d.	n.d.	4.6	21	4.8	n.d.
Li	ICP-MS	ppm	n.d.	n.d.	14	34	12	n.d.
Mn	ICP-MS	ppm	490	650	270	600	410	420
Mn	ICP-AES	ppm	435	556	n.d.	n.d.	n.d.	362
Mo	ICP-MS	ppm	n.d.	n.d.	15	6.4	16	n.d.
Nb	ICP-MS	ppm	n.d.	n.d.	2	6.8	2.4	n.d.
Nb	ICP-AES	ppm	<10	10	n.d.	n.d.	n.d.	<10
Ni	ICP-MS	ppm	16	21	9	31	12	9
Pb	ICP-MS	ppm	42	45	49	33	50	46
Rb	ICP-MS	ppm	n.d.	n.d.	42	67	53	n.d.
Sb	ICP-MS	ppm	<0.1	0.1	<0.1	<0.1	0.1	0.2
Sc	ICP-MS	ppm	n.d.	n.d.	8.4	11	7.9	n.d.
Se	ICP-MS	ppm	n.d.	n.d.	22	11	31	n.d.
Sr	ICP-MS	ppm	n.d.	n.d.	63	140	46	n.d.
Sr	ICP-AES	ppm	44	31	n.d.	n.d.	n.d.	37
Te	ICP-MS	ppm	n.d.	n.d.	< 0.1	< 0.1	< 0.1	n.d.
Te	HYD	ppm	0.3	0.5	n.d.	n.d.	n.d.	0.3
Th	ICP-MS	ppm	n.d.	n.d.	1.1	4.7	0.72	n.d.
Tl	ICP-MS	ppm	0.8	0.7	<0.1	<0.1	<0.1	0.8
Tl	HYD	ppm	0.8	0.7	n.d.	n.d.	n.d.	0.8
U	ICP-MS	ppm	n.d.	n.d.	0.52	1.2	0.5	n.d.
V	ICP-MS	ppm	100	84	76	93	83	81
Y	ICP-MS	ppm	n.d.	n.d.	5.2	14	5.9	n.d.
Y	ICP-AES	ppm	<10	13	n.d.	n.d.	n.d.	<10
Zn	ICP-MS	ppm	370	450	300	320	480	380
Zr	ICP-AES	ppm	105	87	n.d.	n.d.	n.d.	94
			Carbon, water, and sulfur					
Total C	LECO	%	n.d.	0.11	0.2	0.43	0.12	0.1
CO_2	LECO	%	n.d.	0.01	0.01	0.2	<0.01	0.01
$C=CO_2$	LECO	%	n.d.	<0.003	<0.003	0.05	<0.003	<0.003
$C_{organic}$	LECO	%	n.d.	0.11	0.2	0.38	0.12	0.1
Total H_2O	LECO	%	n.d.	n.d.	3.9	3.5	5.8	n.d.
H_2O^+	LECO	%	n.d.	n.d.	3.3	2.9	4.8	n.d.
H_2O^-	LECO	%	n.d.	n.d.	0.6	0.6	1	n.d.
Total S	LECO	%	n.d.	1.39	1.04	0.56	2.2	2.31
			Selected metal ratios and calculated parameters					
BM		ppm	706	680	1064	542	709	584
Cu/BM			0.33	0.14	0.64	0.22	0.18	0.21
Zn/BM			0.52	0.66	0.28	0.59	0.68	0.65
Pb/BM			0.06	0.07	0.05	0.06	0.07	0.08
Cu/Zn			0.62	0.21	2.27	0.38	0.27	0.32
Fe/Al			3	7	2	1	4	4

Table 7. Geochemical data for tailings profiles.

[See Appendix B for explanation of methods; n.d., not determined; LOI, loss on ignition; $C=CO_2$, carbonate carbon; BM, total base metal concentration in ppm. See Appendix A for sample locations.]

			TP1 profile near base of north slope					TP1 pond area	
Key			1	2	3	4	5	6	7	8
Element	Method	Units								
					Major elements					
Al	ICP-MS	%	3.9	4.5	2.7	4.4	3.2	4.1	5.3	2.4
Al	ICP-AES	%	3.68	4.37	2.78	4.29	2.95	3.75	5.65	2.49
Ca	ICP-MS	%	2.6	4.7	1.6	1.1	1.9	2.1	1.8	0.3
Ca	ICP-AES	%	2.21	4.28	1.58	1.12	1.68	1.84	2.66	0.25
Fe	ICP-MS	%	12	0.68	20	15	16	9	14	31
Fe	ICP-AES	%	10.5	0.62	18.2	11.5	12.7	7.33	16	28.1
K	ICP-MS	%	1.1	0.74	0.76	1.1	0.94	1.4	1.4	1.8
K	ICP-AES	%	0.92	0.62	0.74	0.83	0.84	1.07	1.51	1.79
Mg	ICP-MS	%	0.39	0.39	0.37	0.65	0.33	1	1.3	0.4
Mg	ICP-AES	%	0.38	0.42	0.38	0.6	0.28	0.82	1.12	0.37
Na	ICP-MS	%	1.3	1.5	0.72	1.3	1	0.95	0.9	0.49
Na	ICP-AES	%	1.18	1.35	0.68	1.19	0.82	0.81	0.74	0.4
P	ICP-AES	%	0.03	0.06	0.03	0.04	0.01	0.09	0.05	0.04
Si	ICP-AES	%	20.9	26.6	12.9	25.5	15.9	17.4	21.3	9.62
Ti	ICP-AES	%	0.73	0.93	0.35	0.35	0.35	0.46	0.33	0.22
					Minor elements					
Ag	ICP-MS	ppm	2.9	4	1.5	2.7	1.6	2.3	0.42	2.5
As	ICP-MS	ppm	14	12	33	2	24	110	6.2	7.3
As	HYD	ppm	14.5	12.8	33	1.9	36.3	125	n.d.	n.d.
Au	GFAA	ppm	0.023	0.027	0.024	0.093	0.19	0.021	0.015	0.016
Ba	ICP-MS	ppm	110	110	52	210	66	110	140	260
Ba	ICP-AES	ppm	72	78	43	141	50	79	121	133
Be	ICP-MS	ppm	0.6	0.8	0.4	1.5	0.7	0.6	1	0.4
Cd	ICP-MS	ppm	0.4	1.7	18	1	1.3	120	16	0.4
Co	ICP-MS	ppm	11	4	300	46	38	2,200	250	68
Cr	ICP-MS	ppm	64	54	80	69	58	100	99	75
Cr	ICP-AES	ppm	201	79	122	63	58	86	124	67
Cu	ICP-MS	ppm	120	240	970	5,700	770	29,000	590	930
Hg	CVAC	ppm	0.1	0.13	0.06	0.02	0.06	0.1	0.08	0.16
Mn	ICP-MS	ppm	350	320	150	1,900	140	220	410	320
Mn	ICP-AES	ppm	304	272	142	2,190	115	193	428	315
Nb	ICP-AES	ppm	14	18	15	14	<10	<10	10	<10
Ni	ICP-MS	ppm	6.2	1.7	63	15	8.1	320	72	22
Pb	ICP-MS	ppm	52	37	32	50	38	44	33	65
Sb	ICP-MS	ppm	0.1	0.3	<0.1	0.2	<0.1	<0.1	<0.1	0.2
Sr	ICP-AES	ppm	46	44	25	69	30	28	59	40
Te	FAA	ppm	0.4	<0.1	0.4	0.7	0.2	0.3	n.d.	n.d.
Tl	ICP-MS	ppm	0.8	0.3	0.5	0.5	0.6	1.3	0.7	1
Tl	FAA	ppm	1	0.2	0.5	0.4	0.5	1.2	n.d.	n.d.
V	ICP-MS	ppm	90	53	59	120	51	85	92	99
Y	ICP-AES	ppm	<10	15	<10	10	<10	<10	19	<10
Zn	ICP-MS	ppm	440	87	1,400	210	1,100	1,900	2,600	590
Zr	ICP-AES	ppm	128	151	76	102	79	81	129	58
					Carbon and sulfur					
Total C	LECO	%	0.12	0.06	0.25	0.26	0.17	0.21	0.12	0.72
C=CO2	LECO	%	0.01	<0.003	0.01	0.01	0.01	0.01	0.04	0.01
$C_{organic}$	LECO	%	0.11	0.06	0.24	0.25	0.16	0.2	0.08	0.71
CO_2	LECO	%	0.03	<0.01	0.04	0.02	0.04	0.02	0.13	0.03
Total S	LECO	%	2.9	3.01	15.6	1.8	9.43	14.5	9.96	3.62

Key				TP1 profile near base of north slope					TP1 pond area	
			1	2	3	4	5	6	7	8
Element	Method	Units								
				Selected metal ratios						
BM		ppm	630	371	2,783	6,022	1,955	33,584	3,561	1,675
Cu/BM			0.19	0.65	0.35	0.95	0.39	0.86	0.17	0.56
Zn/BM			0.70	0.23	0.50	0.03	0.56	0.06	0.73	0.35
Pb/BM			0.08	0.10	0.01	0.01	0.02	0.00	0.01	0.04
Cu/Zn			0.27	2.76	0.69	27.14	0.70	15.26	0.23	1.58
Fe/Al			3.08	0.15	7.41	3.41	5.00	2.20	2.64	12.92

Table 7.Continued.

Key Element	Method	Units	Tailings pile 2 profile 9	10	11	12	13
			Major elements				
Al	ICP-MS	%	5.5	5.7	7.3	5.8	6.1
Al	ICP-AES	%	5.11	6.75	0.46	6.78	5.91
Ca	ICP-MS	%	0.9	1.3	1.1	1.2	1.2
Ca	ICP-AES	%	0.79	1.42	0.09	1.22	1.12
Fe	ICP-MS	%	10	10	5.2	9.5	10
Fe	ICP-AES	%	7.73	10.4	0.29	9.56	8.62
K	ICP-MS	%	1.9	1.2	2.1	1.3	1.3
K	ICP-AES	%	1.59	1.27	0.12	1.47	1.27
Mg	ICP-MS	%	1.4	2.1	2.3	1.8	1.8
Mg	ICP-AES	%	1.12	2.11	0.12	1.7	1.62
Na	ICP-MS	%	1.4	1.6	1.8	1.3	1.5
Na	ICP-AES	%	1.26	1.58	<0.01	1.4	1.31
Si	ICP-AES	%	23.4	26.1	1.76	23.8	20.9
Ti	ICP-AES	%	0.37	0.43	0.02	0.39	0.32
			Minor elements				
Ag	ICP-MS	ppm	1	0.32	0.54	0.34	0.55
As	ICP-MS	ppm	5.8	2	2	3	3
As	HYD	ppm	5.9	n.d.	n.d.	n.d.	4.5
Au	GFAA	ppm	0.01	0.013	0.024	0.012	0.017
Ba	ICP-MS	ppm	150	83	210	90	97
Ba	ICP-AES	ppm	112	66	97	81	79
Be	ICP-MS	ppm	0.9	0.8	1.1	0.9	0.9
Cd	ICP-MS	ppm	<0.1	6.8	0.7	16	22
Co	ICP-MS	ppm	3.8	95	8.1	160	180
Cr	ICP-MS	ppm	160	280	190	170	160
Cr	ICP-AES	ppm	161	279	18	178	208
Cu	ICP-MS	ppm	290	2,800	640	3,200	2,900
Hg	CVAC	ppm	0.04	0.03	0.03	0.04	0.03
Mn	ICP-MS	ppm	340	450	420	400	410
Mn	ICP-AES	ppm	303	474	<100	423	377
Nb	ICP-AES	ppm	<10	<10	<10	<10	<10
Ni	ICP-MS	ppm	3.4	33	5.2	60	63
P	ICP-AES	%	0.04	0.04	0.01	0.06	0.05
Pb	ICP-MS	ppm	35	33	37	32	37
Sb	ICP-MS	ppm	<0.1	<0.1	0.6	<0.1	<0.1
Sr	ICP-AES	ppm	42	51	<10	49	38
Te	FAA	ppm	0.4	n.d.	n.d.	n.d.	0.3
Tl	ICP-MS	ppm	1.2	0.6	1.3	0.7	0.8
Tl	FAA	ppm	1.2	n.d.	n.d.	n.d.	0.8
V	ICP-MS	ppm	140	110	150	100	100
Y	ICP-AES	ppm	<10	<10	<10	11	<10
Zn	ICP-MS	ppm	96	1,100	200	1,600	1,800
Zr	ICP-AES	ppm	95	53	18	70	86
			Carbon and sulfur				
Total C	LECO	%	0.11	0.09	0.1		0.05
$C=CO_2$	LECO	%	<0.003	<0.003	0.01	0.01	0.01
$C_{organic}$	LECO	%	0.11	0.09	0.09	0.04	0.04
CO_2	LECO	%	<0.01	0.01	0.03	0.03	0.02
Total S	LECO	%	1.52	5.54	1.18	5.27	5.85
BM		ppm	428	4068	891	5068	5002

Key Element	Method	Units	Tailings pile 2 profile 9	10	11	12	13
			Selected metal ratios				
Cu/BM			0.7	0.7	0.7	0.6	0.6
Zn/BM			0.2	0.3	0.2	0.3	0.4
Pb/BM			0.08	0.01	0.04	0.01	0.01
Cu/Zn			3.0	2.6	3.2	2.0	1.6
Fe/Al			1.8	1.8	0.7	1.6	1.6

Key	Field no.	Sample description
1	TP1-4F	Oxidized topsoil at the surface of tailings profile TP1-4 (near base of north slope of tailings pile 1 above seeps). Sample TP1-4F overlies TP1-4E; TP1-4E overlies TP1-4D, etc.
2	TP1-4E	Gray layer at 25 cm depth
3	TP1-4D	Hardpan layer at 46 cm depth
4	TP1-4C	Yellow-orange soil layer at 50 cm depth
5	TP1-4B	Orange hardpan at 61 cm depth
6	TP1-4A	Pyrrhotite-rich black tailings at 64 cm depth
7	TP1-A-12	Pyrrhotite-rich black tailings at 30 cm depth below flat top surface at the south end of tailings pile 1 in the area between the pond and the base of tailings pile 2
8	TP1-POND	Wet sediment collected from the bottom of the pond on tailings pile 2, about 2 meters from the shore
9	TP2-1D	Yellow-orange clayey soil layer 30 to 56 cm below the top surface of tailings pile 2. Topsoil overlying this layer (not sampled) contains abundant roots.
10	TP2-1C-HP	Hardpan layer at 56 cm below top surface of tailings pile 2
11	TP2-1B	Yellow-green clayey layer 2.5 cm thick overlies unoxidized tailings (occurs 58 cm below top surface of pile)
12	TP2-1A	Black, unoxidized tailings at 61 cm depth
13	TP2-1A (R)	Replicate sample for TP2-A

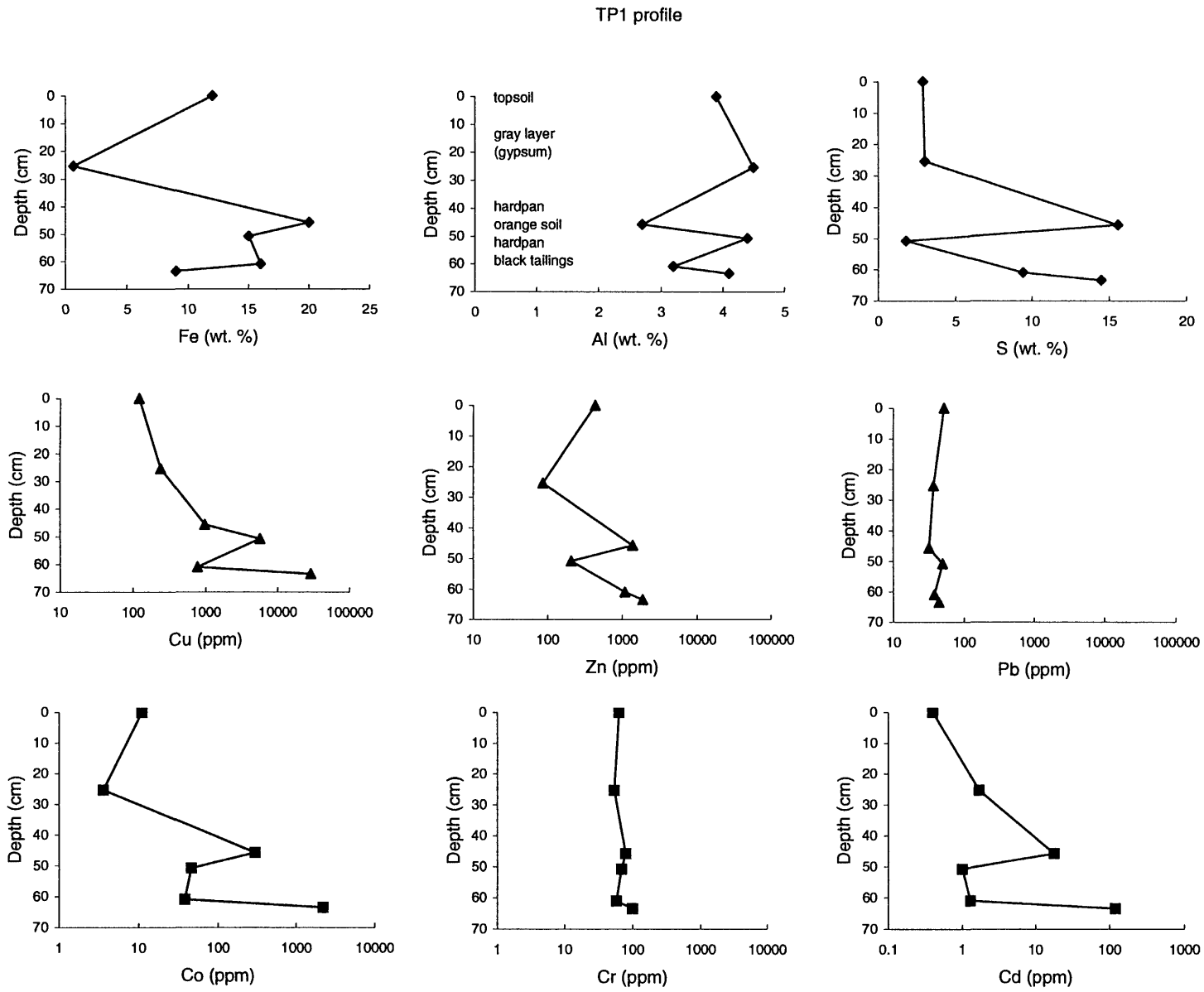

Figure 10. Geochemical profiles of upper surfaces of tailings.

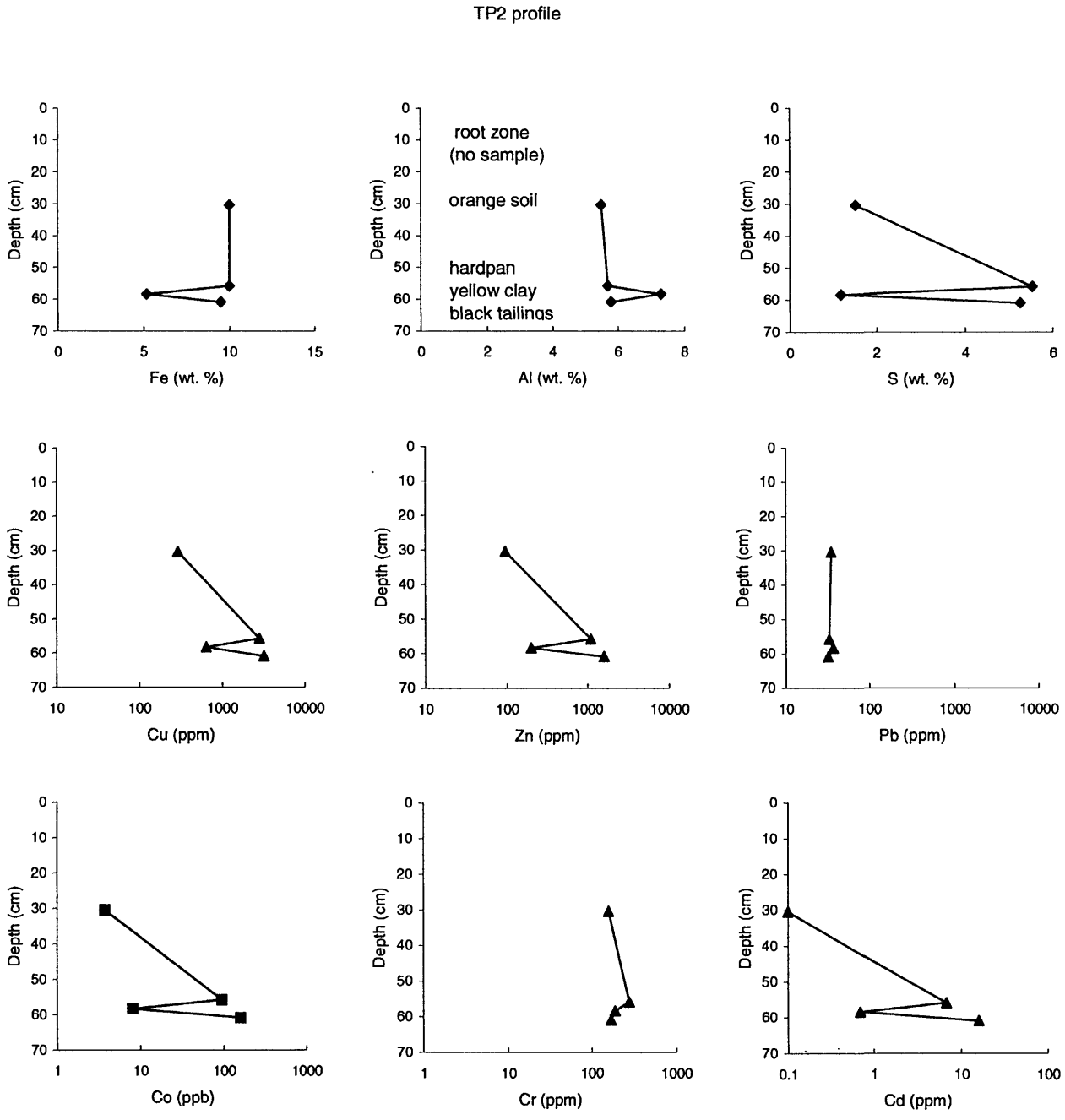

Figure 10. Continued.

Stream sediments

Stream sediments represent a composite of all materials upstream from the sampling site. Stream sediments (table 8) were collected at 22 sites including water sampling sites near the mine, at the seeps, along Copperas Brook, at the air shaft, upriver and downriver from the air shaft, at Lord Brook and Blaisdell Brook (background samples away from mine area), and along the West Branch and main Ompompanoosuc River several kilometers downstream from the mine workings (fig. 11A). The percentage of fine-grained (<80 mesh) material in the sediments varies from 5 % to 36 % (table 8). The highest percentages (>25 %) of fine-grained material are associated with the mud-rich seeps at the base of TP1, where flow rates are fairly low and the stream gradient is not steep. Total base metal concentrations of <80 mesh stream sediments in Copperas Brook decrease with increasing distance from the mine area (fig. 11B). The sample from the West Branch of the Ompompanoosuc River upstream from the air vent (table 8, site 14) has the lowest total base metal concentrations of all samples and the lowest copper concentration. Although geochemical landscapes vary as a function of type of bedrock, comparison of stream sediment data with crustal abundances (CI, Clarke Index values; from Fortescue, 1992) gives an overall perspective on the geochemistry of an area. Crustal abundances are included at the end of table 10B for reference. Detection levels for many of the elements in our data set are too high to warrant comparison with low level crustal abundances. However, many of the values for environmentally sensitive elements for which we do have data, such as mercury, are below expected crustal abundance levels.

Contaminated stream sediments can affect aquatic ecosystems and human health because of their potential toxicity to benthic organisms and to humans who ingest organisms exposed to contaminated sediments (EPA, 1997). Sediments can serve as sources and sinks as well as reservoirs for heavy metals. The use of stream sediment data for aquatic life toxicity assessment is controversial and cannot substitute for bioassay toxicity data; different sediments can represent different degrees of bioavailability for the same total concentration of a trace metal (Di Toro and others, 1990). Nevertheless, stream sediment data provide a useful screening tool to alert investigators to areas that may need further detailed sampling. We have included a subset of EPA's preferred sediment chemistry screening data in table 8; these are reference values above which metal concentrations could pose a significant threat to aquatic life. The values reported in table 8 are effects range-median (ERM) values developed by Long and others (1997). These values were developed by comparing dry weight sediment metal concentrations with biological effects data. Values above the reported value are in the "probable effects range" and have been shown to be a useful screening tool for predicting toxicity (EPA, 1997, Appendix B). All 22 stream sediment samples analyzed in our study are below ERM values for silver, arsenic, cadmium, chromium, mercury, nickel, and lead. With the exception of the muddy sediments at the seeps at the base of TP1, all sediments from Copperas Brook exceed ERM values for copper (table 8, sites 1-5, 11, 18). Two samples from the seeps (table 8, sites 4 and 6) exceed ERM values for zinc. Samples from the haulageway at the south pit (table 8, sites 1 and 2) exceed ERM values for copper. No water was present in the haulageway when these sites were sampled; because of a drainage divide between the south and north pit areas, surface flow from the south pit area does not contribute water to Copperas Brook. None of the river sediment samples exceeds any of the ERM values.

Slack and others (1990) described geochemical anomalies in the Elizabeth mine area in their regional stream sediment survey of the Orange County copper district. Their study, conducted in the 1980s using semi-quantitative spectroscopy (SQS), sampled 37 sites that span several drainage basins in the mine area and showed that geochemical anomalies in stream sediments and heavy mineral concentrates reflected multiple sources of elements including stratabound massive sulfide deposits (anomalous Cu, Zn, Ag, Co, Cd, Mn, and B), metamorphic bedrock, and possibly, undiscovered mineral deposits related to granites in the region. Because SQS data have higher detection limits and greater uncertainties than the analytical techniques used in the present study, data are not directly comparable.

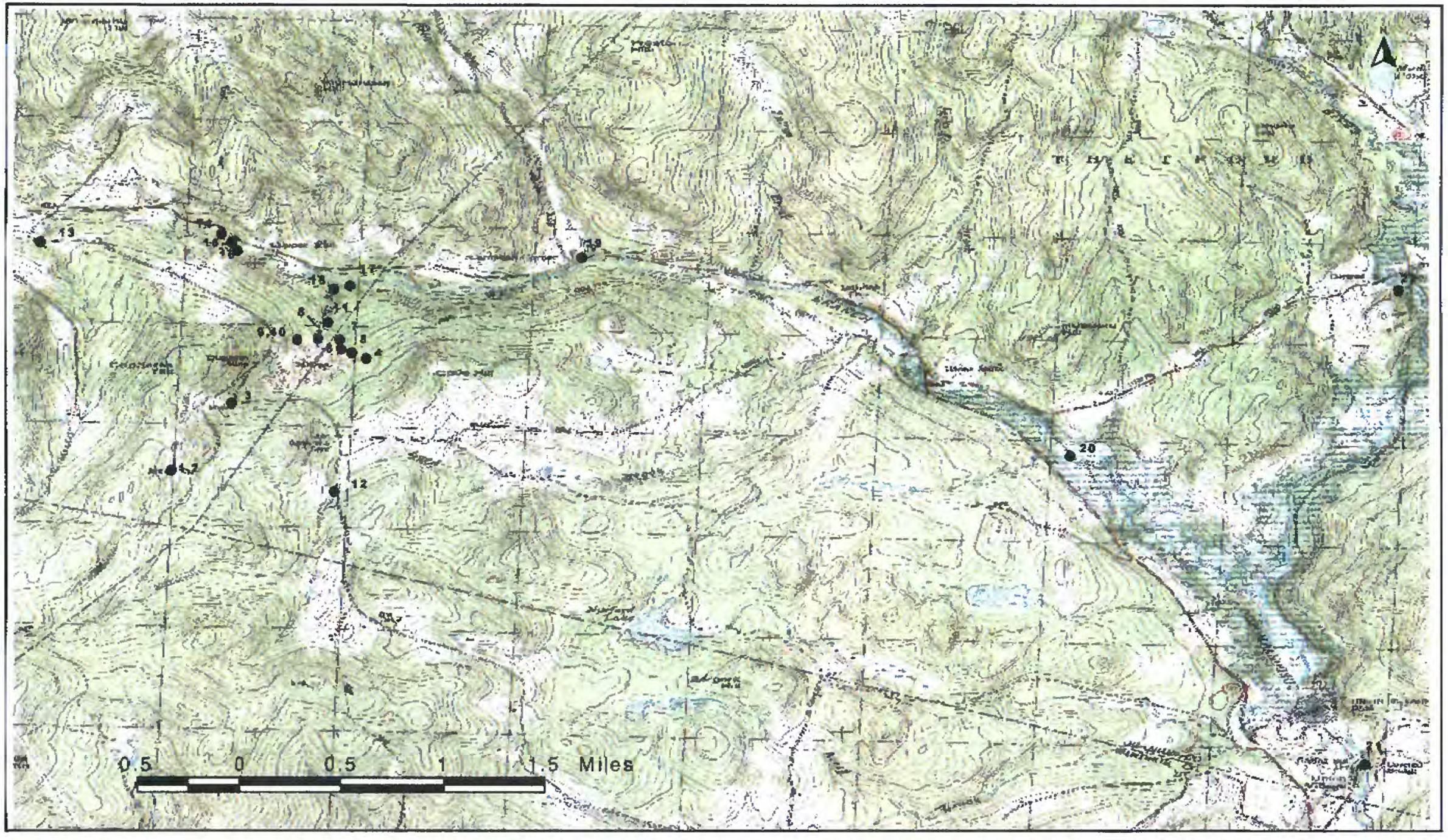

Figure 11. Stream sediment samplas. A, Localities plotted on the South Strafford quadrangle. Note that the actual map is at a scale of 1:24,000 (see fig. 2), but is plotted here at a scale of t:48,000 to show all tha sample sites on a singla page. Sae table 8A for sample key and locations of sample sites.

B

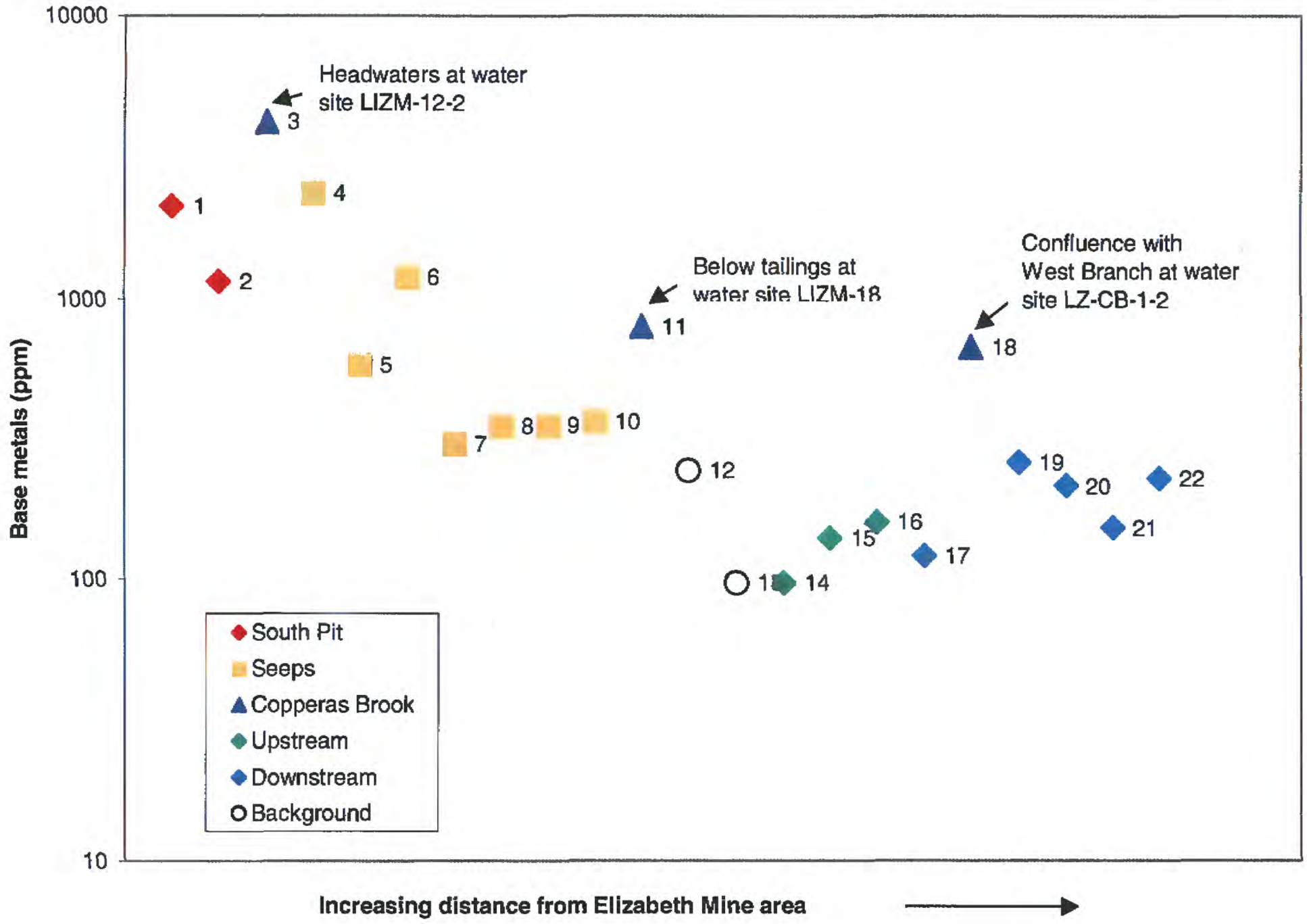

Figure 11. Stream sediment samples. B , Total base metals in <80 mesh stream sediments plotted as a function of increasing distance (approximate) from the Elizabeth mine area. See table 8A for sample key and figure 11A for location key.

Table 8. Stream sediments.

A. Sample key.

[See figure 11A for plotted locations; * denotes replicate samples submitted for chemistry; n.r., not recorded]

Key	Location	Sample	Latitude (N)	Longitude (W)	Description	% Fines
1	South pit	SP-SS1	43° 48' 58.7"	72° 20' 20.2"	Stream sediment at haulageway intersection with pit.	22
2	South pit	SP-SS2	43° 48' 58.7"	72° 20' 20.2"	Stream sediment at end of haulageway above the road.	22
3*	Copperas Brook headwaters above tailings piles 1 and 2, below tailings pile 3	LIZM-12-2 SS	43° 49' 17"	72° 20' 8"	Stream sediment from headwaters of Copperas Brook at water sample site LIZM12-2; sampled just above the waterfall for a distance of 10 m along the stream (10 traverses of 3 samples across the stream width).	n.r.
4	Decant drainage outlet at northeast corner of base of tailings pile 1	LIZM-2-SS	43° 49' 30"	72° 19' 32"	Stream sediment at outlet of TP1 drainage into Copperas Brook at NE corner of TP1 at water sample site LIZM-2-2.	29
5	Seep along north base of tailings pile 1	LIZM-3-SS	43° 49' 27"	72° 19' 33"	Stream sediment at outlet of seep from TP1 west of LIZM-2-2 at water sample site LIZM-3-2..	n.r.
6	Seep along north base of tailings pile 1	LIZM-4-SS	43° 49' 33"	72° 19' 39"	Stream sediment at seep draining TP1 in birches; hardpan forming at waterfall. Water sample site LIZM-4-2.	n.r.
7	Seep along north base of tailings pile 1	LIZM-5-SS	43° 49' 36"	72° 19' 36"	Stream sediment at seep draining TP1 at end of wetlands (cattails); very mucky here.; water sample site LIZM-5-2.	n.r.
8	Seep along north base of tailings pile 1	LIZM-6-SS	43° 49' 37"	72° 19' 32"	Stream sediment at red area of big protohardpan area at base of TP1 at water sample site LIZM-6-2.	31

Key	Location	Sample	Latitude (N)	Longitude (W)	Description	% Fines
9	Seep along north base of tailings pile 1	LIZM-7-SS	43° 49' 38"	72° 19' 45"	Stream sediment at red seep with red to black hardpan edges forming at base of TP1 near its western edge at water sample site LIZM-7-2.	n.r.
10*	Seep along north base of tailings pile 1	LIZM-8-SS	43° 49' 38"	72° 19' 45"	Stream sediment at orange seep draining area immediately west of LIZM7; less hardpan forming, more orange color. Water sample site LIZM-8-2.	36
11	Copperas Brook (east tributary) below tailings pile 1	LIZM-18-2 -SS	43° 49' 40"	72° 19' 37"	Stream sediment at water sample site LIZM-18-2 in woods below tailings on east tributary just above confluence with main Copperas Brook.	n.r.
12	Lord Brook at New Boston Road; above culvert and bridge	LIZR-1-2-SS	43° 48' 36"	72° 19' 38"	Stream sediment at LIZR-1-2 water sample site.	n.r.
13	Unnamed stream (Blaisdell Brook on old maps) on mine road between the mine and S. Strafford, above bridge.	LIZR-2-2-SS	43° 50' 7"	72° 20' 52"	Stream sediment at LIZR-2-2 water sample site sampled for background away from mined area.	n.r.
14	West Branch of the Ompompanoosuc River, 18 m upstream from the air shaft discharge (location reported for air shaft)	OMPR-1-2-SS	43° 50' 7"	72° 20' 4"	Stream sediment at water sample site OMPR-1-2.	5
15	Air shaft along river	98JHAV-SS	43° 50' 7"	72° 20' 4"	Stream sediment along side drainage fed by air shaft drainage just above the river at water sample site LZAS.	22
16	West Branch of the Ompompanoosuc River, 78 meters downstream from the air shaft	OMPR-2-2-SS	43° 49' 59"	72° 18' 36"	Stream sediment at water sample site OMPR-2-2.	14

Key	Location	Sample	Latitude (N)	Longitude (W)	Description	% Fines
17	West Branch of the Ompompanoosuc River 126.3 meters downstream from confluence of Copperas Brook	OMPR-3-2-SS	43° 50' 8"	72° 19' 38"	Stream sediment at water sample site OMPR-3-2.	15
18	Copperas Brook	LIZ-CB-1-2-SS	43° 49' 53"	72° 19' 38"	Stream sediment from Copperas Brook at river confluence, LZCB-1-2 water site.	n.r.
19	West Branch of the Ompompanoosuc River downstream from Copperas Brook and upstream from side drainage confluence at Miller Pond Road	OMPR-4-SS	43° 49' 59"	72° 18' 36"	Stream sediment at water sample site OMPR-4-2. Note that the whole width of the river here has orange floc and coated rocks whereas at the area upstream (just below the Copperas Brook confluence), only the eastern third of the river appeared to be affected. Thick (0.5 cm) orange slime coats river rocks.	n.r.
20	Green bridge across West Branch of the river; south of Tucker Hill Road	OMPR-GB	43° 48' 58"	72° 16' 31"	This is not a water sample site.	24
21	USGS gauging station along the Ompompanoosuc River below Union Dam	OMPR-5-SS	43° 47' 20"	72° 15' 16"	Main Ompompanoosuc River downstream from mine area at water sample site OMPR-5-2.	9
22	Ompompanoosuc River below the covered bridge on Tucker Hill Road	OMPR-7-SS	43° 49' 51"	72° 15' 7"	Stream sediment from main part of the river at a covered bridge at water sample site OMPR-7-2. River is healthy here - no orange flocs or coated rocks.	n.r.

Table 8. Stream sediments.

B. Geochemical data

[Note replicates for samples 3 and 10; CI, Clarke Index values for crustal abundance from Fortescue, 1985; ERM, Effects Range median sediment quality guidelines from Long and others, 1995]

	Key		1	2	3	3	4	5	6	7	8
Element	Method	Units									
Al	ICP40	%	5.865	6.175	3.57	3.48	4.07	1.26	3.37	1.805	1.55
Ca	ICP40	%	2	1.465	0.605	0.59	0.88	0.45	1.68	1.065	0.67
Fe	ICP40	%	18.1	11.3	16.5	16.3	19.6	34.4	21.3	29.8	28.6
K	ICP40	%	0.77	1.09	0.79	0.78	0.94	0.19	1.05	0.49	0.39
Mg	ICP40	%	1.325	1.245	0.45	0.43	0.53	0.145	0.785	0.31	0.205
Na	ICP40	%	2.295	1.575	1.43	1.42	0.855	0.38	0.878	0.605	0.473
P	ICP40	%	0.025	0.06	0.01	0.01	0.015	0.01	0.02	0.02	0.015
Ti	ICP40	%	0.24	0.456	0.192	0.2	0.198	0.024	0.116	0.06	0.072
Ag	ICP40	ppm	<2	<2	<2	<2	<2	<2	<2	<2	<2
As	ICP40	ppm	<10	<10	<10	<10	<10	<10	<10	<10	<10
As	HYD	ppm	0.9	4.4	7.3	n.d.	n.d.	2.2	n.d.	3.2	n.d.
Au	GFAA	ppm	0.016	0.14	0.027	n.d.	n.d.	0.021	n.d.	0.02	n.d.
Au	ICP40	ppm	<8	<8	<8	<8	<8	<8	<8	<8	<8
Ba	ICP40	ppm	82	218	66	66	147	25	136	76	52
Be	ICP40	ppm	1	2	<1	<1	1	<1	<1	<1	<1
Bi	ICP40	ppm	<50	<50	<50	<50	<50	64	<50	55	<50
Cd	ICP40	ppm	2	2	2	3	3	4	7	3	4
Ce	ICP40	ppm	<5	17	13	<5	22	84	39	79	40
Co	ICP40	ppm	9	11	20	24	31	<2	71	7	8
Cr	ICP40	ppm	161	172	89	82	100	68	95	75	61
Cu	ICP40	ppm	1870	925	3800	3930	1860	377	228	91	180
Eu	ICP40	ppm	<2	2	<2	<2	<2	<2	<2	<2	<2
Ga	ICP40	ppm	<4	5	<4	<4	<4	<4	<4	<4	<4
Hg	CVAC	ppm	<0.02	0.02	0.07	0.08	0.05	<0.02	0.06	0.03	0.03
Ho	ICP40	ppm	<4	4	4	<4	<4	4	<4	<4	<4
La	ICP40	ppm	3	10	<2	<2	7	50	32	67	24
Li	ICP40	ppm	13	32	9	8	11	3	13	5	4
Mn	ICP40	ppm	295	423	453	440	403	152	4400	1330	251
Mo	ICP40	ppm	27	10	37	37	7	15	11	18	8
Nb	ICP40	ppm	11	9	13	18	15	18	8	13	19
Nd	ICP40	ppm	<9	9	<9	<9	<9	<9	<9	<9	<9
Ni	ICP40	ppm	19	35	6	7	10	<3	20	<3	<3
Pb	ICP40	ppm	30	19	47	56	35	24	31	28	25
Sc	ICP40	ppm	13	11	6	6	7	<2	6	<2	<2
Sn	ICP40	ppm	<50	<50	<50	<50	<50	<50	<50	<50	<50
Sr	ICP40	ppm	88	142	46	45	64	21	72	65	40
Ta	ICP40	ppm	<40	<40	<40	<40	<40	<40	<40	<40	<40
Th	ICP40	ppm	<6	<6	<6	7	8	<6	<6	10	<6
U	ICP40	ppm	<100	<100	<100	<100	<100	<100	<100	<100	<100
V	ICP40	ppm	130	89	75	71	66	23	66	36	25
Y	ICP40	ppm	7	9	4	4	8	22	13	15	13
Yb	ICP40	ppm	<1	<1	<1	<1	<1	1	<1	<1	<1
Zn	ICP40	ppm	190	160	322	301	414	177	836	176	136

Element	Key Method	Units	1	2	3	3	4	5	6	7	8
Total C	LECO	%	n.d.	n.d.	n.d.	0.18	n.d.	n.d.	n.d.	n.d.	n.d.
CO2	LECO	%	n.d.	n.d.	n.d.	<0.01	n.d.	n.d.	n.d.	n.d.	n.d.
C=CO2	LECO	%	n.d.	n.d.	n.d.	<0.003	n.d.	n.d.	n.d.	n.d.	n.d.
$C_{organic}$	LECO	%	n.d.	n.d.	n.d.	0.18	n.d.	n.d.	n.d.	n.d.	n.d.
Total S	LECO	%	n.d.	n.d.	n.d.	1.72	n.d.	n.d.	n.d.	n.d.	n.d.
Base metals(BM)			2,120	1,152	4,197	4,321	2,353	582	1,193	305	353
Cu/BM			0.88	0.80	0.91	0.91	0.79	0.65	0.19	0.30	0.52
Zn/BM			0.09	0.14	0.08	0.07	0.18	0.31	0.70	0.58	0.39
Pb/BM			0.01	0.02	0.01	0.01	0.01	0.04	0.03	0.09	0.07

Table 8.–Continued.

Element	Key Method	Units	9	10	10	11	12	13	14	15	16
Al	ICP40	%	3.305	3.85	3.75	3.995	4.2	3.02	3.93	4.17	4.64
Ca	ICP40	%	1.02	1.075	1	0.88	1.06	1.35	2.23	1.665	2.26
Fe	ICP40	%	16.8	11	11.5	9.61	3.38	2.31	3.11	5.19	3.1
K	ICP40	%	1.04	0.93	0.93	0.97	0.69	0.46	0.48	0.52	0.62
Mg	ICP40	%	0.3	0.31	0.3	0.505	0.885	0.675	0.96	0.865	1.15
Na	ICP40	%	1.03	1.242	1.29	1.415	0.785	0.685	0.88	0.95	1
P	ICP40	%	0.005	0.005	0.01	0.015	0.04	0.03	0.08	0.06	0.08
Ti	ICP40	%	0.108	0.138	0.138	0.156	0.408	0.39	0.975	0.715	0.725
Ag	ICP40	ppm	<2	<2	<2	<2	<2	<2	<2	<2	<2
As	ICP40	ppm	<10	12	<10	<10	<10	<10	<10	12	<10
As	HYD	ppm	7.5	n.d.	n.d.	5.5	0.8	1	n.d.	n.d.	n.d.
Au	GFAA	ppm	0.016	n.d.	n.d.	0.017	0.017	0.009	n.d.	n.d.	n.d.
Au	ICP40	ppm	<8	<8	<8	<8	<8	<8	<8	<8	<8
Ba	ICP40	ppm	85	70	76	94	187	120	148	132	204
Be	ICP40	ppm	<1	<1	<1	1	2	2	2	2	2
Bi	ICP40	ppm	<50	<50	<50	<50	<50	<50	<50	<50	<50
Cd	ICP40	ppm	<2	2	<2	<2	<2	<2	<2	<2	<2
Ce	ICP40	ppm	73	24	31	7	28	28	21	36	25
Co	ICP40	ppm	13	10	13	11	15	6	9	10	12
Cr	ICP40	ppm	79	65	53	54	75	89	98	84	99
Cu	ICP40	ppm	94	133	128	520	118	33	12	42	34
Eu	ICP40	ppm	<2	<2	2	2	<2	<2	<2	<2	<2
Ga	ICP40	ppm	<4	<4	<4	<4	<4	13	9	<4	5
Hg	CVAC	ppm	0.04	0.03	0.04	0.03	<0.02	<0.02	<0.02	<0.02	0.02
Ho	ICP40	ppm	<4	<4	4	<4	<4	<4	6	<4	<4
La	ICP40	ppm	35	9	7	3	13	15	9	11	14
Li	ICP40	ppm	7	7	6	9	24	14	19	19	29
Mn	ICP40	ppm	340	494	477	539	2050	829	1100	921	1070
Mo	ICP40	ppm	18	10	10	15	3	<2	3	<2	2
Nb	ICP40	ppm	12	9	15	10	5	<4	12	11	11
Nd	ICP40	ppm	22	<9	<9	<9	16	15	13	14	<9
Ni	ICP40	ppm	<3	4	<3	5	28	14	20	16	24
Pb	ICP40	ppm	29	35	35	28	<4	<4	4	9	15
Sc	ICP40	ppm	6	7	6	7	16	9	11	10	11
Sn	ICP40	ppm	<50	<50	<50	<50	<50	<50	<50	<50	<50
Sr	ICP40	ppm	39	39	44	60	102	151	254	168	292
Ta	ICP40	ppm	<40	<40	<40	<40	<40	<40	<40	<40	<40
Th	ICP40	ppm	<6	<6	<6	<6	<6	6	<6	<6	<6
U	ICP40	ppm	<100	<100	<100	<100	<100	<100	<100	<100	<100
V	ICP40	ppm	58	51	52	59	63	56	70	69	77
Y	ICP40	ppm	20	9	9	5	22	12	16	15	16
Yb	ICP40	ppm	1	1	<1	<1	3	2	2	3	2
Zn	ICP40	ppm	219	183	191	233	85	44	52	63	75

Element	Key Method	Units	9	10	10	11	12	13	14	15	16
Total C	LECO	%	n.d.	n.d.	0.14	n.d.	n.d.	n.d.	0.63	n.d.	1.04
CO2	LECO	%	n.d.	n.d.	<0.01	n.d.	n.d.	n.d.	0.33	n.d.	0.34
C=CO2	LECO	%	n.d.	n.d.	<0.003	n.d.	n.d.	n.d.	0.09	n.d.	0.09
$C_{organic}$	LECO	%	n.d.	n.d.	0.14	n.d.	n.d.	n.d.	0.54	n.d.	0.95
Total S	LECO	%	n.d.	n.d.	1.08	n.d.	n.d.	n.d.	0.04	n.d.	0.03
Base metals(BM)			355	367	367	797	246	97	97	140	160
Cu/BM			0.26	0.36	0.35	0.65	0.48	0.34	0.12	0.30	0.21
Zn/BM			0.62	0.50	0.52	0.29	0.35	0.45	0.54	0.45	0.47
Pb/BM			0.08	0.10	0.10	0.04	--	--	0.04	0.06	0.09

Table 8.–Continued.

Element	Key Method	Units	17	18	19	20	21	22	Reference Values CI	Reference Values ERM
Al	ICP40	%	3.915	3.71	4.56	4.415	4.26	4.42	*8.4*	
Ca	ICP40	%	1.975	0.91	2.32	2.07	1.85	1.63	*4.7*	
Fe	ICP40	%	2.24	10.9	3.19	3.19	2.33	2.77	*6.2*	
K	ICP40	%	0.49	0.86	0.61	0.54	0.57	0.71	*1.8*	
Mg	ICP40	%	0.93	0.57	1.13	1.005	0.83	0.87	*2.8*	
Na	ICP40	%	0.797	1.155	1.09	0.932	1.058	1.17	*2.3*	
P	ICP40	%	0.06	0.02	0.07	0.075	0.06	0.06	*0.1*	
Ti	ICP40	%	0.435	0.252	0.613	0.803	0.545	0.7	*0.6*	
Ag	ICP40	ppm	<2	<2	<2	<2	<2	<2	*0.08*	***3.7***
As	ICP40	ppm	<10	<10	<10	17	12	<10	*2*	***70***
As	HYD	ppm	n.d.	3.1	n.d.	n.d.	n.d.	n.d.	*2*	***70***
Au	GFAA	ppm	n.d.	0.026	n.d.	n.d.	n.d.	n.d.	*0.004*	
Au	ICP40	ppm	<8	<8	<8	<8	<8	<8	*0.004*	
Ba	ICP40	ppm	147	121	198	167	151	190	*390*	
Be	ICP40	ppm	2	1	2	2	2	2	*2*	
Bi	ICP40	ppm	<50	<50	<50	<50	<50	<50	*0.008*	
Cd	ICP40	ppm	<2	<2	<2	<2	<2	<2	*0.16*	***9.6***
Ce	ICP40	ppm	24	13	20	38	33	40	*66.4*	
Co	ICP40	ppm	7	9	18	13	9	13	*29*	
Cr	ICP40	ppm	87	76	66	66	72	89	*122*	***370***
Cu	ICP40	ppm	30	484	85	82	56	104	*68*	***270***
Eu	ICP40	ppm	<2	2	<2	<2	<2	<2	*2*	
Ga	ICP40	ppm	<4	<4	19	<4	<4	9	*19*	
Hg	CVAC	ppm	0.03	0.02	<0.02	<0.02	<0.02	<0.02	*0.086*	***0.71***
Ho	ICP40	ppm	<4	<4	<4	<4	<4	<4	*1.26*	
La	ICP40	ppm	10	4	14	15	11	14	*34.6*	
Li	ICP40	ppm	23	12	28	24	21	26	*18*	
Mn	ICP40	ppm	738	737	1170	1100	883	1100	*1060*	
Mo	ICP40	ppm	<2	15	2	<2	<2	<2	*1.2*	
Nb	ICP40	ppm	<4	12	14	12	<4	7	*20*	
Nd	ICP40	ppm	<9	<9	10	13	<9	9	*39.6*	
Ni	ICP40	ppm	18	8	24	21	17	21	*99*	***52***
Pb	ICP40	ppm	9	19	23	10	10	15	*13*	***220***
Sc	ICP40	ppm	8	8	10	11	9	9	*25*	
Sn	ICP40	ppm	<50	<50	<50	<50	<50	<50	*2*	
Sr	ICP40	ppm	219	83	286	219	203	225	*384*	
Ta	ICP40	ppm	<40	<40	<40	<40	<40	<40	*2*	
Th	ICP40	ppm	<6	<6	<6	<6	<6	<6	*8*	
U	ICP40	ppm	<100	<100	<100	<100	<100	<100	*2*	
V	ICP40	ppm	56	62	74	72	53	58	*136*	
Y	ICP40	ppm	13	8	16	18	15	16	*31*	
Yb	ICP40	ppm	2	<1	2	3	2	2	*3.1*	
Zn	ICP40	ppm	57	152	111	89	60	75	*76*	***410***

Element	Key Method	Units	17	18	19	20	21	22	Reference Values CI	Reference Values ERM
Total C	LECO	%	n.d.	n.d.	1.09	n.d.	n.d.	0.86	*0.02*	
CO2	LECO	%	n.d.	n.d.	0.47	n.d.	n.d.	<0.01		
C=CO2	LECO	%	n.d.	n.d.	0.13	n.d.	n.d.	<0.003		
$C_{organic}$	LECO	%	n.d.	n.d.	0.96	n.d.	n.d.	0.86		
Total S	LECO	%	n.d.	n.d.	0.03	n.d.	n.d.	0.02	*0.03*	
Base metals(BM)			121	672	261	215	152	228		
Cu/BM			0.25	0.72	0.33	0.38	0.37	0.46		
Zn/BM			0.47	0.23	0.43	0.41	0.39	0.33		
Pb/BM			0.07	0.03	0.09	0.05	0.07	0.07		

Sulfide and gangue minerals in ore and tailings

Pyrrhotite is the major component of the ores at Elizabeth (table 1) and chalcopyrite was the main source of the copper produced. Pyrite can be locally abundant, but tends to be rare overall relative to pyrrhotite. In many other types of hydrothermal ore, including other types of massive sulfide deposits and coal, most acid mine drainage results from the oxidation of pyrite. Pyrrhotite and pyrite are both iron sulfide minerals; pyrite contains more sulfur than pyrrhotite. However, pyrrhotite weathers more easily than pyrite and rapid oxidation of pyrrhotite forms marcasite, a mineral that has the same composition as pyrite. The stability of pyrrhotite is variable, depending on its composition. We used EMPA to study the composition of the ore minerals in one of the weathered ore "snowballs" from TP3-F and in the tailings (table 9). Samples of black tailings from TP3 oxidized in the plastic sample bag en route to the lab and grew white salts sitting at room temperature in air. Tailings were placed in the heavy liquid methylene iodide (specific gravity 3.3), to facilitate concentration of sulfide minerals by density contrast with gangue minerals such as quartz and feldspar. The material that sank in the heavy liquid was drained, washed with acetone, and studied by XRD, SEM, and EMPA. The heavy mineral suite is dominated by non-magnetic pyrrhotite with minor magnetic pyrrhotite, pyrite, sphalerite, and chalcopyrite.

Pyrrhotite oxidizes much more rapidly than pyrite. The amount of acid produced or consumed by pyrrhotite weathering depends on the particular oxidation path followed and the pyrrhotite composition. The general chemical formula for pyrrhotite is $Fe_{1-x}S$, where x can vary from 0.125 to 0. Thus, pyrrhotite can vary from Fe_7S_8 to FeS. Pyrrhotite grains in the tailings are typically less than 100 microns in diameter. The pyrrhotite in the ore and in the nonmagnetic fraction of the tailings has the same composition with an Fe:S ratio of 0.89. This corresponds to a pyrrhotite composition of Fe_8S_9. The pyrrhotite contains traces of cobalt, but no other metals were detected by EMPA.

Reactions that have been proposed to describe pyrrhotite oxidation are as follows (from Jambor and Blowes, 1994):

(1) Complete reaction (amount of acid produced depends on pyrrhotite composition):

$$Fe_{1-x}S + (2 + x/2)O_2 + xH_2O = (1- x)Fe^{2+} + SO_4^{2-} + 2xH^+$$

(2) Partial reaction to produce native S (not observed at Elizabeth to date):

$$Fe_{1-x}S + (2 - 2x)Fe^{3+} = (3- 3x)\,Fe^{2+} + S^\circ$$

(3) Rapid oxidation to pyrite/marcasite (FeS_2) consumes acid:

$$2Fe_{1-x}S + (1/2 - x)O_2 + (2-4x)\,H^+ = FeS_2 + (1- 2x)Fe^{2+} + (1-2x)\,H_2O$$

Evidence of reaction (3), which consumes rather than produces acidity, is observed on weathered pyrrhotite-rich ore sitting on the mine dumps (TP3) in the north pit area. Backscatter electron images and x-ray spectra obtained with the SEM show the development of FeS_2 along cracks and grain margins of pyrrhotite (fig. 12A). The metastable pyrite/marcasite can react with oxygen and water through a series of reactions. The initial reaction (4) releases ferrous iron and acidity.

(4) Initiator reaction:

$$FeS_2 + 3.5\,O_2 + H_2O = Fe^{2+} + 2\,SO_4^{2-} + 2H^+$$

Ferrous iron released from initial pyrite/marcasite oxidation is oxidized by bacteria (reaction 5). This is one of the most significant steps in the generation of acid drainage because the oxidation of ferrous iron by bacteria is orders of magnitude faster than abiotic oxidation (Singer and Stumm, 1970). Recent

experiments suggest that the rate of pyrite oxidation via this reaction in air at high relative humidity, such as the environment in many waste piles, is faster than oxidation in solution by dissolved oxygen (Jerez and Rimstidt, 1999).

(5) Propagation reaction:

$$Fe^{2+} + 0.25\ O_2 + H^+ = 0.5\ H_2O + Fe^{3+}$$

Ferric iron is a powerful oxidant that can attack pyrite (equation 6) and release significant amounts of ferrous iron and acidity that can further propagate the cycle:

(6) Propagation reaction:

$$14\ Fe^{3+} + FeS_2 + 8\ H_2O = 15\ Fe^{2+} + 2\ SO_4^{2-} + 16H^+$$

Metastable FeS_2 in exposed ore oxidizes, releases sulfur, iron, and acidity. Iron is sequestered in rusty iron oxyhydroxide (goethite) rinds, or in efflorescent salts that develop on exposed surfaces. The reaction of pyrrhotite to pyrite to goethite is illustrated by mapping the distribution of elements across an area of altered pyrrhotite (fig. 12B) for iron, sulfur, and oxygen. The hotter colors on fig. 12B represent higher concentrations of each element. For example, the oxygen concentration is nil (black or blue) where sulfide minerals are present, and highest (red) along the iron oxide vein near the bottom of the map. On the sulfur map, the red areas represent marcasite (higher S) rimming and invading pyrrhotite (lower S than pyrite). Areas that are enriched in aluminum represent mica grains intergrown with the ore.

Other sulfide minerals occurring in ore such as chalcopyrite and sphalerite are subject to similar oxidation reactions that involve oxygen, water, microbes, and ferric iron . Such reactions can produce acidity and release metal cations that remain dissolved in waters, precipitate as secondary minerals, or be adsorbed on hydrous metal-oxide minerals, clays, or organic matter.

Quartz and white mica are abundant as primary rock-forming minerals in wallrock and as gangue minerals in the ore. Therefore, it is not surprising that these minerals are ubiquitous in the tailings. White mica (muscovite) weathers slowly relative to other silicate minerals and quartz is essentially inert (table 1). However, white mica breakdown to aluminum hydroxides (equation 7) and to kaolinite clay (equation 8) produces a major source of aluminum and potassium in soils, and theoretically at least, can consume acidity.

$$(7)\ KAl_3Si_3O_{10}(OH)_2 + H^+ + 9H_2O = K^+ + 3H_4SiO_4 + 3Al(OH)_3$$

$$(8)\ KAl_3Si_3O_{10}(OH)_2 + H^+ + 3/2H_2O = K^+ + 3/2Al_2Si_2O_5(OH)_{4(S)}$$

Table 9. Compositions of minerals in ore and tailings determined by electron microprobe (EMPA).
[n, number of analyses; s.d., standard deviation]

	Sulfide minerals in weathered ore on TP3-F					
	pyrrhotite		marcasite		chalcopyrite	
	n=49		n=7		n=7	
	Wt. %	s.d.	Wt. %	s.d.	Wt. %	s.d.
Fe	60.45	0.65	45.85	1.52	30.39	0.16
Cu	0.02	0.04	0.01	0.01	34.74	0.37
S	39.01	0.44	48.19	5.00	35.25	0.76
Mn	0.00	0.01	0.00	-	0.00	0.01
Co	0.05	0.00	0.11	0.16	0.01	0.00
Pb	0.00	0.00	n.d.	-	0.00	0.00
Ag	0.02	0.02	0.02	0.02	0.02	0.03
Sb	0.01	0.01	0.01	0.01	0.00	0.00
As	0.00	0.01	0.00	0.01	0.01	0.01
Cd	0.00	0.00	n.d.	-	0.00	0.00
Se	0.01	0.01	0.00	0.01	0.00	0.00
Zn	0.00	0.01	0.00	0.00	0.03	0.02
Total	99.6		94.2		100.5	
Fe:S	0.89		0.55			

	Sulfide minerals in tailings (TP1)				Silicate minerals in weathered ore (TP3)		
	pyrrhotite		pyrite			white mica	
	n=8		n=3			n=14	
	Wt. %	s.d.	Wt. %	s.d.		Wt. %	s.d.
Fe	59.02	0.79	45.12	0.79	SiO_2	49.0	0.9
Cu	0.02	0.01	0.03	0.01	Al_2O_3	35.7	0.9
S	37.95	0.56	52.10	0.19	FeO	1.68	0.44
Mn	0.00	0.00	0.00	0.00	MgO	1.22	0.17
Co	0.15	0.02	0.34	0.34	MnO	0.01	0.02
Pb	0.00	0.00	0.00	0.00	Cr_2O_3	0.07	0.06
Ag	0.02	0.02	0.00	0.00	V_2O_3	0.08	0.02
Sb	0.00	0.01	0.01	0.01	TiO_2	0.57	0.17
As	0.00	0.00	0.14	0.22	K_2O	10.00	0.25
Cd	0.00	0.00	0.00	0.00	BaO	0.19	0.19
Se	0.01	0.01	0.01	0.01	Na_2O	0.23	0.12
Zn	0.04	0.07	0.01	0.01	CaO	0.00	0.00
Total	97.2		97.8		Cl	0.00	0.01
					F	0.00	0.00
Fe:S	0.89				Total	98.7	

A

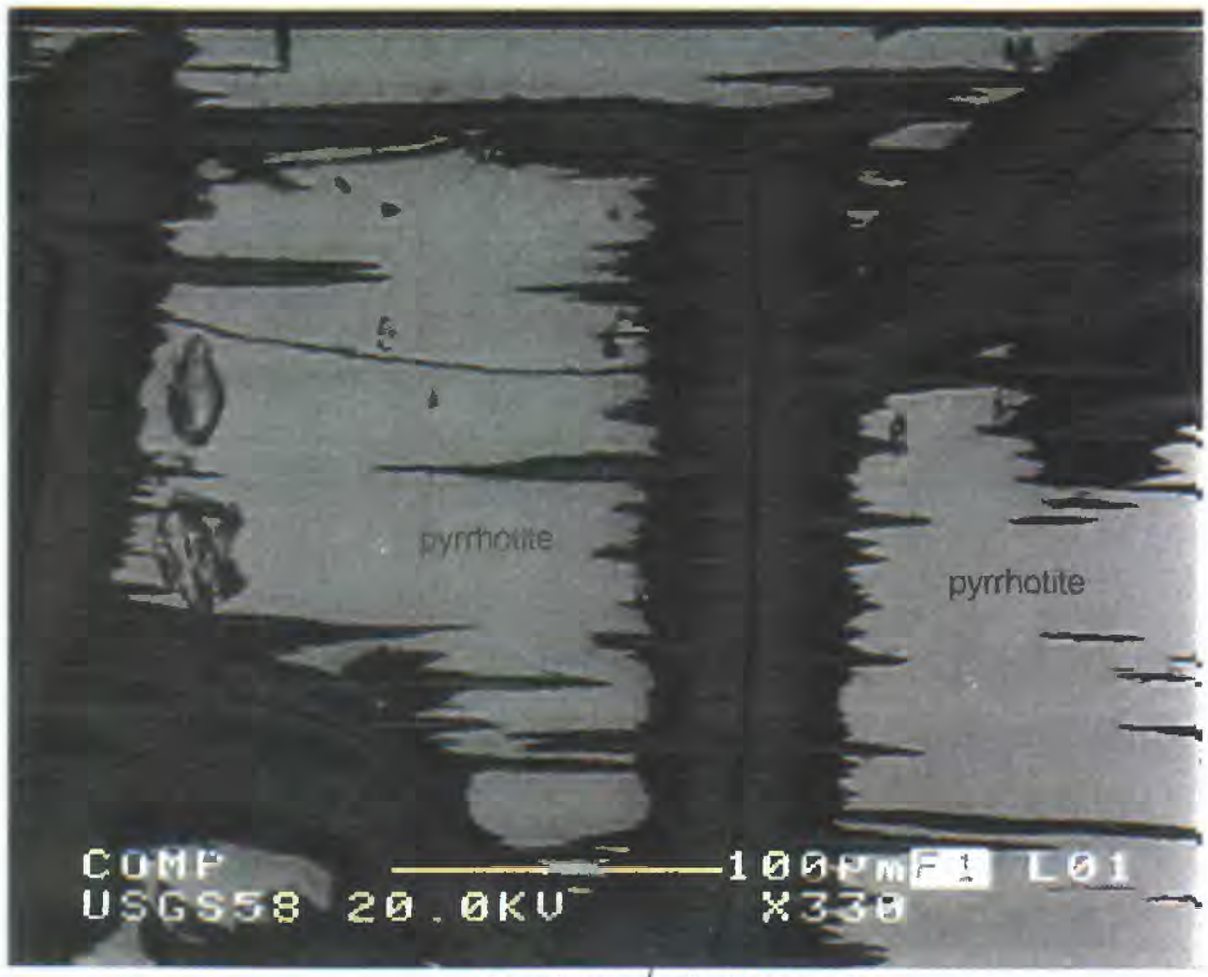

alteration to pyrite/marcasite

B

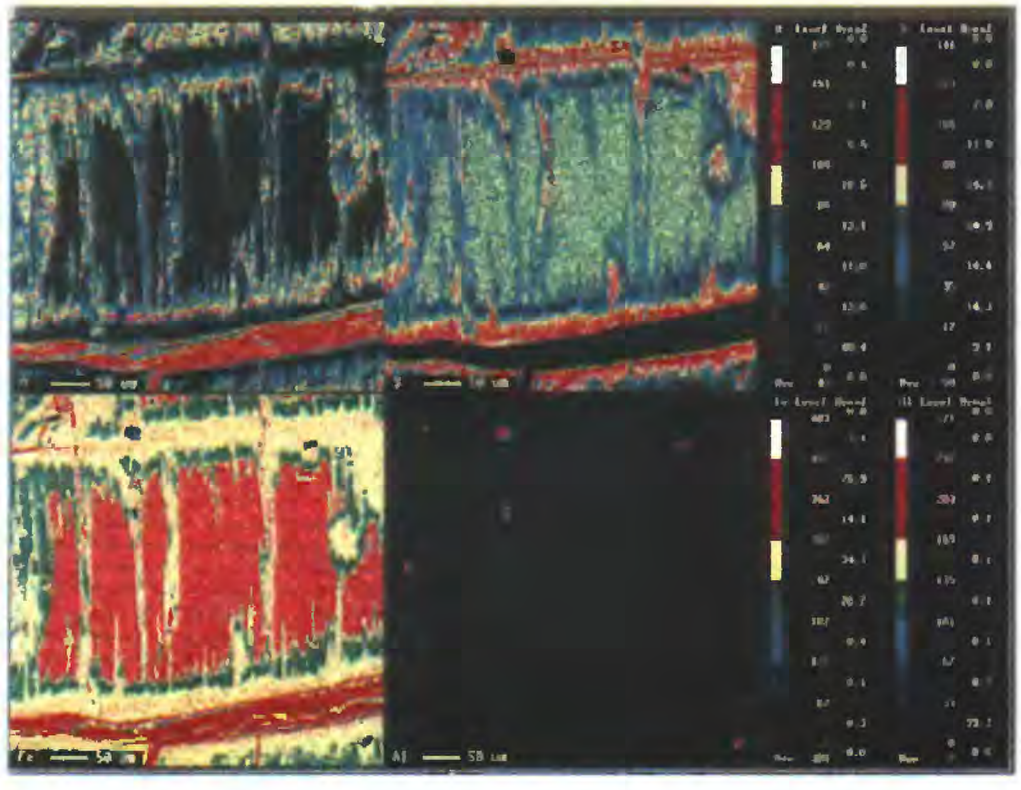

Figure 12. Pyrrhotite alteration in oxidized ore on TP3-F. A, Backscattered electron SEM image showing alteration of pyrrhotite (bright areas) to marcasite. B, EMPA map of distribution of O, S, Fe, and Al in altering pyrrhotite (see text). Hotter colors represent higher concentrations of the

Efflorescent salts

Efflorescent salts are secondary metal-sulfate minerals that form from the weathering of sulfide minerals. Many salts are highly soluble, hydrated solid solution minerals that react in changing weather conditions; salts exert an important control on metal mobility from mine wastes. On dry days, salts are ubiquitous on the tailings at the Elizabeth mine. During rainstorms, the soluble salts dissolve and contribute metals and acidity to surface runoff. Efflorescent salts are observed in several settings at the mine: (1) as thick (up to 2 cm) crusts and coatings on bedrock on pit walls, where protective overhangs shelter the rock faces from continuous exposure to rain and snow; (2) as rinds on weathered pieces of ore exposed to precipitation; and (3) as thin, drusy coatings on tailings surfaces. Capillary action draws waters to tailings, soil, or rock surfaces where it evaporates to form salt crusts. Observations of storm runoff at the Sulfur massive sulfide mine in central Virginia (Dagenhart, 1980) demonstrated that dissolution of efflorescent salts from mine tailings can elevate the peak metal load in a nearby creek to as much as fifty times base- flow metal loads. At Elizabeth, salts were collected from protected overhangs on bedrock outcrops along pit walls, from weathered rinds on loose blocks of oxidized ore in the north pit area, and from tailings pile surfaces. Because salts store acidity that can be released on dissolution, minor amounts of salts within tailings and mine dump soils contribute to low paste pH values.

Most of the thick encrusted coating on protected parts of pit walls is gypsum. Gypsum also forms "organpipe" crystals on eroded tailings surfaces that are fine-grained near the tailings substrate and coarsen outwards (fig. 13A). Highly soluble efflorescent salts of the halotrichite-pickeringite group grow as felted mats of white to yellowish crystals on the surface of tailings pile 3 (fig. 13B). SEM spectra of different "strands" of the curved fibers show that their composition is variable; all of the fibers analyzed contained sulfur, aluminum, magnesium, and iron but varied in minor element content (copper, manganese, silicon). Blue salts contain substantial copper (fig. 14). However, XRD acquired on the blue salts showed no discrete copper minerals, but produced a pattern consistent with a siderotil mixed with minor amounts of pickeringite and melanterite. None of the end-members of these mineral groups contains copper (table 1); however, copper readily substitutes for divalent iron or magnesium in these minerals complicating unequivocal identification by XRD. At high magnification (1,000x) in the SEM, the blue salts include at least two different copper-bearing minerals. One forms curved fibers (fig. 14A) that contain sulfur>aluminum> iron>copper>magnesium (fig. 14B), consistent with a mineral of the halotrichite-pickeringite group that incorporated copper. Micas are typically present in the substrate on which the salts grow. Weathering of micas in the top soil layer of the tailings releases aluminum. The solubility of aluminum, an element that can be poisonous to plants (phytotoxic), increases in acid mine soils. Therefore, in addition to release of copper, sulfur, and iron on dissolution, these salts can recycle aluminum. The other mineral identified by SEM (fig. 14C) has a more equant rounded to hexagonal crystal form and contains significant amounts of iron and copper but lacks aluminum (fig. 14D), suggesting a copper-substituted siderotil group mineral.

The white salts that form "snowball" coatings on weathered ore are mixtures of the ferrous iron sulfate minerals melanterite (copperas) and rozenite. Melanterite is one of the most common minerals found in association with acid-mine drainage. Melanterite (7 waters of hydration) dehydrates to rozenite (4 waters of hydration). Melanterite is typically pale blue-green whereas rozenite is white (table 1). The salts were white rather than green when sampled, and they may have dehydrated further en route to the lab. Although melanterite group minerals can accommodate significant amounts of other metals (manganese, copper, etc.), SEM spectra confirm that the snowball salts are composed solely of iron and sulfur (in addition to oxygen and hydrogen).

A

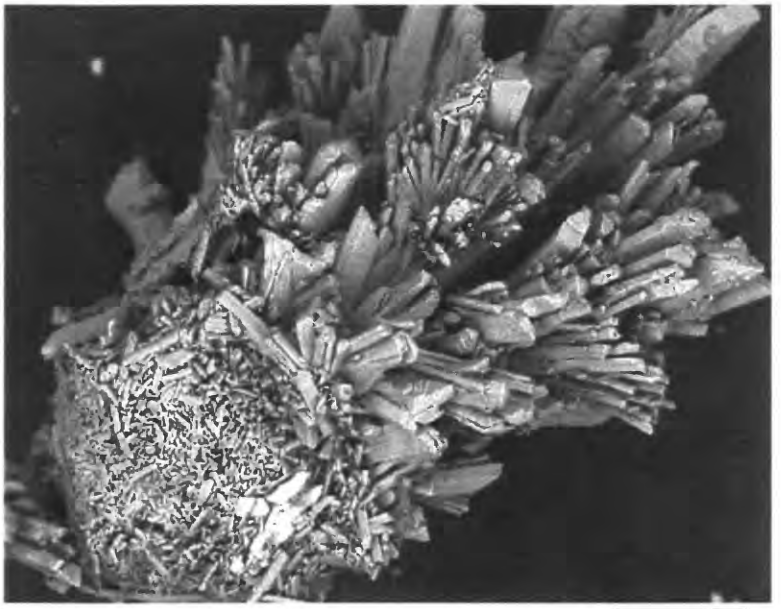

100 microns

B

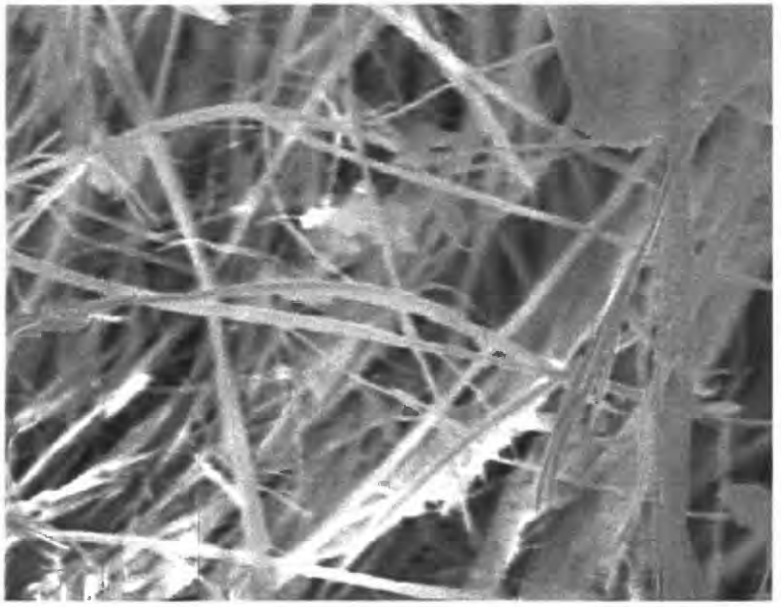

10 microns

Figure 13. Secondary electron SEM images. A, "Organpipe" gypsum crystals that coarsen outwards (200x). B, Hairlike needles of pickeringite (2,000x).

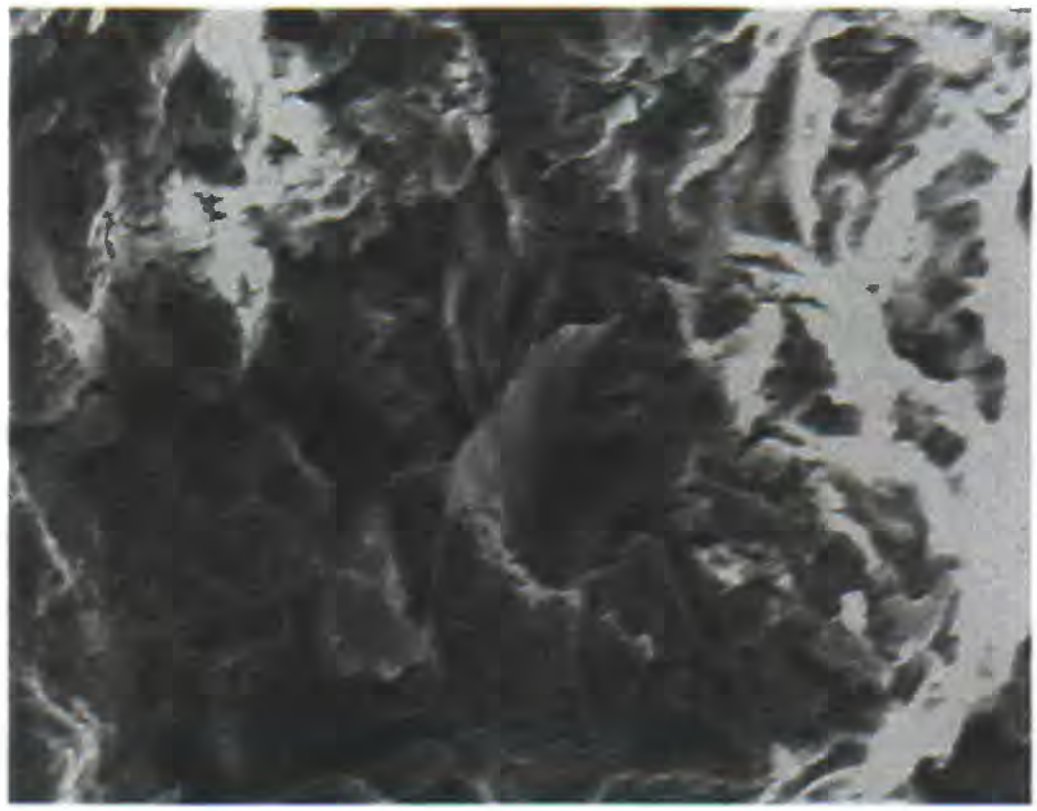

A

B

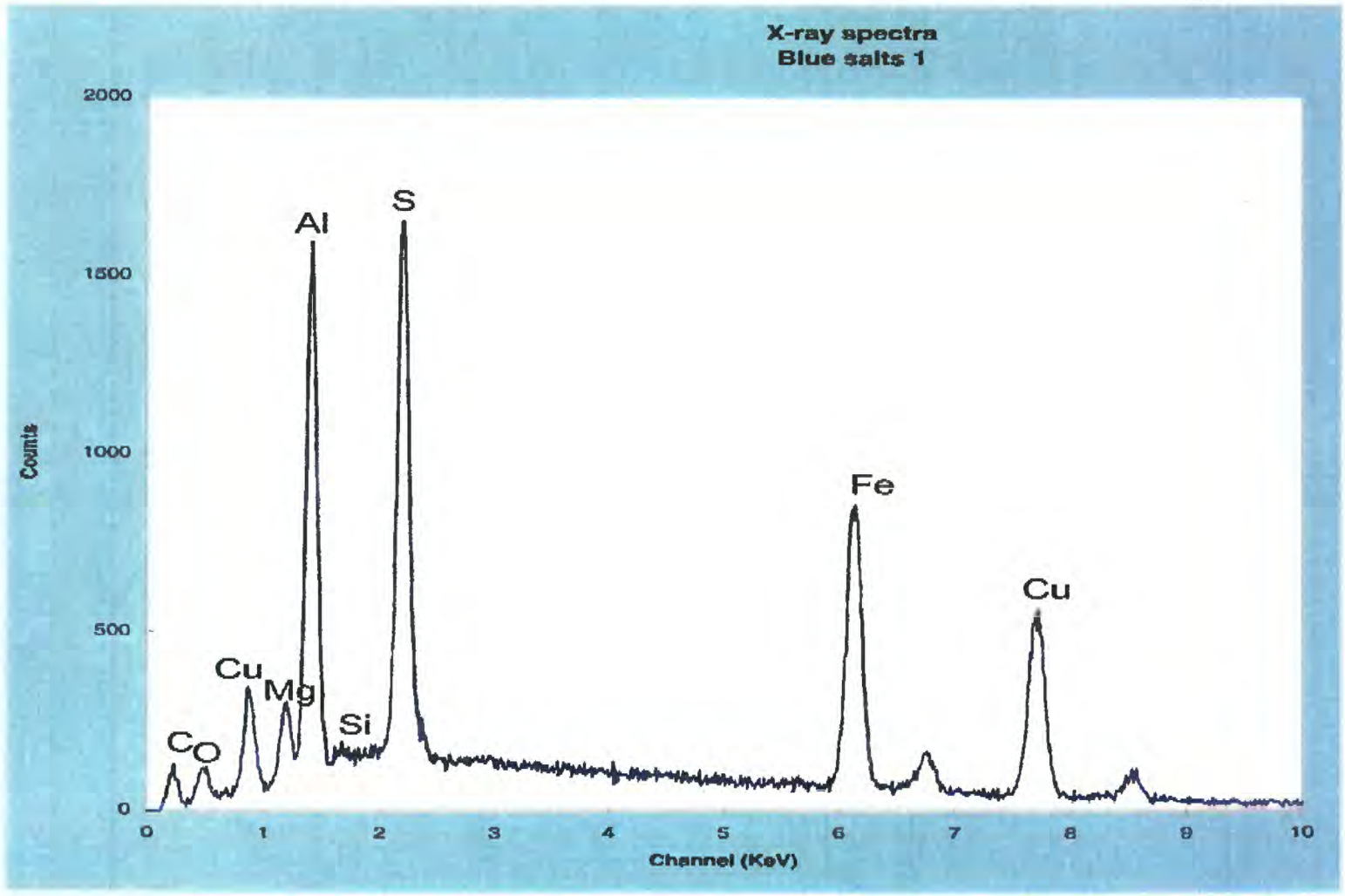

Figure 14. Blue efflorescent salts growing on the surface of TP3. XRD pattern is consistent with a siderotil group rnineral; however SEM shows that there are two different crystal forms that have different cornpositions. A, Curved, sheaf-like crystals (secondary electron irnage, 1000x). B, Energy dispersive x-ray spectrum collected for the crystal at the center of image A.

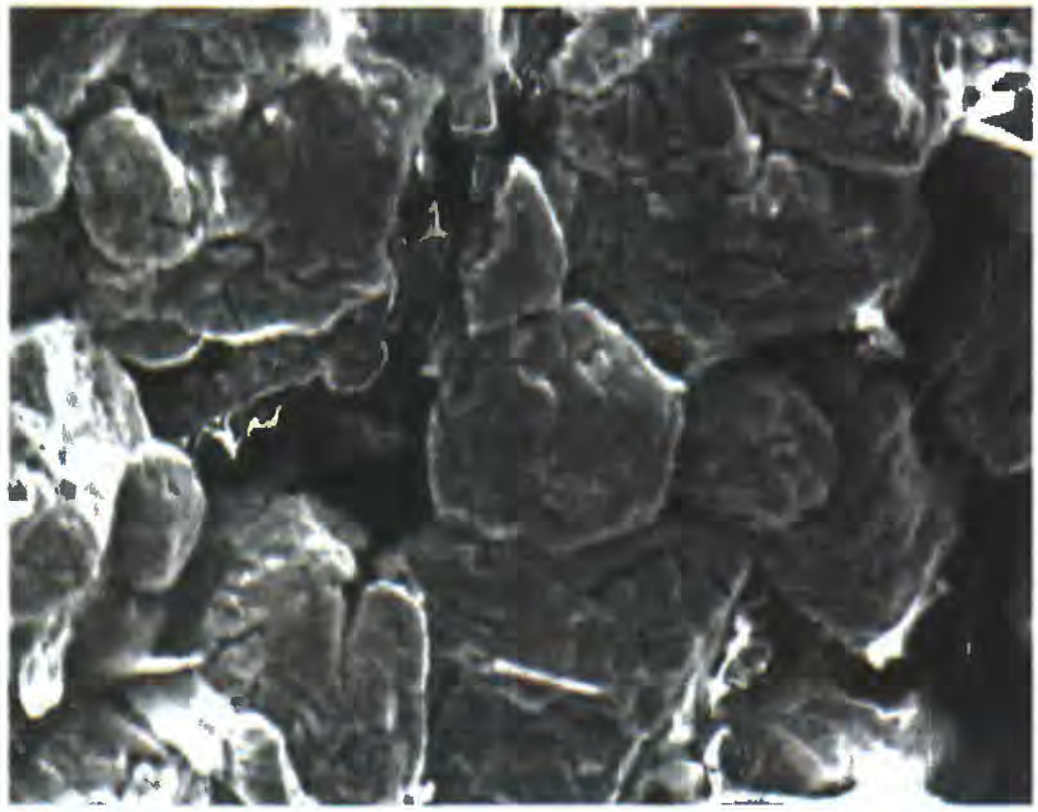

C

D

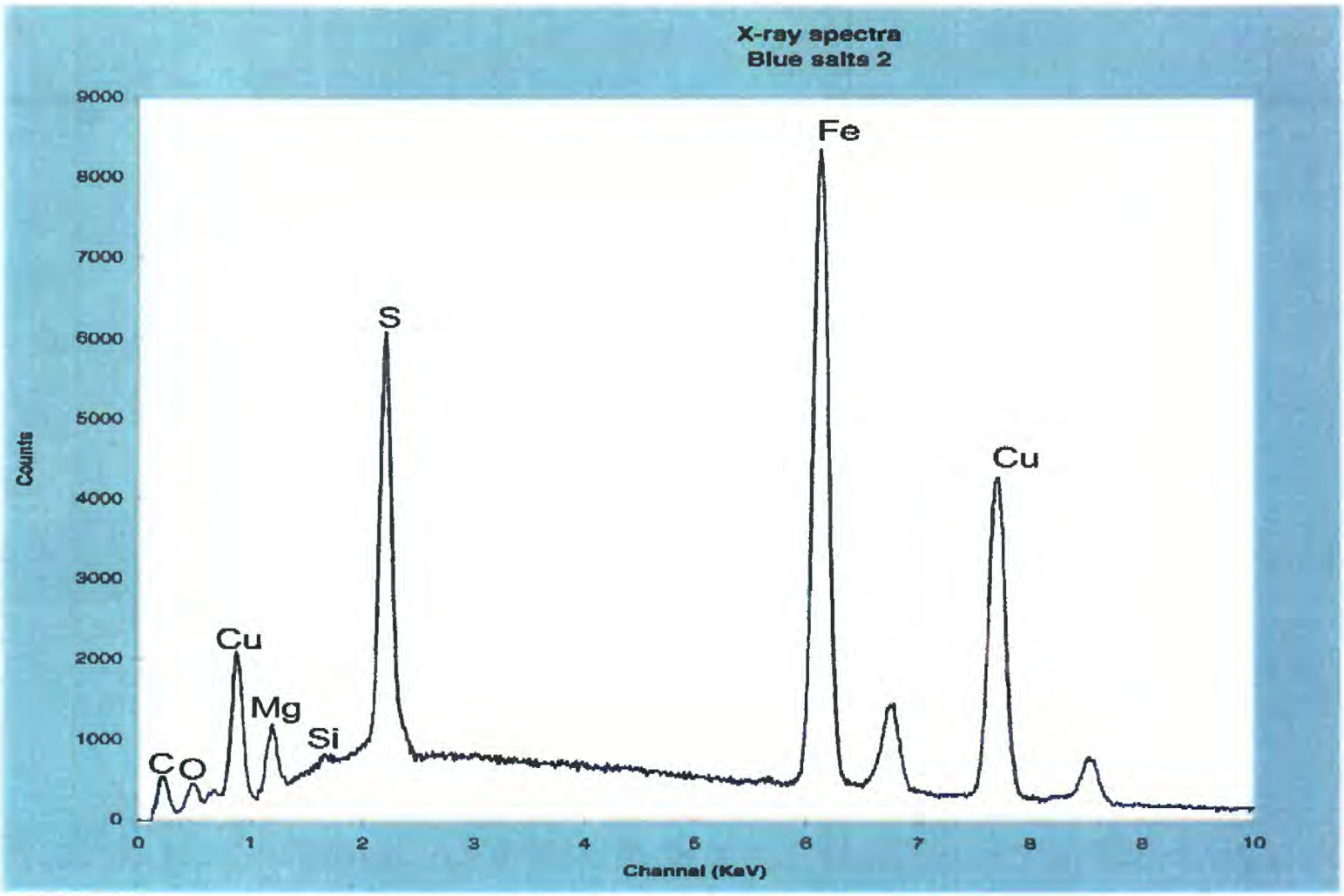

Figure 14. Continued. C, Hexagonal crystals (secondary electron image, 1000x). D, Energy dispersive x-ray spectrum collected for the crystal at the center of image C.

Ochre deposits

Ochre deposits are concentrations of secondary iron- and aluminum-oxides and oxyhydroxides that form from the weathering and oxidation of sulfide minerals (Bigham, 1994). Ochres present at the Elizabeth mine include hardpan layers in and along streams, layers in tailings piles, soft crusts, and wet (typically slimy) precipitates and flocs that range from amorphous ferric hydroxide to well-crystallized minerals such as goethite and jarosite. Ochres were sampled by a variety of methods, depending on the degree of compaction of the material.

The multicolored iron ochre minerals that contribute to soil color on oxidized tailings surfaces, form muds at seeps, coat the Copperas Brook streambed, and form hardpans are goethite, jarosite, and schwertmannite (table 1). "Yellowboy" in and along streams is a hallmark of acid mine drainage. Yellowboy is an informal name for the mineral schwertmannite, a poorly crystalline mineral that has only recently been characterized. In the past, it was commonly referred to only as a "mine drainage mineral" (Bigham, 1994). Such minerals form by hydrolysis and precipitation (equation 9) of the iron available from sulfide oxidation reactions, such as the reactions described above in equations 1-6. Hydrous-oxide minerals form initially as amorphous solid phases (too poorly crystalline to produce an XRD pattern). These minerals can play a critical role in trace metal transport because they (1) produce acid on formation; (2) adsorb metals at the solid-water interface, effectively removing them from contaminated waters; and (3) consume acid and release any adsorbed metals when they dissolve. All of these reactions are pH dependent. For example, iron and aluminum hydrous oxides adsorb Cu, Pb, and Hg in the pH range 3 to 5, and adsorb Zn, Co, Ni, and Cd at higher pH values (5 to 6.5).

The particular ochre minerals that form vary as a function of pH, dissolved sulfate content, and availability of elements such as K, Na, or Si. Goethite is the most widespread mineral associated with acid drainage. Other ochre minerals are all transient relative to goethite as a stable end-product, following dissolution and reprecipitation of other minerals as conditions vary (Bigham, 1994). Low pH (3 to 4) and moderately high concentrations of dissolved sulfate (1,000 to 3,000 ug/L) favor schwertmannite formation. Jarosite tends to form at lower pH and higher concentrations of dissolved sulfate. The jarosite crystal structure can incorporate K, Na, or H_3O^+ resulting in the end-member minerals jarosite, natrojarosite, and hydronium jarosite, respectively. The jarosite at Elizabeth is the potassium-hydronium variety, as shown by XRD and by SEM spectra. In some mine processing operations, natrojarosite is produced as part of a zinc refining process. We have no documentation of this occurring at Elizabeth, but the very jarosite-rich, straw yellow, clayey layers present near the base of TP1 (most recent mine operation) may have discharged as jarosite from a flotation circuit rather than having formed in situ in the tailings. A sample of this material was analyzed (table 10C). Although sodium is present, K>Na. The relatively high silica content (11 wt. %) reflects a minor amount of quartz detected in the XRD pattern. Base metal content of this material is low (129 ppm), but it has elevated Sr (290 ppm) which may reflect its source. Jarosite is also present in hardpans along Copperas Brook (fig. 14B), proximal to tailings (sample CBW-HP). Goethite and schwertmannite occur in all hardpans sampled along Copperas Brook (fig. 14B). Sample 98JH-CB2-HP is just downstream from water sample site LIZM-18-2, and 98JHCB2-R-HP was collected just above water sample site LIZ-CB near the river. The occurrence of jarosite in sample CBW-HP is consistent with the low pH (~3) and high dissolved sulfate content (3,000 mg/L) of the water in Copperas Brook at this locality.

(9) Precipitation of hydrous-oxide minerals: acid-producing reaction:

$$Fe^{2+} + 0.25O_2 + 2.5\ H_2O = Fe(OH)_3\ (solid) + 2H^+$$

$$Fe^{3+} + 3H_2O = Fe(OH)_3\ (solid) + 3H^+$$

$$Al^{3+} + 3H_2O = Al(OH)_3\ (solid) + 3H^+$$

Geochemical data for ochre deposits at Elizabeth are given in table 10 and plotted in fig. 16. Samples analyzed include hardpans forming along the Copperas Brook, hardpan layers in tailings, "red slimes" that form proto hardpans and organic-rich hardpan terraces at seeps, jarosite, and "white" slime

at the air vent along the river. The highest concentrations of base metals (Cu>Zn>Pb) are present in the hardpans in and on tailings. The protohardpan muds associated with the near-neutral seeps however, are more iron-rich and in most cases have Zn>Cu>Pb, reflecting the mobility of zinc relative to copper and most likely, sorption of zinc onto the secondary iron minerals that comprise the ochres. Downstream from the seeps along Copperas Brook, hardpans again have Cu>Zn>Pb. Zinc is very difficult to remove from acidic waters, because pH must be raised to at least 5 for effective sorption of dissolved zinc onto hydrous iron and aluminum oxides. Our data indicate that some zinc is being sequestered in solid phases at the near-neutral seeps. At the air vent, a thin layer of "white slime" covers red-orange hardpan. SEM confirms that the white slime is aluminum-rich. A small, impure sample of the white slime (18 on fig. 16) has the highest concentration of copper and zinc of any samples, and almost an order of magnitude more than the associated hardpan (sample 17).

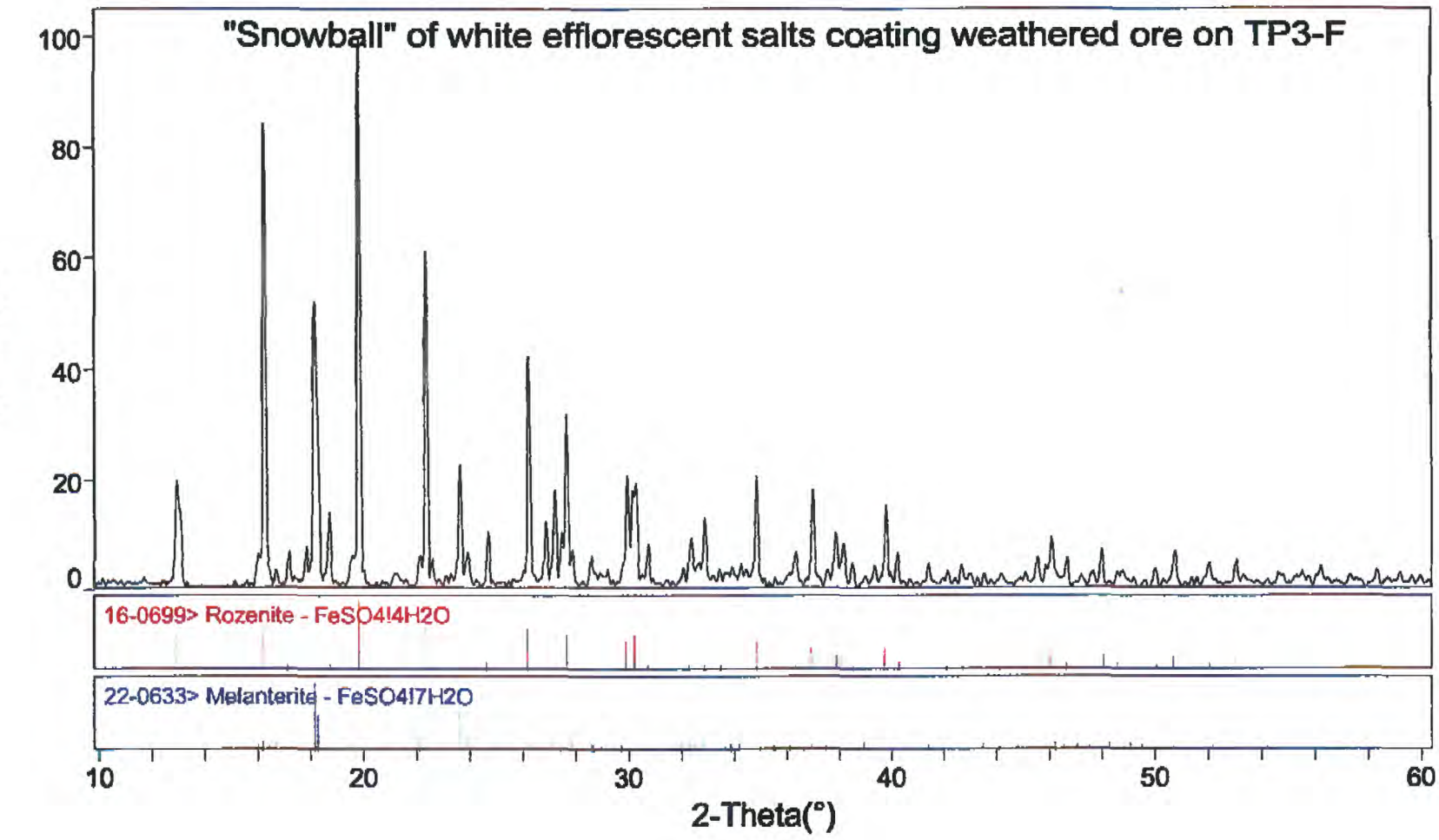

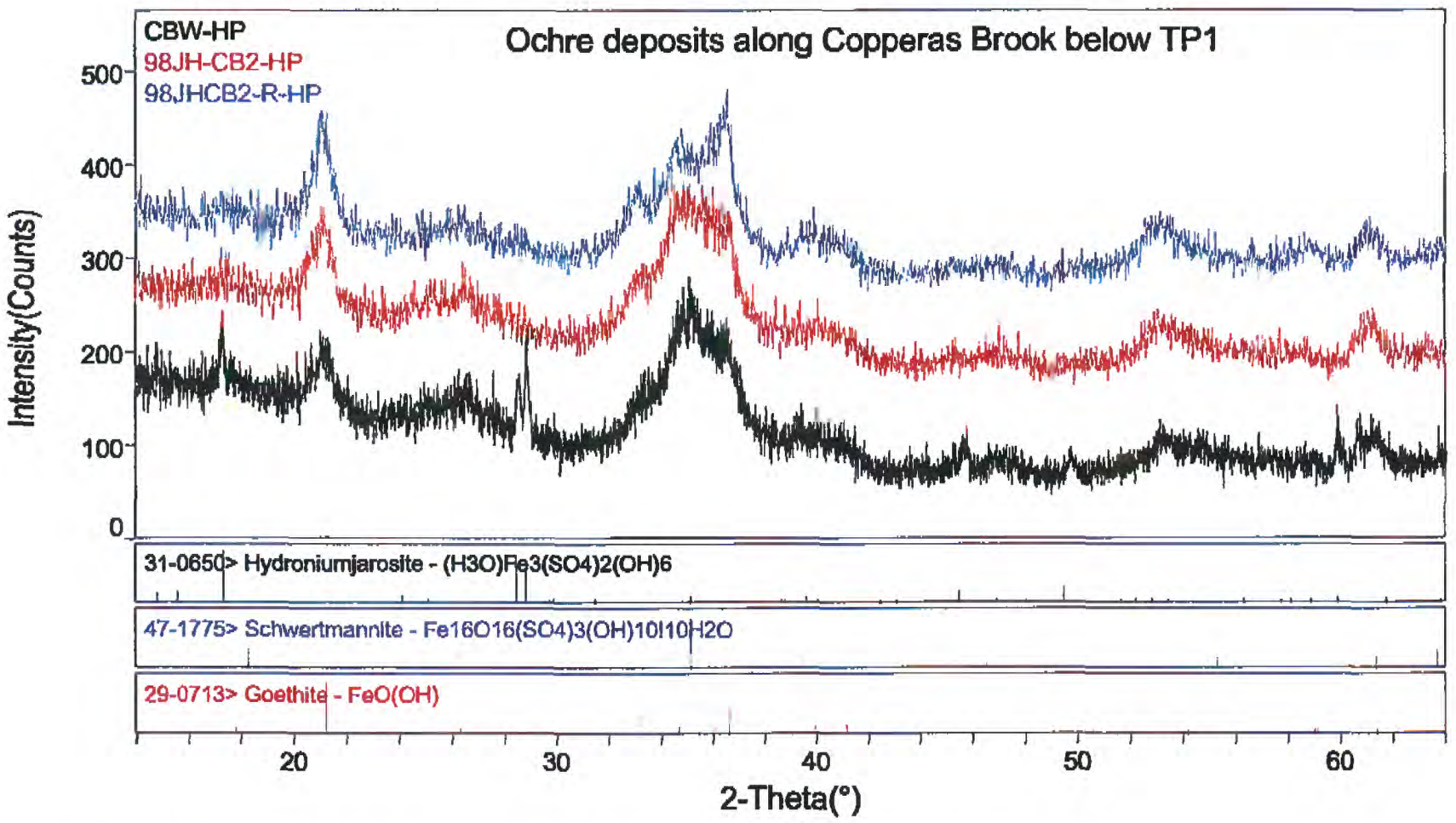

Figure 15. X-ray powder diffraction patterns. A, "Snowballs" of white efflorescent salts coating weathered ore on TP3-F. Comparison with standard reference patterns (stick diagrams) shows that the snowballs are a mixture of rozenite and melanterite. SEM data confirms that Fe and S are the major components of the minerals. B, Iron minerals in ochre deposits along Copperas Brook below TP1.

Table 10. Ochres.

A. Sample key, descriptions, and water data.

[NA, no water flowing at the site when sampled; n.d., not determined. pH and conductivity were measured in the field; $SO_4^=$, dissolved sulfate in filtered water samples determined by ion chromatography in USGS (Water Resources Division) laboratories in Ocala, FL; EMSG, Elizabeth Mine Study Group sample sites; LIZM, USGS water sample sites; see Barg and others (1999) for locations and other water data for EMSG and USGS sample sites]

Key	Sample no.	Description and mineralogy	Water data		
			pH	conductivity (uS/cm)	$SO_4^=$ (mg/L)
1	98JH-NP-HP1	Hardpan in dry (8/20/98) gully on west side above road.	NA	NA	NA
2	98JH-NP-HP2	Hardpan at headwaters of water that drains into LIZM-13 water site	2.1	5480	3200
3	98JH-NP-HP3	Hardpan above LIZM-12-2 water site; varved layers. XRD shows quartz, mica, feldspar, jarosite, goethite, and hematite.	2.4	3140	210
4	TP-2A-HP	Hardpan at base of TP2 (not part of TP2-1 profile) ; dug out section that showed cemented black tailings (A) at base overlain by 0.6 cm of gray mica , 2.5 cm of yellow clay, earthy orange soil, hardpan (E), and orange soil at uppermost surface). XRD shows pyrrhotite, mica, and chlorite.	NA	NA	NA
5	TP2-E-HP	Hardpan at base of TP2 (not part of TP2-1 profile) ; dug out section that showed cemented black tailings (A) at base overlain by 0.6 cm of gray mica, 2.5 cm of yellow clay, earthy orange soil, hardpan (E), and orange soil at uppermost surface. Hardpan contains the heavy minerals rutile, spessartine, and mica (no sulfides detected by XRD).	NA	NA	NA
6	98JH-TP1-HP	Hardpan forming on surface of TP1 at stream that feeds the tailings pond. Heavy minerals include pyrrhotite, mica, chlorite.	n.d.	n.d.	n.d.
7	LIZM-4A-HP	Yellow-orange 1/4" thick piecrust terraced hardpan at E edge of cattails below LIZM-4-2 water sample site; cut with knife to sample	6.8	2790	600
8	LIZM-4B-HP	Yellowboy in stream below LIZM-4-2 water sample site-wet when sampled	6.8	2790	600
9	LIZM-4-HP	Protohardpan at LIZM-4-2 water site - looks hard but you sink in when you step on it	6.8	2790	600
10	LIZM-6-HP	Red area of big hardpan terraced seep draining north edge of TP1 at seep water sample site LIZM-6-2. XRD shows gypsum, goethite, and jarosite.	6.5	3460	1900
11	LIZM-7-HP	Red to black hardpan edges forming at red seep at base of TP1 (near western edge) at water sample site LIZM-7-2.	6.1	4410	2900
12	98JHCBW-HP	Hardpan terraces with leaves above LIZM-18-2 along west tributary of Copperas Brook just below wetland. XRD shows schwertmannite, goethite, quartz.	n.d.	n.d.	n.d.

Key	Sample no.	Description and mineralogy		Water data	
13	98JHCB1-HP	Hardpan in eastern tributary of Copperas Brook a few m above confluence with drainage from LIZM-18-2. XRD shows goethite, schwertmannite, quartz, plagioclase, and minor jarosite. Schwertmannite forms a thin surface layer on goethite.	n.d.	n.d.	n.d.
14	LIZM-18-2-HP	Hardpan at LIZM-18-2 USGS water site. XRD shows quartz, mica, and goethite.	3.1	4410	3000
15	98JH-CB2-HP	Hardpan in Copperas Brook at flag "8" (EMSG H2 water site) downstream from LIZM-18-2 USGS water site.	3.1	4410	1380
16	98JHCB2-R-HP	Hardpan in Copperas Brook at waterfalls just above confluence with W. Ompompanoosuc River at water sample site LZCB-1-2. XRD shows goethite and schwertmannite.	2.7	3600	1900
17	AV-HP	Hardpan at air shaft site along the West Branch of the Ompompanoosuc River (USGS water sample site LZAS).	5.0	984	540
18	AV	White slime precipitate coating the grate at the air shaft vent at water sample site LZAS. Broad, indistinct XRD pattern, may be consistent with aluminite.	5.0	984	540
19	LIZM6	Yellow, clayey layer at base of TP1 above seep LIZM-6-2. Nearly pure jarosite (minor quartz).	NA	NA	NA

Table 10. Ochres.

B. Geochemical data.

[See Appendix B for explanation of methods. n.d., not determined; LOI, loss on ignition; $C=CO_2$, carbonate carbon; BM, total base metal concentration in ppm.]

			North Pit Area (TP3)			TP2		TP1		Seeps	
	Key		1	2	3	4	5	6	7	8	9
Element	Method	Units				Major elements					
Al	ICP-AES	%	3.29	3.83	2.93	7.08	3.33	4.22	1.36	1.28	1.11
Al	ICP-MS	%	2.6	3.2	2.6	6.1	2.6	3.4	1.3	0.97	0.99
Ca	ICP-AES	%	0.46	0.34	0.35	1.64	0.57	1.23	0.28	0.42	2.14
Ca	ICP-MS	%	0.5	0.4	0.4	1.5	0.53	1.2	0.4	0.4	2.2
Fe	ICP-AES	%	26.2	21.8	24.4	9.39	26	11.4	>30	>30	>30
Fe	ICP-MS	%	25	22	20	9.1	25	11	29	38	40
K	ICP-AES	%	1.03	1.4	0.88	1.46	1.86	0.89	1.13	1.21	0.3
K	ICP-MS	%	0.85	1.2	0.7	1.3	1.7	0.77	1	1	0.28
Mg	ICP-AES	%	0.45	0.67	0.25	1.77	0.76	0.63	0.2	0.19	0.4
Mg	ICP-MS	%	0.4	0.65	0.25	1.7	0.62	0.5	0.23	0.16	0.4
Na	ICP-AES	%	0.67	0.46	0.87	1.61	1.05	1.26	0.38	0.49	0.19
Na	ICP-MS	%	0.7	0.55	1	1.7	1.1	1.3	0.54	0.5	0.24
P	ICP-AES	%	0.05	0.04	0.03	0.05	0.02	<0.01	<0.01	0.03	<0.01
Si	ICP-AES	%	16.7	19.3	17.6	25.4	14.9	26.1	6.5	7.07	5.73
Ti	ICP-AES	%	0.26	0.38	0.2	0.44	0.32	0.49	0.2	0.15	0.09
						Minor elements					
Ag	ICP-MS	ppm	0.36	0.52	1.5	0.51	0.58	0.14	0.22	0.37	0.45
As	ICP-MS	ppm	4	1	10	3	5	3	2	2	2
Au	GFAA	ppm	0.01	0.011	0.027	0.014	0.015	0.009	0.016	0.014	0.017
Ba	ICP-AES	ppm	170	229	59	82	38	65	29	32	62
Ba	ICP-MS	ppm	190	280	61	100	47	74	43	35	76
Be	ICP-MS	ppm	0.8	0.4	0.3	0.9	0.2	0.6	0.3	0.2	0.2
Cd	ICP-MS	ppm	0.3	0.4	0.8	3.3	<0.1	0.5	<0.1	<0.1	6.2
Co	ICP-MS	ppm	11	11	24	160	3.6	18	7	8.6	99
Cr	ICP-AES	ppm	60	77	55	173	109	64	39	38	27
Cr	ICP-MS	ppm	57	81	48	160	96	48	22	22	24
Cu	ICP-MS	ppm	930	1200	620	4600	220	220	73	150	190
Hg	CVAC	ppm	0.05	0.03	0.26	<0.02	0.06	0.03	27.8	0.03	0.03
Mn	ICP-AES	ppm	259	458	220	458	310	441	213	145	907
Mn	ICP-MS	ppm	220	430	210	430	280	380	280	100	460
Nb	ICP-AES	ppm	<10	<10	<10	<10	<10	<10	<10	<10	<10
Ni	ICP-MS	ppm	12	12	6	45	1.2	5.4	2.8	2.3	28
Pb	ICP-MS	ppm	16	38	42	45	21	25	13	15	8.1
Sb	ICP-MS	ppm	<0.1	<0.1	<0.1	<0.1	<0.1	<0.1	<0.1	<0.1	<0.1
Sr	ICP-AES	ppm	99	63	74	48	66	50	35	116	99
Tl	ICP-MS	ppm	0.4	0.4	0.4	0.7	0.5	0.3	0.2	0.2	0.2
V	ICP-MS	ppm	73	81	73	98	86	59	31	56	22
Y	ICP-AES	ppm	<10	<10	<10	11	<10	10	<10	<10	20
Zn	ICP-MS	ppm	80	200	300	490	86	220	100	98	870
Zr	ICP-AES	ppm	110	107	47	91	47	71	42	28	37

			North Pit Area (TP3)				TP2	TP1	Seeps		
			Carbon, water, and total sulfur								
Total C	LECO	%	0.56	0.56	0.27	0.07	0.14	0.15	1.11	0.49	2.7
$C=CO_2$	LECO	%	<0.003	<0.003	<0.003	<0.003	0.01	0.01	0.02	0.01	0.62
$C_{organic}$	LECO	%	0.56	0.56	0.27	0.07	0.13	0.14	1.09	0.48	2.08
CO_2	LECO	%	0.01	0.01	0.01	0.01	0.03	0.02	0.08	0.03	2.28
Total S	LECO	%	1.95	1.36	1.94	6.04	4.11	2.37	5.6	4.9	3.82
			Selected metal ratios and calculated parameters								
BM			1,049	1,461	993	5,343	332	489	196	274	1,201
Cu/BM			0.89	0.82	0.62	0.86	0.66	0.45	0.37	0.55	0.16
Zn/BM			0.08	0.14	0.30	0.09	0.26	0.45	0.51	0.36	0.72
Pb/BM			0.02	0.03	0.04	0.01	0.06	0.05	0.07	0.05	0.01
Cu/Zn			11.6	6.0	2.1	9.4	2.6	1.0	0.7	1.5	0.2
Fe/Al			9.6	6.9	7.7	1.5	9.6	3.2	22.3	39.2	40.4

Table 10B. Continued.

			Seeps			Copperas Brook				Air vent	
	Key		10	11	12	13	14	15	16	17	18
Element	Method	Units				Major elements					
Al	ICP-AES	%	0.35	1.56	n.d.	n.d.	0.2	0.09	n.d.	4.59	n.d.
Al	ICP-MS	%	0.3	1.5	0.13	1.8	0.4	0.06	0.04	4	2.1
Ca	ICP-AES	%	0.69	0.71	n.d.	n.d.	0.07	0.06	n.d.	1.23	n.d.
Ca	ICP-MS	%	0.63	0.7	0.1	0.54	0.2	0.06	0.05	1.2	0.05
Fe	ICP-AES	%	>30	>30	n.d.	n.d.	>30	>30	n.d.	14	n.d.
Fe	ICP-MS	%	46	34	41	33	38	40	41	14	44
K	ICP-AES	%	0.11	0.79	n.d.	n.d.	0.08	0.03	n.d.	0.57	n.d.
K	ICP-MS	%	0.1	0.74	0.12	0.4	0.2	0.02	0.03	0.52	0.06
Mg	ICP-AES	%	0.08	0.14	n.d.	n.d.	0.05	0.01	n.d.	0.77	n.d.
Mg	ICP-MS	%	0.09	0.15	0.06	0.33	0.1	0.02	0.02	0.75	0.04
Na	ICP-AES	%	0.05	0.37	n.d.	n.d.	0.01	<0.01	n.d.	0.6	n.d.
Na	ICP-MS	%	0.08	0.49	0.03	0.38	0.13	0.01	0.01	0.67	<0.01
P	ICP-AES	%	<0.01	<0.01	n.d.	n.d.	<0.01	<0.01	n.d.	0.04	n.d.
Si	ICP-AES	%	4.16	9.89	n.d.	n.d.	0.92	0.44	n.d.	28.3	n.d.
Ti	ICP-AES	%	0.03	0.19	n.d.	n.d.	0.05	0.03	n.d.	0.48	n.d.
						Minor elements					
Ag	ICP-MS	ppm	0.25	1	0.2	0.48	0.2	0.14	0.28	0.45	0.43
As	ICP-MS	ppm	<0.5	5.7	3	2	0.5	<0.5	1	2	1
Au	GFAA	ppm	0.008	0.027	n.d.	n.d.	0.033	0.007	n.d.	0.065	n.d.
Ba	ICP-AES	ppm	32	39	n.d.	n.d.	<10	<10	n.d.	138	n.d.
Ba	ICP-MS	ppm	30	53	7	120	19	4	4	150	8
Be	ICP-MS	ppm	0.1	0.2	<0.1	0.6	<0.1	<0.1	<0.1	1.6	0.4
Bi	ICP-MS	ppm	n.d.	n.d.	0.1	0.3	n.d.	n.d.	0.05	n.d.	n.d.
Cd	ICP-MS	ppm	0.2	0.1	<0.1	<0.1	<0.1	<0.1	<0.1	0.3	4
Ce	ICP-MS	ppm	n.d.	n.d.	0.8	13	n.d.	n.d.	0.9	n.d.	n.d.
Co	ICP-MS	ppm	4.1	12	0.69	4.4	2.4	0.5	0.3	86	100
Cr	ICP-AES	ppm	<10	25	n.d.	n.d.	10	13	n.d.	57	n.d.
Cr	ICP-MS	ppm	5	24	6	52	18	10	10	48	42
Cs	ICP-MS	ppm	n.d.	n.d.	< 0.1	1.8	n.d.	n.d.	< 0.1	n.d.	n.d.
Cu	ICP-MS	ppm	100	60	23	530	110	92	180	300	1500
Ga	ICP-MS	ppm	n.d.	n.d.	1	5.9	n.d.	n.d.	0.7	n.d.	n.d.
Ge	ICP-MS	ppm	n.d.	n.d.	0.3	0.6	n.d.	n.d.	0.3	n.d.	n.d.
Hg	CVAC	ppm	<0.02	0.04	<0.02	<0.02	<0.02	<0.02	<0.02	<0.02	n.d.
In	ICP-MS	ppm	n.d.	n.d.	< 0.1	< 0.1	n.d.	n.d.	< 0.1	n.d.	n.d.
La	ICP-MS	ppm	n.d.	n.d.	0.5	6.5	n.d.	n.d.	0.5	n.d.	n.d.
Li	ICP-MS	ppm	n.d.	n.d.	0.6	14	n.d.	n.d.	< 0.5	n.d.	n.d.
Mn	ICP-AES	ppm	230	184	n.d.	n.d.	<100	<100	n.d.	5580	n.d.
Mn	ICP-MS	ppm	170	170	23	190	78	34	16	5600	38
Mo	ICP-MS	ppm	n.d.	n.d.	1.2	1.6	n.d.	n.d.	0.6	n.d.	n.d.
Nb	ICP-AES	ppm	<10	<10	n.d.	n.d.	<10	<10	n.d.	403	n.d.
Nb	ICP-MS	ppm	n.d.	n.d.	< 0.2	3.9	n.d.	n.d.	0.2	n.d.	n.d.
Ni	ICP-MS	ppm	1.6	3	<2	8.2	4	0.58	<2	19	45
Pb	ICP-MS	ppm	2.6	20	2.3	13	3.6	1	1.4	10	8.5
Rb	ICP-MS	ppm	n.d.	n.d.	2.5	25	n.d.	n.d.	1.2	n.d.	n.d.
Sb	ICP-MS	ppm	<0.1	<0.1	<0.1	<0.1	<0.1	<0.1	<0.1	0.2	<0.1

			Seeps			Copperas Brook				Air vent	
Sc	ICP-MS	ppm	n.d.	n.d.	< 0.5	4	n.d.	n.d.	< 0.5	n.d.	n.d.
Se	ICP-MS	ppm	n.d.	n.d.	4	5	n.d.	n.d.	3	n.d.	n.d.
Sr	ICP-AES	ppm	40	26	n.d.	n.d.	<10	<10	n.d.	129	n.d.
Sr	ICP-MS	ppm	n.d.	n.d.	7.4	71	n.d.	n.d.	3.2	n.d.	n.d.
Te	ICP-MS	ppm	n.d.	n.d.	< 0.1	< 0.1	n.d.	n.d.	< 0.1	n.d.	n.d.
Th	ICP-MS	ppm	n.d.	n.d.	0.2	3	n.d.	n.d.	0.29	n.d.	n.d.
Tl	ICP-MS	ppm	<0.1	0.3	<0.1	<0.1	<0.1	<0.1	<0.1	0.2	<0.1
U	ICP-MS	ppm	n.d.	n.d.	< 0.05	0.4	n.d.	n.d.	< 0.05	n.d.	n.d.
V	ICP-MS	ppm	6	32	12	38	14	8	7	65	5
Y	ICP-AES	ppm	11	37	n.d.	n.d.	<10	<10	n.d.	33	n.d.
Y	ICP-MS	ppm	n.d.	n.d.	0.4	6.2	n.d.	n.d.	0.5	n.d.	n.d.
Zn	ICP-MS	ppm	46	180	20	46	31	9	< 8	180	1400
Zr	ICP-AES	ppm	22	48	n.d.	n.d.	18	13	n.d.	95	n.d.
						Carbon, water, and total sulfur					
Total C	LECO	%	0.93	0.83	0.61	0.62	0.47	0.29	0.26	0.72	n.d.
$C = CO_2$	LECO	%	0.21	0.12	<0.003	<0.003	0.01	0.01	<0.003	0.06	n.d.
$C_{organic}$	LECO	%	0.72	0.71	0.61	0.62	0.46	0.28	0.26	0.66	n.d.
CO_2	LECO	%	0.78	0.45	0.01	0.01	0.04	0.03	<0.01	0.22	n.d.
H_2O	LECO	%	n.d.	n.d.	22.3	14.9	n.d.	n.d.	21.3	n.d.	n.d.
H_2O-	LECO	%	n.d.	n.d.	8.7	5.1	n.d.	n.d.	8.2	n.d.	n.d.
H_2O+	LECO	%	n.d.	n.d.	13.6	9.8	n.d.	n.d.	13.1	n.d.	n.d.
Total S	LECO	%	0.74	2.5	5.49	2.97	5.31	5.15	4.93	0.44	n.d.
						Selected metal ratios and calculated parameters					
BM			155	275	46	602	151	103	182	595	3058
Cu/BM			0.65	0.22	0.50	0.88	0.73	0.89	0.99	0.50	0.49
Zn/BM			0.30	0.65	0.43	0.08	0.21	0.09	--	0.30	0.46
Pb/BM			0.02	0.07	0.05	0.02	0.02	0.01	0.01	0.02	0.00
Cu/Zn			2.2	0.3	1.2	11.5	3.5	10.2	--	1.7	1.1
Fe/Al			153.3	22.7	315.4	18.3	95.0	666.7	1025.0	3.5	21.0

Table 10. Ochres.

C. Geochemical data for yellow, jarosite-rich material at the base of TP1 (sample LIZM6)

[See Appendix B for explanation of methods. n.d., not determined; LOI, loss on ignition; $C{=}CO_2$, carbonate carbon; $FeTO_3$, total iron reported as Fe_2O_3; BM, total base metal concentration in ppm.]

Major elements (as oxides)				Metals and minor elements			
Element	Method	Units		Element	Method	Units	
SiO_2	WD-XRF	%	11.1	Ag	ICP-MS	ppm	1
Al_2O_3	WD-XRF	%	1.76	As	ICP-MS	ppm	2
FeTO3	WD-XRF	%	42.2	Ba	ICP-MS	ppm	25
MgO	WD-XRF	%	0.22	Be	ICP-MS	ppm	0.2
CaO	WD-XRF	%	<0.03	Bi	ICP-MS	ppm	0.4
Na_2O	WD-XRF	%	0.33	Cd	ICP-MS	ppm	<0.1
K_2O	WD-XRF	%	0.92	Ce	ICP-MS	ppm	2.6
TiO_2	WD-XRF	%	5.26	Co	ICP-MS	ppm	5.2
P_2O_5	WD-XRF	%	0.31	Cr	ICP-MS	ppm	11
MnO	WD-XRF	%	<0.14	Cs	ICP-MS	ppm	0.8
LOI	WD-XRF	%	33.7	Cu	ICP-MS	ppm	60
Total			95.8	Ga	ICP-MS	ppm	2
	Volatiles			Ge	ICP-MS	ppm	0.4
Total C	LECO	%	0.12	Hg	CVAC	ppm	<0.02
$C{=}CO_2$	LECO	%	<0.003	In	ICP-MS	ppm	< 0.1
CO_2	LECO	%	<0.01	La	ICP-MS	ppm	2.3
$C_{organic}$	LECO	%	0.12	Li	ICP-MS	ppm	2.9
				Mn	ICP-MS	ppm	110
Total S	LECO	%	10.6	Mo	ICP-MS	ppm	3.2
				Nb	ICP-MS	ppm	0.7
Total H_2O	LECO	%	12.1	Ni	ICP-MS	ppm	<2
H_2O^-	LECO	%	0.3	Pb	ICP-MS	ppm	11
H_2O^+	LECO	%	11.8	Rb	ICP-MS	ppm	57
	Major elements			Sb	ICP-MS	ppm	<0.1
Al	ICP-MS	%	0.84	Sc	ICP-MS	ppm	2
Ca	ICP-MS	%	0.2	Se	ICP-MS	ppm	7
Fe	ICP-MS	%	28	Sr	ICP-MS	ppm	290
K	ICP-MS	%	3.7	Te	ICP-MS	ppm	< 0.1
Mg	ICP-MS	%	0.1	Th	ICP-MS	ppm	0.21
Na	ICP-MS	%	0.69	Tl	ICP-MS	ppm	<0.1
	Selected ratios			U	ICP-MS	ppm	0.1
Base metals		ppm	129	V	ICP-MS	ppm	18
				Y	ICP-MS	ppm	1.9
Cu/BM			0.46	Zn	ICP-MS	ppm	53
Zn/BM			0.41				
Pb/BM			0.09				

A

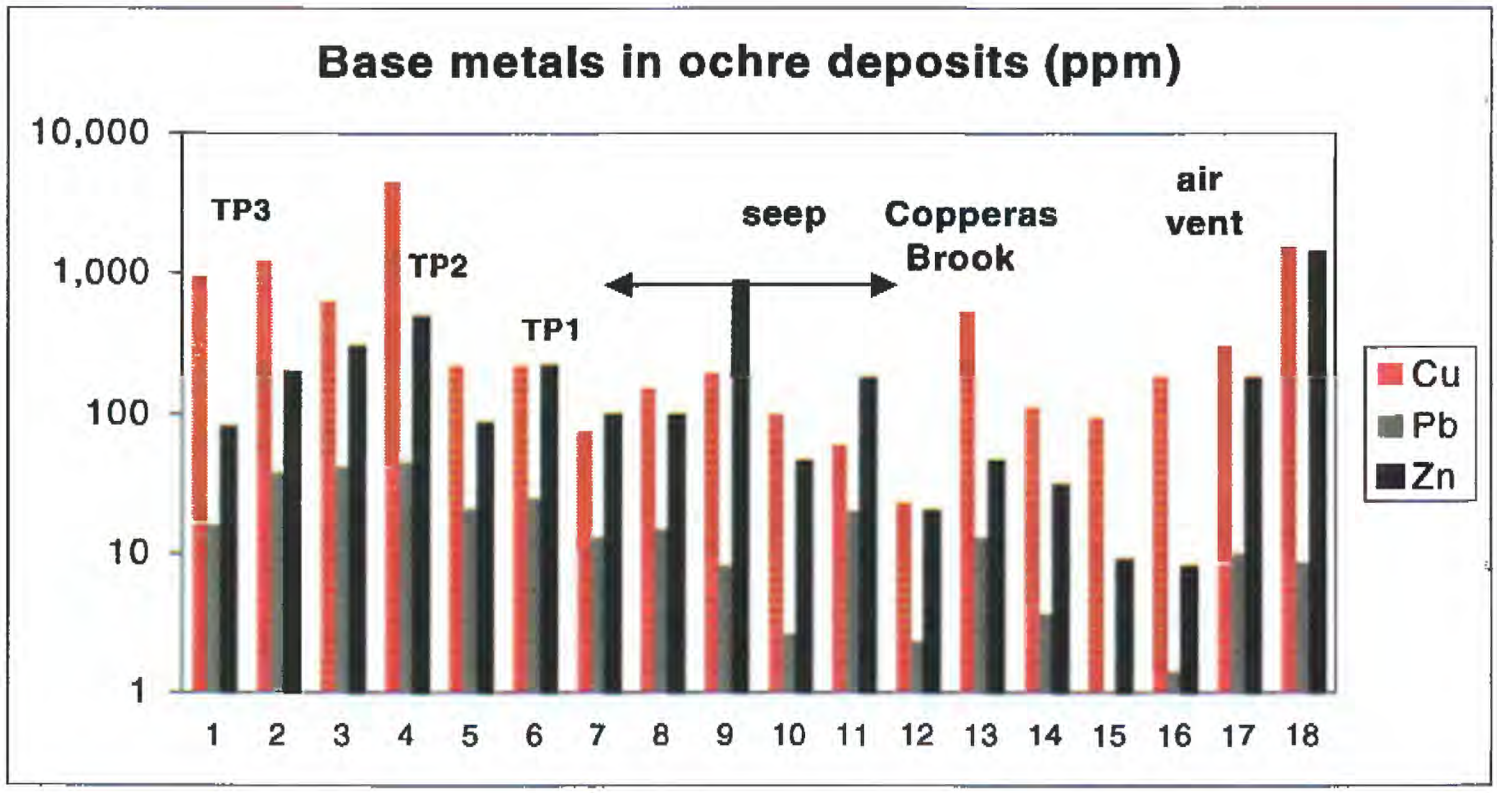

B

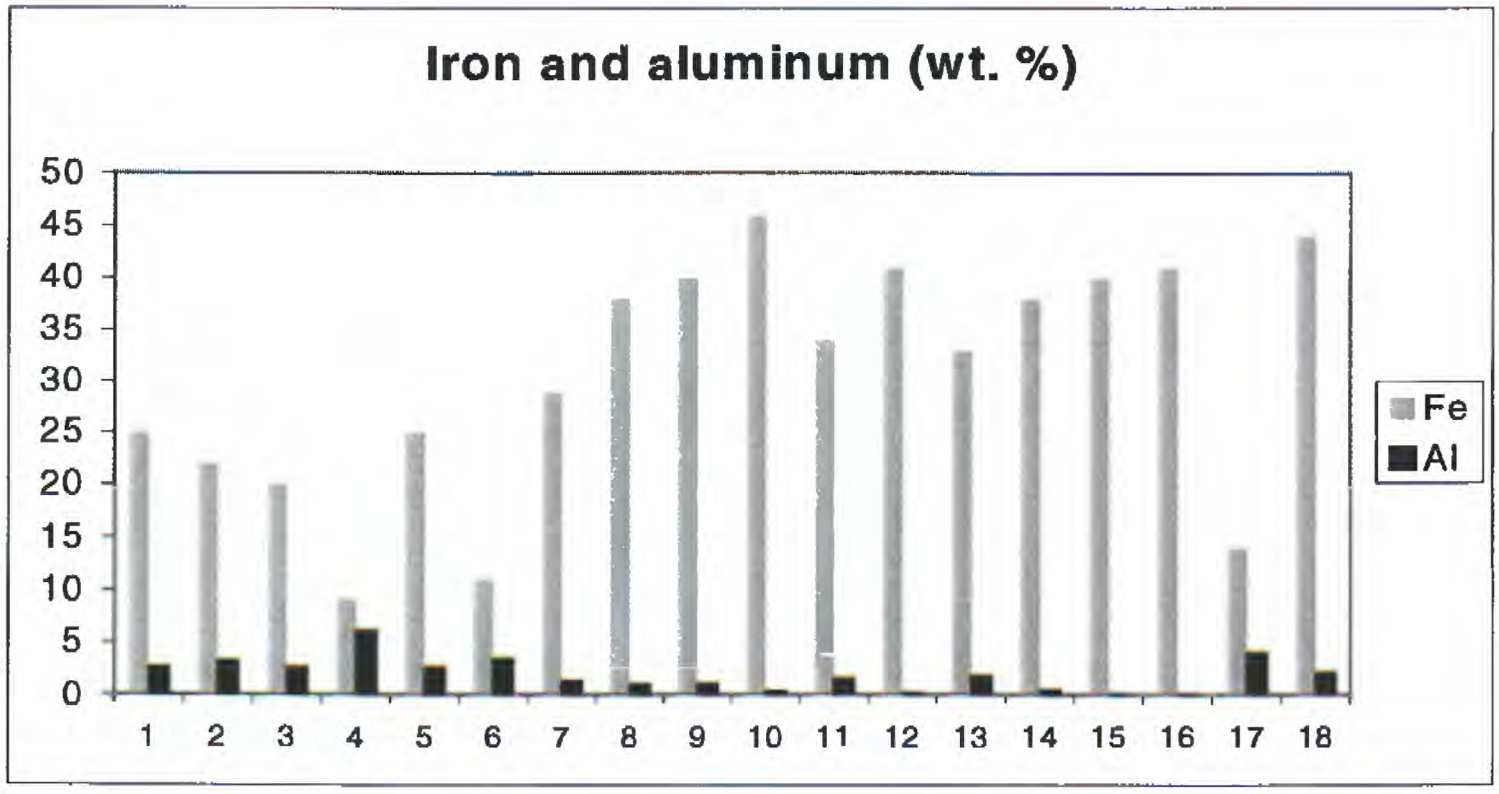

Figure 16. Bar graphs showing chemical variations in ochre deposits associated with tailings, seeps, surface waters, and ground water discharge at the air shaft. See table 10A for key to sample numbers listed along the x-axis of the charts. A, Base metals. B, Iron and aluminum.

IMPLICATIONS FOR REMEDIATION

The pyrrhotite-rich nature of the ore and tailings in the mine area should be considered in any reclamation planning. Pyrrhotite weathers faster than pyrite, but does not generate as much acid as an equal volume of pyrite. However, some pyrite occurs in the ore and tailings. This study demonstrates that pyrrhotite at Elizabeth is actively oxidizing to marcasite, which is chemically identical to, and more reactive than, pyrite. Although some acidity may be consumed in this alteration process, once the pyrite is formed it has the potential to produce huge amounts of acidity. Complete oxidation of pyrrhotite having the composition observed at Elizabeth produces 0.22 moles of acidity (H^+) for every mole of pyrrhotite oxidized. Given the very large volumes of unoxidized tailings and the fine-grained nature of the tailings, the potential for further acid generation is great. Any activities that would promote oxidation, such as moving the large volumes of fine-grained pyrrhotite-rich tailings on TP1 and TP2, could exacerbate the problem. Damp or wet, unoxidized, black tailings develop efflorescent salt crusts in a matter of hours to days when exposed to air. Tailings are chemically and texturally heterogeneous, both laterally across the mine area and vertically within waste piles. Concentrations of base metals and total sulfur in unoxidized black tailings can exceed 3 % and 10 %, respectively. Locally, zinc exceeds copper in tailings; lead concentrations are uniformly low, reflecting the low lead content of the ore.

The fact that near-neutral waters emanate from the base of TP1 suggests that flow through TP1 is not the main cause of acid drainage in Copperas Brook downstream. Once the waters leave the pile, however, dissolved ferrous iron oxidizes and hydrolyzes to produce acid and form the distinctive red, orange, and yellow ferric iron minerals that accumulate as ochre deposits and coat the streambed all the way to the West Branch of the Ompompanoosuc River; zinc tends to accumulate in these ochre deposits. This "natural" process that has developed at Elizabeth is analogous to ochre precipitation and metal sequestration accomplished by raising the pH of acidic streams via limestone amendment or other remediation methods. The abundance of organic debris may be fortuitous or may facilitate ochre formation in seep areas and promote local reduction. Ochres occur within tailings as hardpan layers that may represent paleosurfaces; such layers have been shown to limit diffusion of oxygen in other tailings piles by Blowes and others (1994).

The base metal, iron, and total sulfur content of the surface soils on TP3 is much higher than on the more recent tailings (TP1 and TP2) due to efficiency of the more modern mineral processing. Tailings of TP1 and TP2 are finer-grained and richer in aluminum, which can be a problem in establishing vegetation. Jarosite and gypsum layers within TP1 probably represent chemical residues from the flotation process that were discharged onto the pyrrhotite-rich tailings at different times as the pile was built up.

Surface runoff from acidic and metal-rich soils on TP3 and dissolution of efflorescent salt minerals that coat all tailings surfaces are important factors to consider in developing a viable remediation plan. A number of different, highly soluble efflorescent salt minerals form on the site and recycle iron, aluminum, copper, sulfur and other elements from solid phases to the aquatic ecosystem depending on weather conditions. Critical considerations for development of effective strategies to improve water quality in Copperas Brook include (1) the role that these salts play, and (2) the potential for exacerbating salt development if the large volumes of fine-grained tailings buried beneath a shallow (less than a meter thick in most places), deeply eroded oxidized cover become exposed to wet/dry cycles and air.

ACKNOWLEDGMENTS

We would like to thank Bob Walker, coordinator of the Elizabeth Mine Study Group, and other members of the group for welcoming our participation in this study and for arranging site access. We also thank the landowners, Leonard Cook, Richard Josler, and Ted Zagaeski for permitting us on the site. Johnny Johnsson, mining historian, provided historic references on the Elizabeth mine. John Slack, USGS, kindly allowed us to incorporate his unpublished geochemical data on Elizabeth mine ore samples, and supplied background information on the mine. Harvey Belkin, USGS, gave advice on SEM sample preparation and analysis.

Helen Folger, USGS, and John Slack, USGS, reviewed a draft of this report and provided many helpful suggestions. Adam Johnson assisted with final compilation.

REFERENCES

Adrian, B.M., Arbogast, D.F., Detra, D.E., and Mays, R.E., 1990, Direct-current arc emission spectrographic method for the semiquantitative analysis of rock, stream-sediment, soil, and heavy-mineral-concentrate samples, *in* Arbogast, B.F., ed., Quality assurance manual for the Branch of Geochemistry, U.S. Geological Survey: U.S.;Geological Survey Open-File Report 90-668, p. 100-106.

Anderson, C.S., 1931, Mining and milling in the Vermont copper district: Engineering and Mining Journal, v. 131, p. 208-210.

Annis, M.P., Slack, J.F., and Rolph, A.L., 1983, Stratabound massive sulphide deposits of the Elizabeth mine, Orange County, Vermont, *in* Sangster, D.F., ed. , Field trip guidebook to stratabound sulphide deposits, Bathurst area, N.B., Canada and west-central New England, U.S.A.: Geological Survey of Canada, Miscellaneous Report 36, p. 41-51.

Arbogast, B.F., 1996, Analytical methods manual for the Mineral Resource Surveys Program, U.S. Geological Survey: U.S. Geological Survey Open- File Report 96-525.

Barg, L.D., McLeary, Eric, and Kepler, Doug (Step by Step & Damariscotta), 1999, Hydrologic characterization and remediation options for the Elizabeth mine, South Strafford, Vermont: Unpublished Report prepared for the Elizabeth Mine Study Group, 57 p.

Barth, R.C., 1984, Water quality implications and control techniques associated with the proposed Union Village hydroelectric project: Unpublished report prepared by the Colorado School of Mines Research Institute, 32 p.

Benson, C.B., Wangaard, J.C., and Johnson, H.A., 1950, Elizabeth mine reorganized for efficient production: Mining Congress Journal, v. 36, no. 7, p. 18-23.

Bigham, J.M., 1994, Mineralogy of ochre deposits formed by sulfide oxidation, *in* Jambor, J.L., and Blowes, D.W., eds., 1994, The environmental geochemistry of sulfide mine-wastes: Mineralogical Association of Canada, Short Course Handbook, v. 22, p. 103-132.

Blowes, D.W., Ptacek, C.J., and Jambor, J.L., 1994, Remediation and prevention of low-quality drainage from tailings impoundments, *in* Jambor, J,L., and Blowes, D.W., eds., 1994, The environmental geochemistry of sulfide mine-wastes: Mineralogical Association of Canada, Short Course Handbook, v. 22, p. 365-379.

Canney, F.C., 1965, Geochemical prospecting investigations in the copper belt of Vermont: U.S. Geological Survey Bulletin 1198-B, 28 p.

Crock, J.G., Lichte, F.E., and Briggs, P.H., 1983, Determination of elements in National Bureau of Standards geological reference materials SRM 278 obsidian and SRM 688 basalt by inductively coupled plasma-atomic emission spectroscopy: Geostandards Newsletter, v. 7, no. 2, p. 335-340.

Dagenhart, T.V., Jr., 1980, The acid mine drainage of Contrary Creek, Loiuisa County, Virginia - Factors causing variations in stream water chemistry: University of Virginia, M.S. Thesis, 215 p.

Department of the Army, 1989, Hydraulic evaluation and revegetation study for the Elizabeth mine site, Vermont: Report prepared for the State of Vermont by the New England Division, Corps of Engineers, Waltham, MA, 35 p.

Di Toro, D.M., Mahoney, J.D., Hansen, D.J., Scott, K.J., Hicks, M.B., Mays, S.M., and Redmond, M.S., 1990, Toxicity of cadmium in sediments - The role of acid-volatile sulfide: Environmental Toxicology and Chemistry, v. 9, p. 1487-1502.

Environmental Protection Agency, 1997, The incidence and severity of sediment contamination in surface waters of the United States. Volume 1: National stream sediment survey: EPA-823-R-97-006.

Fay, A.H., 1909, The Vermont Copper Co.: Engineering and Mining Journal, v. 88, p. 364-365.

Ferris, F.G., Tazaki, K., and Fyfe, W.S., 1989, Iron oxides in acid mine drainage environments and their association with bacteria: Chemical Geology, v. 74, p. 321-330.

Fortescue, J.A.C., 1992, Landscape geochemistry: Retrospect and prospect-1990: Applied Geochemistry, v. 7, p. 1-53.

Gair, J.E., and Slack, J.F., 1980, Stratabound massive sulfide deposits of the U.S. Appalachians, *in*

Vokes, F.M. , and Zachrisson, Ebbe, eds., Review of Caledonian Appalachian stratabound sulphides: Geological Survey of Ireland, Special Paper No. 5, p. 68-81.
Hitchcock, Edward, Hitchcock, Edward, Jr., Haager, A. D., and Hitchcock, C.H., 1861, Report on the geology of Vermont, vol. II, Claremont, N.H..
Howard, P.F., 1959a, Structure and rock alteration at the Elizabeth mine, Vermont. Part I. Structure at the Elizabeth mine: Economic Geology, v. 54, p. 1214-1249.
_____ 1959b, Structure and rock alteration at the Elizabeth mine, Vermont. Part II. Rock alteration at the Elizabeth mine: Economic Geology, v. 54, p. 1414-1443.
_____ 1969, The geology of the Elizabeth mine, Vermont: Vermont Geological Survey, Economic Geology No. 5, 73 p.
Howe, H.M., 1886, The Elizabeth copper mine, Vermont: Engineering and Mining Journal, v. 42, p. 327.
International Centre for Diffraction Data, 1997, Powder Diffraction File Sets 1-47.
Jacobs, E.C., 1944, The Vermont Copper Company, Inc.: Vermont Geological Survey, Report of the State Geologist, 24th, 1943-1944, p. 1-13.
Jambor, J.L., 1994, Mineralogy of sulfide-rich tailings and their oxidation products, *in* Jambor, J.L., and Blowes, D.W., eds., 1994, The environmental geochemistry of sulfide mine-wastes: Mineralogical Association of Canada, Short Course Handbook, v. 22, p. 103-132.
Jambor, J.L., and Blowes, D.W., eds., 1994, The environmental geochemistry of sulfide mine-wastes: Mineralogical Association of Canada, Short Course Handbook, v. 22, 438 p.
Jenks, W.F., 1968, Origin of Vermont copper ores and its bearing on exploration: Society of Mining Engineers, Preprint, 10 p.
Jerez, J.K., and Rimstidt, J.D., 1999, Rate of pyrite oxidation in air (abs.): Geological Society of America, Abstracts with Programs, v. 31, no. 7, p. A-27.
Judson, J.N., 1909, The Vermont Copper Co.: Engineering and Mining Journal, v. 88, p. 524-525.
Kwong, Y.T.J., 1993, Prediction and prevention of acid rock drainage from a geological and mineralogical perspective: Canadian National Hydrology Research Centre Contribution CS-92054, 47 p.
Kwong, Y.T.J. and Lawrence, J.R., 1994, Mineralogical controls of sulfide oxidation: Canadian National Hydrology Research Centre Contribution No. 94010, 87 p.
Lichte, F.E., Meier, A.L., and Crock, J.G., 1987, Determination of rare earth elements in geological materials by inductively coupled plasma mass spectrometry: Analytical Chemistry, v. 59, no. 8, p. 1150-1157.
Long, E.R., MacDonald, D.D., Smith, S.L., and Calder, F.D., 1995, Incidence of adverse biological effects within ranges of chemical concentrations in marine and estuarine sediments: Environmental Management, v. 19, no. 1, p. 81-97.
Lutjen, G.P., and Kearney, J.H., 1953, New life for Vermont's 160 year-old copper mine: Engineering and Mining Journal, v. 154, p. 72-75.
Mandarino, J.A., 1999, Fleischer's glossary of mineral species 1999: The Mineralogical Record, Inc., Tucson, 225 p.
McKinstry, H.E., and Mikkola, A.K., 1954, The Elizabeth copper mine, Vermont: Economic Geology, v. 49, p. 1-20.
Mee, J.S., Siems, D.F., and Taggart, J.E., Jr., 1996, Major element analysis by wavelength dispersive X-ray fluorescence spectrometry, *in* Arbogast, B.F., ed., Analytical methods manual for the Mineral Resource Surveys Program, U.S. Geological Survey: U.S. Geological Survey Open- File Report 96-525, p. 237-242.
Meier, A.L., 1980, Flameless atomic absorption determination of gold in geological materials: Journal of Geochemical Exploration, v. 13, p. 75-85.
Nordstrom, D.K., and Alpers, C.N., 1999, Negative pH, efflorescent mineralogy, and consequences for environmental restoration at the Iron Mountain Superfund site, California: Proceedings of the National Academy of Sciences, v. 96, p. 3455-3462.
Power, M.S. and Milton, N.M., 1990, Detection of geobotanical anomalies associated with mineralization in the Glens Falls 1°x2° quadrangle, *in* Slack, J.F., ed., 1990, Summary results of the Glens Falls CUSMAP project, New York, Vermont, and New Hampshire: U.S. Geological Survey Bulletin

1887, p. I1-I8.
Plumlee, G.S., 1999, The environmental geology of mineral deposits, *in* Plumlee, G.S., and Logsdon, M.J., eds., The environmental geochemistry of mineral deposits, Part A, Processes, techniques, and health issues: Society of Economic Geologists, Reviews in Economic Geology, v. 6A, p. 71-116.
Price, W.A., 1997, DRAFT, Guidelines and recommended methods for the prediction of metal leaching and acid rock drainage at minesites in British Columbia: British Columbia Ministry of Employment and Investment, Energy and Minerals Division, Smithers, BC, 143 p.
Seal, R.R., II, Haffner, D.P., Meier, A.L., Krishnaswamy, Rama, and Hammarstrom, J.M., 1999, Geochemistry of acid mine drainage from the abandoned Elizabeth copper mine, South Strafford, Vermont:(abs.): Geological Society of America, Abstracts with Programs, v. 31, no. 2, p. A-66.
Singer, P.C., and Stumm, W., 1970, Acidic mine drainage: The rate determining step: Science, v. 167, p. 1121-1123.
Slack, J.F., ed., 1990, Summary results of the Glens Falls CUSMAP project, New York, Vermont, and New Hampshire: U.S. Geological Survey Bulletin 1887, Chapters A-R.
Slack, J.F., 1993, Descriptive and grade-tonnage models for Besshi-type massive-sulphide deposits, in Kirkham, R.V., Sinclair, W.D., Thorpe, R.I., and Duke, J.M., eds., Mineral deposit modeling: Geological Association of Canada, Special paper 40, p. 343-371.
Slack, J.F., Atelsek, P.J., and Whitlow, J.W., 1990, Geochemistry of stream sediments and heavy-mineral concentrates from the Orange County Copper District, east-central Vermont, *in* Slack, J.F., ed., 1990, Summary results of the Glens Falls CUSMAP project, New York, Vermont, and New Hampshire: U.S. Geological Survey Bulletin 1887, p. Q1-Q21.
Slack, J.F., Offield, T.W., Shanks, W.C., III, and Woodruff, L.G., 1993, Besshi-type massive sulfide deposits of the Vermont copper belt:: Society of Economic Geologists Guidebook Series , v. 17, p. 32-73.
Slack, J.F., Moore, Roosevelt, Fletcher, J.D., and Aruscavage, P.J., 1986, Trace elements in New England massive sulfide deposits (abs.): Society of Mining Engineers, American Institute of Mining, Metallurgical, and Petroleum Engineers, Program and Abstracts, p. 22.
Smith, K.S., Plumlee, G.S., and Ficklin, W.H., 1994, Predicting water contamination from metal mines and mining wastes: U.S. Geological Survey Open-File Report 94-264, 112 p.
Smyth, H.L., and Smith, P.S., 1904, The copper deposits of Orange County, Vermont: Engineering and Mining Journal, v. 77, p. 677-678.
Taylor, C.D., Zierenberg, R.A., Goldfarb, R.J., Kilburn, J.E., Seal, R.R., II, and Kleinkopf, M.D., 1995, Volcanic-associated massive sulfide deposits, *in* du Bray, E.A., ed., 1995, Preliminary compilation of descriptive geoenvironmental mineral deposit models: U.S. Geological Survey Open-File Report 95-831, p. 137-144.
Weed, W.H., 1904, Notes on the copper mines of Vermont: U.S. Geological Survey Bulletin 225, p. 190-199.
Wheeler, H.W., 1883, Copper deposits of Vermont: Columbia University School of Mines Quarterly, v. 4, p. 219-224.
White, W.S., 1943, Geology of the Elizabeth copper mine, Vermont: U.S. Geological Survey Strategic Mineral Investigations, Open-File Report, 9 p.
White, W.S., and Eric, J.H., 1944, Preliminary report on the geology of the Orange County copper district, Vermont: U.S. Geological Survey Open-File Report, 36 p.
Yapp, J.J. and Poths, Harald, 1986, Carbon in natural goethites: Geochimica et Cosmochimica Acta, v. 50, p. 1213-1220.
Young, Michael, 1991, Elizabeth Mine, Old Mine Road, Strafford, Vermont: EPA ID# VTD988366621, Potential Hazardous Waste Site, Screening Site Inspection conducted by the Hazardous Materials Management Division, Department of Environmental Conservation, Vermont Agency of Natural Resources, 19 p.

APPENDIX A
Sample key for rock, slag, mineral, tailings, and ochre samples.

Sample	Type	Field Description	Latitude (N)			Longitude (W)			Water sample site
		South Pit Area							
SP-R1	rock	Garnet-amphibolite schist with tourmaline from outcrop at corner of N side of haulageway and pit.	43°	48'	58"	72°	20'	20"	
SP-R4	rock	Weathered mica schist.	43°	48'	58"	72°	20'	20"	
SP-Salts1	salts	Thin, white coating - most common salts observed at the site (sampled dry).	43°	48'	58"	72°	20'	20"	
SP-Salts 2	salts	Coarser white salts at protected overhang.	43°	48'	58"	72°	20'	20"	
SP-Salts 3	salts	Thin coatings that cause vertical color band stripes locally on pit wallrock. a, orange; b, blue-white;c, white	43°	48'	58"	72°	20'	20"	
SP-Salts 4	salts	Coarse efflorescent salts on E wall of south end of pit developed over a distance of several vertical feet. Sampled dry (large sample of crusts) and in oil.	43°	48'	58"	72°	20'	20"	
SP-slime	ochre-PPT	Red slime from pit pond surface.	43°	48'	58"	72°	20'	20"	LIZM-11-1
		North Pit Area (Tailings Pile 3)							
NP-HP1	ochre-HP	Hardpan in gully on west side above road	43°	49'	21"	72°	20'	13"	
NP-HP2	ochre-HP	Hardpan at headwaters of water that drains into LIZM-13 water site	43°	49'	13"	72°	20'	11"	LIZM-13
NP-HP3	ochre-HP	Hardpan above LIZM-12-2 water site; varved layers	43°	49'	17"	72°	20'	8"	LIZM-12-2
98JHNPA	soil	North Pit area (tailings pile 3) Pile A . Pile A is the westernmost pile north of the road. Soil composite of yellow-brown surface soil; 30 increments, -8 mesh	43°	49'	18.7"	72°	20'	12.0"	
NP-A-18"	soil	Yellow clay	43°	49'	18.7"	72°	20'	12.0"	
NP-A-31"	soil	Shovel auger	43°	49'	18.7"	72°	20'	12.0"	
NP-A-36"-40"	soil	Shovel auger	43°	49'	18.7"	72°	20'	12.0"	
NP-A-37"	soil	Shovel auger	43°	49'	18.7"	72°	20'	12.0"	
NP-A-61"	soil	Shovel auger	43°	49'	18.7"	72°	20'	12.0"	
98JHNPB	soil	North Pit area (tailings pile 3) Pile B . Pile B is the central area north of the road and appears to be the site of historic ore processing. Surface soil is very inhomogeneous, local blue-green Cu iridescent coatings on slag. Soil composite of red to b	43°	49'	15.1"	72°	20'	12.2"	
NP-B-58"	soil	Bottom of shovel auger sampling in black, sooty soil.	43°	49'	15.1"	72°	20'	12.2"	
98JHNP-B-RS	rock	Red clinker rock on soil surface.	43°	49'	15"	72°	20'	12"	
98JHNB-slag	rock	Black slag rock on surface.	43°	49'	15"	72°	20'	12"	
98JHNPC	soil	North Pit area (tailings pile 3) Pile C . Pile C is the easternmost area north of the road. Surface runoff from this area directly affects surface water sample site LIZM13. Soil composite of red to black surface soil; 30 increments, -8 mesh	43°	49'	12.7"	72°	20'	11"	
NP-C-6"	soil	Shovel auger	43°	49'	12.7"	72°	20'	11"	
NP-C-24"	soil	Shovel auger	43°	49'	12.7"	72°	20'	11"	
NP-C-42"	soil	Shovel auger	43°	49'	12.7"	72°	20'	11"	

APPENDIX A
Sample key for rock, slag, mineral, tailings, and ochre samples.

Sample	Type	Field Description	Latitude (N)			Longitude (W)			Water sample site
NP-C-48"-54"	soil	Shovel auger	43°	49'	12.7"	72°	20'	11"	
NP-C-Salts1	salts	Pale blue-white salts on red tailings just above water sample site LIZM13	43°	49'	13"	72°	20'	11"	LIZM-13
NP-C-Salts2	salts	White, powdery salts on paler part of pile C	43°	49'	13"	72°	20'	11"	
NP-C-Salts3	salts	Salts on outcrop under protected overhang at very south end of North pit	43°	49'	13"	72°	20'	11"	
98JHNPD	soil	Elizabeth Mine North Pit Composite Dump "D":Soil composite, 30 increments, -8 mesh	43°	49'	16.1"	72°	20'	15.8"	
NP-D1	soil	Auger sample 0-6" interval - yellow	43°	49'	16.1"	72°	20'	15.8"	
NP-D2	soil	Auger sample 24-30" interval - brownish	43°	49'	16.1"	72°	20'	15.8"	
NP-D3	soil	Auger sample 42-46" interval - yellow clay	43°	49'	16.1"	72°	20'	15.8"	
NP-D4	soil	Auger sample 48-54" interval - white	43°	49'	16.1"	72°	20'	15.8"	
NP-D5	soil	Auger sample 55-61" interval - orange	43°	49'	16.1"	72°	20'	15.8"	
98JHNPE	soil	Elizabeth Mine North Pit Composite Dump "E":Soil composite, 30 increments, -8 mesh	43°	49'	17.8"	72°	20'	16.2"	
NP-E1	soil	Auger sample 0-6" interval: red soil	43°	49'	17.8"	72°	20'	16.2"	
NP-E2	soil	Auger sample 30-36" interval: gray, ashy zone that appears to be different from white intervals noted in other auger holes	43°	49'	17.8"	72°	20'	16.2"	
NP-E3	soil	Auger sample 55-61" interval: same gray, ashy material as above	43°	49'	17.8"	72°	20'	16.2"	
98JHNPF	soil	Elizabeth Mine North Pit Composite Dump "F":Soil composite, 30 increments, -8 mesh	43°	49'	21.1"	72°	20'	15.0"	
		Tailings pile 2							
TP2-1 (TP2-veg)	soil	Soil composite of partially vegetated, flat top surface of tailings pile 2; 30 increments; -8 mesh	43°	49'	23"	72°	19'	58"	
TP2-1-A	soil	Black unoxidized tailings at 24"; tailings profile exposed by digging a hole with a shovel.	43°	49'	23"	72°	19'	58"	
TP2-1-B	soil	Yellow-green clay layer 1" thick at 23-24" below surface; tailings profile exposed by digging a hole with a shovel.	43°	49'	23"	72°	19'	58"	
TP2-1-C	ochre-HP	Hardpan layer at 22-23" below surface; overlain by 12-22" yellow-orange clay with no roots and 0-11" reddish soil with roots. Soil profile exposed by digging a hole with a shovel.	43°	49'	23"	72°	19'	58"	
TP2-1-D	soil	Yellow-orange clayey soil layer 12 to 22" below surface; below root zone; tailings profile exposed by digging a hole with a shovel.	43°	49'	23"	72°	19'	58"	
TP2-2 (TP2-LS1)	soil	Soil composite of bare, eroded north face slope of tailings pile 2 above tailings pile 1; 30 increments; -8 mesh	43°	49'	25"	72°	19'	51"	

APPENDIX A
Sample key for rock, slag, mineral, tailings, and ochre samples.

Sample	Type	Field Description	Latitude (N)			Longitude (W)			Water sample site
TP-2A-HP	ochre-HP	Hardpan in at base of TP2 (not part of TP2-1 profile) ; dug out section that showed cemented black tailings (A) at base overlain by 1/4" gray mica, 1" yellow clay, earthy orange soil, hardpan (E), and orange soil at uppermost surface)	43°	49'	23"	72°	19'	53"	
TP2-E-HP	ochre-HP	Hardpan at base of TP2 (not part of TP2-1 profile) ; dug out section that showed cemented black tailings (A) at base overlain by 1/4" gray mica, 1" yellow clay, earthy orange soil, hardpan (E), and orange soil at uppermost surface)	43°	49'	23"	72°	19'	53"	
TP2-Salts	salts	White salts ("organpipes") on tailings							
		Tailings pile 1							
98JHTP1-1	soil	Soil composite of bare area on flat top of tailings pile 1 adjacent to the pond; 30 increments; -8 mesh	43°	49'	24	72°	19'	41"	
98JHTP1-2	soil	Soil composite of vegetated area on flat top of tailings pile 1; 30 increments; -8 mesh	43°	49'	31	72°	19'	39"	
98JHTP1-3	soil	Soil composite of steep, eroded north slope face of tailings pile 1; 60 increments; -8 mesh	43°	49'	27"	72°	19'	33"	
TP1-3R	soil	Replicate soil composite of north slope face of sample TP1-3; 60 increments; -8 mesh	43°	49'	27"	72°	19'	33"	
TP1-4 A	soil	Soil profile at north slope edge of TP1 about 1/3 of the way up from the bottom - dug out cross-section: A, black tailings at bottom of profile	43°	49'	27"	72°	19'	33"	
TP1-4B	soil	Soil profile at north slope edge of TP1 about 1/3 of the way up from the bottom - dug out cross-section: B, gray, micaceous layer overlying A	43°	49'	27"	72°	19'	33"	
TP1-4C	soil	Soil profile at north slope edge of TP1 about 1/3 of the way up from the bottom - dug out cross-section: C, yellow clay overlying B	43°	49'	27"	72°	19'	33"	
TP1-4D	soil	Soil profile at north slope edge of TP1 about 1/3 of the way up from the bottom - dug out cross-section: D, hardpan overlying C	43°	49'	27"	72°	19'	33"	
TP1-4E	soil	Soil profile at north slope edge of TP1 about 1/3 of the way up from the bottom - dug out cross-section: E, gray layer overlying D	43°	49'	27"	72°	19'	33"	
TP1-4F	soil	Soil profile at north slope edge of TP1 about 1/3 of the way up from the bottom - dug out cross-section: F, top layer overlying E	43°	49'	27"	72°	19'	33"	
TP1	soil	Black, unoxidized tailings from pond area approx. 6" below surface	43°	49'	31"	72°	19'	42"	
TP1-pond	soil	Bottom sediments from pond on TP1 at southwest edge of pond	43°	49'	31"	72°	19'	42"	
98JH-TP1-HP	ochre-HP	Hardpan forming along edges of stream that feeds tailings pond on tailings pile 1	43°	49	31	72°	19'	42"	
TP1-Salts	salts	Blue salts on damp tailings surface near pond	43°	49'	31"	72°	19'	42"	

APPENDIX A
Sample key for rock, slag, mineral, tailings, and ochre samples.

Sample	Type	Field Description	Latitude (N)			Longitude (W)			Water sample site
TP1-A-12"	soil	Black,unoxidized tailings from 12" below surface at southwest edge of pond	43°	49'	31"	72°	19'	42"	
TP1-MP3-A	soil	Auger profile adjacent to MP3 piezometer; A, 35 to 36" below surface, black unoxidized tailings	43°	49'	31"	72°	19'	42"	
TP1-MP3-B	soil	Auger profile adjacent to MP3 piezometer;B , 24 to 25" below surface, coarser and drier black tailings than underlying sample MP3-A	43°	49'	31"	72°	19'	42"	
TP1-MP3-C	soil	Auger profile adjacent to MP3 piezometer;C, 20 to 21" wetter, fine-grained black tailings	43°	49'	31"	72°	19'	42"	
TP1-MP3-D	soil	Auger profile adjacent to MP3 piezometer; D, 17 to 18" green clay layer	43°	49'	31"	72°	19'	42"	
TP1-MP3-E	soil	Auger profile adjacent to MP3 piezometer;E, 16 to 17" black tailings layer above clay	43°	49'	31"	72°	19'	42"	
TP1-MP3-F	soil	Auger profile adjacent to MP3 piezometer; F, 15 to 16" wet orange clay layer	43°	49'	31"	72°	19'	42"	
TP1-MP3-G	soil	Auger profile adjacent to MP3 piezometer; G, 4 to 5" drier oxidized orange tailings	43°	49'	31"	72°	19'	42"	
		Seeps along the base of tailings pile 1							
LIZM-4-HP	ochre-HP	Protohardpan at LIZM-4 water site - looks hard but you sink in when you step on it	43°	49	33	72°	19'	39"	LIZM-4
LIZM-4A-HP	ochre-HP	Yellow-orange 1/4" thick piecrust terraced hardpan at E edge of cattails at seep along north base of tailings pile 1; cut with knife to sample	43°	49'	33	72°	19'	39"	LIZM-4
LIZM-4A-PPT	ochre-PPT	Yellow slime and red ochre precipitates (slime) at seep along north base of tailings pile 1.	43°	49'	33	72°	19'	39"	LIZM-4
LIZM-4B-HP	ochre-HP	Yellowboy in stream at seep along north base of tailings pile 1; wet when sampled.	43°	49'	33	72°	19'	39"	LIZM-4
LIZM6-HP	ochre-HP	Red area of big hardpan draining tailings pile 1 along north edge.	43°	49'	37	72°	19'	43"	LIZM-6
LIZM-6-clay	soil	Yellow clay above water sample site LIZM-6 along the north base of tailings pile 1.	43°	49'	37	72°	19'	43"	LIZM-6
		Copperas Brook							
LIZM-18-2-HP	ochre-HP	Hardpan at LIZM-18-2 water site; east tributary of Copperas Brook below tailings pile 1.	43°	49'	40"	72°	19'	37"	LIZM-18-2
LIZM-18-2-PPT	ochre-PPT	Slime at LIZM-18-2	43°	49'	40	72°	19'	37"	LIZM-18-2
98JHCB1-HP	ochre-HP	Hardpan in eastern tributary of Copperas Brook, south and east of water sample site LIZM-18-2 in woods.	43°	49'	40"	72°	19'	37"	
CB2-HP	ochre-HP	Hardpan in Copperas Brook just below the confluence of an eastern and western tributary below water sample site LIZM-18-2.	43°	49'	40"	72°	19'	37"	

APPENDIX A

Sample key for rock, slag, mineral, tailings, and ochre samples.

Sample	Type	Field Description	Latitude (N)			Longitude (W)			Water sample site
CB1-PPT	ochre-PPT	Precipitate in Copperas Brook just below the confluence of an eastern and western tributary below water sample site LIZM-18-2.	43°	49'	40"	72°	19'	37"	
CB2-PPT	ochre-PPT	Precipitate in Copperas Brook just below the confluence of an eastern and western tributary below water sample site LIZM-18-2.	43°	49'	40"	72°	19'	37"	
98JHCBW-HP	ochre-HP	Hardpan terraces with leaves above LIZM-18-2 along west tributary of Copperas Brook just below wetland	43°	49'	36"	72°	19'	38"	LIZM-18-2
CB2-R-HP	ochre-HP	Hardpan on Copperas Brook stream bottom about 80 ft. upstream from confluence with river; thin film of yellowboy on red to orange hardpan substrate.	43°	49'	36"	72°	19'	38"	
98JHCB2R-LS4-1	ochre-PPT	Orange slime at limestone experiment site 4	43°	49'	56"	72°	19'	42"	
98JHCB2R-LS4-2	ochre-PPT	Brown-orange slime (lighter color than 1) at limestone experiment site 4	43°	49'	56"	72°	19'	42"	
		West Branch Ompompanoosuc River							
AV-slime	ochre-PPT	White slime precipitate coating the grate at the air shaft vent at water sample site LZAS.	43°	50'	7"	72°	20'	4"	LZAS
OMPR-2floc	ochre-PPT	Brown floc in West Branch Ompompanoosuc River 78 meters downstream from the air vent .	43°	49'	59"	72°	18'	36"	OMPR-2

APPENDIX B

METHODS

Field measurements

Paste pH

Ten grams of sieved <2 mm surface soil material weighed into a plastic beaker using a battery-operated balance was mixed with distilled water in a 1:1 solid: solution ratio following the recommendations for use in metal mine studies in British Columbia described by Price (1997). An Orion 230A pH meter with a Sure-Flow Ag/AgCl epoxy electrode and temperature probe for automatic temperature compensation was calibrated with pH = 4.00 and 7.00 buffer solutions. Ten milliliters of distilled water (pH = 6) was measured in a plastic graduated cylinder and added to the sample. The paste was stirred with a wooden spatula to wet the powder, and the pH was measured and recorded.

Water measurements

Water data included in this report, and water sampling methods, are given in Barg and others, (1999).

Mineralogy

X-ray powder diffraction (XRD)

X-ray powder diffraction (XRD) was used extensively for mineral identification in this study. Samples were prepared by several different techniques, depending on the nature of the material and the amount available. Splits of the pulverized powders submitted for chemistry were mounted as loosely pressed powders in 1" round aluminum holders. Small samples and minerals (hand picked under a binocular microscope or concentrated with heavy liquids) were ground in an agate mortar and mounted on a 1" round glass or zero-background quartz slide with toluene or isopropyl alcohol as a binder. All samples for XRD were run on a Scintag X1 automated diffractometer equipped with a Peltier detector and using CuKa radiation. Step scans were run using stepping intervals of 0.01 or 0.02 degrees 2-theta, with counting times of 1 to 4 seconds per step. Patterns were interpreted with the aid of Scintag and MDI Applications JADE search/match software and compared with reference patterns in the JCPDS database (International Centre for Diffraction Data, 1997).

Scanning electron microscopy(SEM)

A JEOL JSM-840 SEM was used for detailed examination of minerals to determine crystal shape, size, and texture, and to obtain qualitative information on composition using a PGT x-ray energy dispersive system (EDS). The SEM used in this study is also equipped with a back-scattered electron (BSE) detector and a secondary electron (SEI) detector. The SEM was operated at a voltage of 15 or 20 kV or lower, and a specimen current of about 1 to 2 nA. Samples were attached to carbon planchets with superglue or sticky carbon tape and graphite paint and were carbon coated. The spectra obtained with EDS provide qualitative and semi-quantitative information for elements heavier than carbon.

Electron microprobe (EMPA)

A JEOL JSX-8900 electron microprobe located in USGS laboratories in Reston, VA , was used for quantitative analysis of sulfide minerals and mica and for mapping of pyrrhotite alteration to marcasite. The EMPA, equipped with 5 wavelength dispersive spectrometers, was operated at 20kV (sulfides) or 15kV (silicates) and standardized using natural or synthetic mineral standards. Minerals were analysed in polished thin section or grain mount and samples were carbon coated prior to analysis.

Some samples of efflorescent salts were mounted and dry-polished and run for wavelength scans of the entire range of elements heavier than carbon to determine the presence or absence of minor components. Because the EMPA analyses a very small spot (on the order of 1 to 5 microns), one can obtain chemical information on individual mineral grains or parts of grains.

Mineral separation

Splits of tailings and ochre samples were placed in a heavy liquid (methylene iodide) to separate heavy minerals (those with specific gravity >3.3) including ore minerals and iron minerals from gangue minerals. Gangue minerals such as quartz, mica, and feldspar all have specific gravity <3.3 and therefore float in the heavy liquid whereas the heavy minerals sink and can be readily concentrated. This technique was used to concentrate the heavy minerals for XRD to facilitate identification of minor amounts of minerals and of poorly crystallized minerals.

Chemistry

Samples of materials for chemistry were prepared by the authors using standard sample preparation techniques for geologic materials as described in Arbogast (1996). Materials were pulverized to <100 mesh using an automated a ceramic puck mill. Prepared samples were sent to USGS sample control laboratories in Denver where they were split and grouped with standards and replicate samples and submitted to in-house laboratories or to the contact lab (XRAL, Don Mills, Ontario) depending on the analytical method. The contract lab follows USGS protocols for most methods, as described in Arbogast (1996). Where an element was determined by more than one method, the number for the more sensitive method was used in preparing plots and computing base metal totals. For example, many samples exceed the upper reporting limit for ICP-AES for iron and are reported in the tables as qualified values (> 30 wt. %) but are well within the range for reporting iron by ICP-MS. Two types of analyses were performed in-house (ICP-MS and WD-XRF); all other types of analyses were done by XRAL. Detection limits for different methods are listed in table form below. Abbreviations for methods cited in this report and references for complete details of the analytical techniques and instruments are as follows:

Inductively coupled plasma-mass spectrometry (ICP-MS)

Multi-element technique (USGS method) used for all sample media in this study except stream sediment samples (Arbogast, 1996; Lichte and others,1987). Detection limits for ICP-MS vary and are computed for each batch of analyses based on concentrations measured in blanks. However, detection limits by ICP-MS are orders of magnitude lower than detection limits for other methods, so very low concentrations of elements can be measured by this method.

Inductively coupled plasma-atomic emission spectroscopy (ICP-AES)

Multi-element (40) technique (USGS method) used for stream sediments and to obtain major elements for some other sample types. For samples with >25 wt. % Fe, data by this technique may be biased low. See ICP-MS for preferred values for iron-rich materials (Arbogast, 1996; Crock and others, 1983).

Hydride generation (HYD)

Specialized technique(USGS method) for determination of As, Se, and Sb. Using a multi-acid procedure and atomic absorption spectrophotometer (Arbogast, 1996).

LECO

Technique (XRAL) used for total S, C, and water determinations. Total sulfur is measured with an automated sulfur analyzed by combusting the sample in oxygen in a LECO induction furnace and measuring SO_2 by infrared detector. Total carbon and carbonate carbon are determined; organic carbon is computed by difference. Uses an automated carbon analyzer to determine total carbon in geologic materials. Samples (0.200 g are combusted added to a crucible with LECO cell and iron chips and combusted in an oxygen atmosphere to form carbon dioxide which is measured by infrared detector. Carbonate carbon is determined as carbon dioxide using perchloric acid and evolved gas is measured coulometrically. Essential (structural or crystalline) water is reported as H_2O+ and non-essential (or hydroscopic) water is reported as H_2O-. Both are detected by heating and infra-red absorption.

Graphite furnace atomic absorption spectrophotometry (GFAA)

Specialized technique (USGS method) for accurate analysis of low-level gold using extraction with methyl isobutyl ketone (Meier, 1980).

Cold vapor atomic absorption spectrometry (CVAC)

Specialized technique (USGS method) or mercury analysis in geologic materials (Kennedy and Crock, 1987).

Wavelength dispersive X-ray fluorescence spectroscopy (WD-XRF)

Used for determination of major elements (reported as oxides) in geologic materials. Used in this study primarily to determine silica content of rocks and soils. LOI reported represent loss on ignition and include water and other volatiles released on sample ignition (Mee and others, 1996).

DC-ARC emission spectrography (SQS)

Semi-quantitative method widely used in older (pre-1990s) studies in exploration geochemistry. Values are reported as 6 steps per order of magnitude. Detection limits reported below are from Adrian and others (1990).

Ranges of concentrations or lower detection limits for each method

Element	Units	ICP-AES	ICP-MS	GFAA	LECO	CHM	WD-XRF	HYD	SQS	CVAC
Al	%	0.005 - 50								
Ca	%	0.005 - 50							0.05	
Fe	%	0.02 - 25							0.005	
K	%	0.01 - 50								
Mg	%	0.005 - 5							0.02	
Na	%	0.005 - 50							0.2	
P	%	0.005 - 50	0.01						0.2	
Si	%									
Ti	%	0.05 - 25								
FeO	%				0.01					
SiO_2	%						0.10 -99			
Al_2O_3	%									
Fe_2O_3	%									
MgO	%									
CaO	%									
K_2O	%									
TiO_2	%									
P_2O_5	%									
MnO	%									
LOI	%									
Ag	ppm	2 - 10,000							0.5	
As	ppm	10 - 50,000	0.5					0.6 - 20	200	
Au	ppm	8 - 50,000	0.05	0.002					10	
B	ppm								10	
Ba	ppm	1 - 35,000							20	
Be	ppm	1 - 5,000	0.1						1	
Bi	ppm	10 - 50,000							10	
Cd	ppm	2 - 25,000	0.1						20	
Ce	ppm	5 - 50,000	2							
Co	ppm	2 - 25,000							10	
Cr	ppm	2 - 50,000							10	
Cs	ppm		0.1							
Cu	ppm	2 - 15,000							5	
Ga	ppm	4 - 50,000							5	
Ge	ppm									
Hg	ppm									0.02
In	ppm									
La	ppm	1-50,000	1						50	
Li	ppm	2 - 50,000		0.5						
Mn	ppm	4 - 50,000							10	
Mo	ppm	2 - 50,000							5	
Nb	ppm	4 - 50,000	0.1						20	
Ni	ppm	3 - 50,000							5	
Pb	ppm	4 - 50,000							10	
Rb	ppm									

Element	Units	ICP-AES	ICP-MS	GFAA	LECO	CHM	WD-XRF	HYD	SQS	CVAC
Sb	ppm			0.1				0.6 - 20	100	
Sc	ppm	2 - 50,000	0.5						5	
Se	ppm		1					0.2 - 4		
Sm	ppm		0.05							
Sr	ppm	2 - 15,000							100	
Ta	ppm		0.1							
Te	ppm		0.1					0.1 - 10		
Th	ppm	6 - 50,000	0.05						100	
Tl	ppm		0.1	0.1				0.1 - 10		
U	ppm	100- 100,000	0.05							
V	ppm	2 - 30,000							10	
Y	ppm	2 - 25,000							10	
Zn	ppm	2 - 15,000							200	
Zr	ppm									
CO2	%				0.01 - 50					
Total S	%				0.5 - 35					